Structure and Activities of Beta Toxin: A Virulence Factor of *Staphylococcus aureus*

A DISSERTATION
SUBMITTED TO THE FACULTY OF THE GRADUATE SCHOOL
OF THE UNIVERSITY OF MINNESOTA
BY

Medora Jean Huseby

IN PARTIAL FULFILLMENT OF THE REQUIREMENTS
FOR THE DEGREE OF
DOCTOR OF PHILOSOPHY

Douglas Ohlendorf

May 2009

Acknowledgements

I would like to acknowledge all those who gave me the courage to pursue my dreams and shaped the person I am proud to be.

I acknowledge my family, who always believed in and supported me throughout my entire life.

I acknowledge Cathy and Doug Ohlendorf, who gave me the guidance to become the scientist I am today.

I acknowledge Dr. Ke Shi, who taught me the technical side of crystallography, and always had an answer to every question I could think of.

I acknowledge Andrew Kruse. His outstanding hard work has made this thesis much more comprehensive and interesting.

I acknowledge the scientific community at the University of Minnesota. The openness and sharing everything from knowledge to reagents and equipment is something I will emulate throughout my scientific career.

Dedication

I dedicate this work to my family, my horses, and my friends. Without their support, I would not have been able to accomplish nearly as much. Through their love, I am proud of what I have achieved, and am confident in my future. I specifically dedicate this to Mark Stenglein, who has been my partner through my entire graduate career, and supported me always.

Abstract

Beta toxin is a neutral sphingomyelinase secreted by certain strains of *Staphylococcus aureus*. This virulence factor lyses erythrocytes in order to evade the host immune system as well as to scavenge nutrients. The structure of beta toxin was determined at 2.4 Å resolution using crystals that were merohedrally twinned. This structure is similar to that of the endonuclease HAP1, *Escherichia coli* endonuclease III, bovine pancreatic DNase I, and the endonuclease domain of TRAS1 from *Bombyx mori*. Our biological assays demonstrated for the first time that beta toxin kills proliferating human lymphocytes. Structure-directed active site mutations show the biological activities of hemolysis and lymphotoxicity are due to the sphingomyelinase activity of the enzyme.

The structures of all bacterial neutral sphingomyelinases solved to date reveal a solvent exposed hydrophobic beta hairpin. We examined the role of this beta hairpin in beta toxin virulence. Altering the length but not the content of the beta hairpin attenuates the biological activities associated with beta toxin. The beta hairpin is an important stabilizing structure. X-ray crystallographic analysis of beta hairpin mutants revealed very minimal structural changes. We show for the first time diacylglycerol bound in the beta toxin truncation (275-280) structure near the beta hairpin region. We also show at 1.75 Å resolution Mg^{2+} and phosphate bound to the F277A P289A structure.

Neutral sphingomyelinases belong to the DNase I super-family of proteins (CATH class 3.60). Beta toxin shares the overall fold of DNase I with an RMSD value 3.3 Å over 220 Cαs. Beta toxin does not function as a DNase and instead precipitates nucleic acid. DNA causes beta toxin to non-specifically cross-link to other proteins. Extracellular DNA is a major structural component of the *S. aureus* biofilm matrix. Here we demonstrate that beta toxin has a profound effect on forming the matrix on which biofilms grow through the nucleic acid-dependent formation of cross-linked beta toxin monomers as well as other proteins. These links, plus the ability to bind eDNA, enables formation of the underlying nucleoprotein matrix essential to establish a biofilm.

The goal of this thesis project is to understand the structural foundations for the role of the virulence factor beta toxin in order to understand the biological mechanism that allows *S. aureus* to successfully invade, colonize, and attack a host.

Table of Contents

List of Tables

List of Figures

CHAPTER 1
INTRODUCTION TO CRYSTALLOGRAPHY

This chapter is an overview of crystallography. It describes the crystallization and data collection processes used in this thesis project and details the difficulties encountered with perfect merohedrally twinned crystals.

SUMMARY

Crystallography is a common technique used by the scientific community to determine the three dimensional positions of all atoms in a protein. Beta toxin was crystallized using both sitting and hanging drop vapor diffusion techniques. The crystals of native beta toxin, as well as those of the active site mutants H150N and H289N were perfect merohedral twins. The structures were solved using molecular replacement techniques. The crystal structures of beta toxin hairpin mutants were not twinned and were solved by molecular replacement.

INTRODUCTION

Crystallography is a powerful tool that allows researchers to determine the three dimensional positions of all atoms in a molecule. It can be applied to systems as simple as a salt or as complex as the ribosome. The limits are ever being pushed as technology and ideas progress. To date, there are 57,558 structures deposited in the RSCB protein data bank (10). Many of these structures are from crystallography and have directly impacted human health by aiding drug design, revealing how a variant protein causes disease, or giving insight into previously unknown functions of proteins.

DISCUSSION

Crystallization

To perform crystallography, one must first crystallize a biomolecule of interest. This process is often the rate limiting step of crystallography. By definition, a crystal is a repeating unit that extends in three dimensions. The smallest translationally repeating unit of a crystal is known as the unit cell. A crystal should be composed of homogenous species, as heterogeneity will decrease the quality and order of the crystal. Heterogeneity can be in the form of impurities from the purification of the species, or from flexible domains within the species itself. Furthermore, post-translational modifications of proteins, such as glycosylation, and the presence of co-factors can introduce heterogeneity.

There are many different ways to crystallize a protein. This is done based on a trial-and-error search of different conditions, as it is currently not possible to predict how a protein will crystallize based on sequence or secondary structure predictions. Commercial screens are available of known conditions that have produced crystals of other proteins. Salts, organics, and polymers such as polyethylene glycol (PEG) are used as precipitating agents. When crystallizing a biomolecule, many variables can be changed to produce crystals. Temperature, precipitant concentration, protein

concentration, the pH of the buffer, the mother liquor volume, or adding ions or detergents are a few examples.

Vapor diffusion is a common method used to crystallize a protein. This involves the supersaturation of a solution, allowing the protein to precipitate in a controlled fashion to produces crystals (Figure 1.1). This is a tightly regulated step; if the protein spends too much time in the nucleation zone it will form many crystals too small to give quality data. However, if it the protein remains in the soluble zone, it will not nucleate or grow at all. Ideally, the right conditions will cause a protein to form ordered aggregates in the nucleation zone. If the ordered aggregates reach a size where crystal growth is favored over dissolution, the decrease in the protein concentration will cause the aggregate to enter the crystal growth zone. The crystal will grow until there is no longer any protein in the solution.

The process of finding conditions that produce crystals of a suitable size and quality can require milligrams of protein. Getting such amounts of protein is problematic as some proteins are not soluble, such as membrane proteins, or are not easy to produce in large quantities, such as some eukaryotic proteins. Crystallization robots, such as the OryxNano from Douglas Instruments Ltd, the Mosquito from Molecular Dimensions Ltd, or the CrystalMation™ from Rigaku, have been developed to alleviate this problem. Using this technology, nanoliter drops can be used to screen for initial conditions and then the protocol scaled up to produce protein crystals of a suitable size.

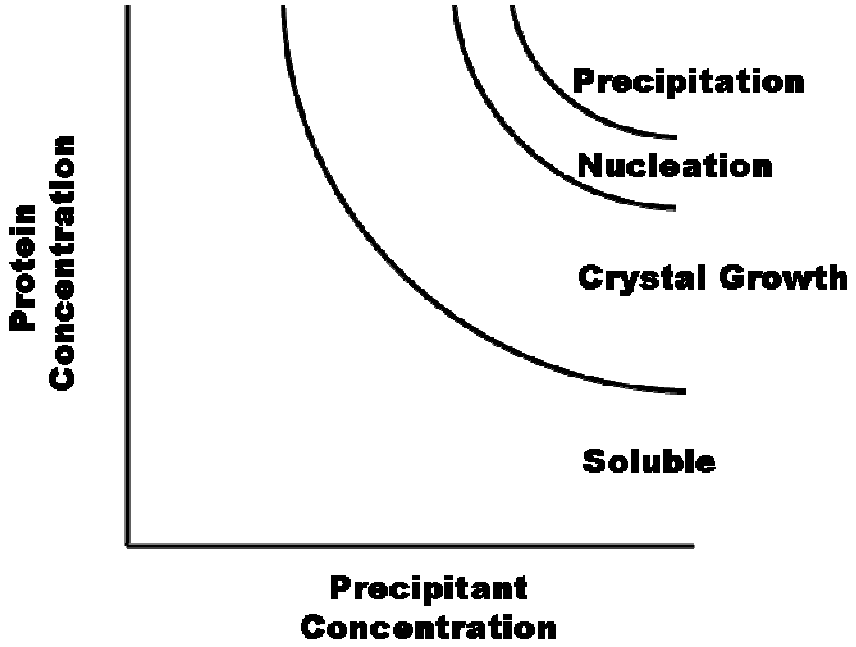

Figure 1.1 Plot of protein and precipitating reagent concentration. Everything above the soluble curve is supersaturated. The zones where precipitation, nucleation, and crystal growth occur are indicated.

Sitting drop and hanging drop are two common techniques that use vapor diffusion for crystallization of proteins (Figure 1.2). In these techniques, a protein/precipitant solution is equilibrated with a larger aqueous reservoir in a sealed container. Purified protein is dissolved in buffer containing the precipitant at a concentration that is just below the maximum precipitate concentration in which the protein is still soluble. The water vapor from the protein mixture slowly evaporates to the reservoir of mother liquor until equilibrium is reached. This causes an increase in the precipitant concentration allowing the protein to nucleate and then form ordered aggregates. This step is followed by crystal growth. Both hanging and sitting drop diffusion were used to crystallize all forms of beta toxin.

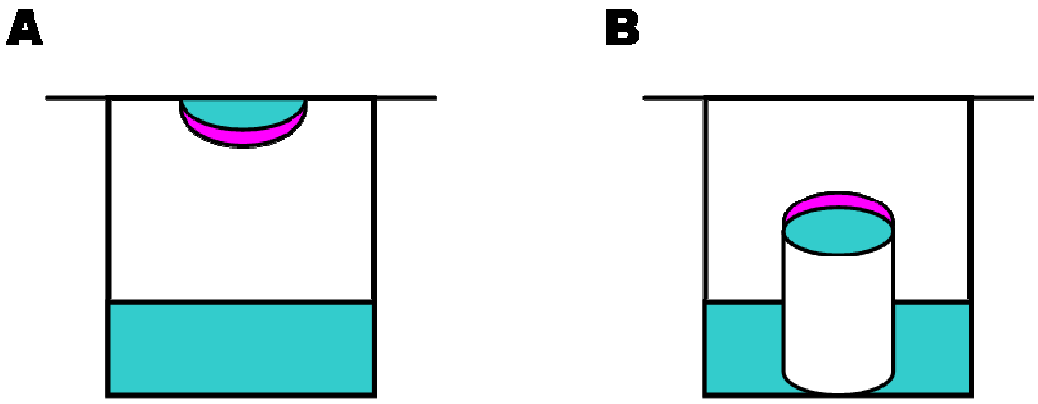

Figure 1.2 Hanging and sitting drop vapor diffusion. (A) Hanging drop vapor diffusion. The protein (pink) is mixed with mother liquor (blue) and suspended above the reservoir of mother liquor. (B) Sitting drop vapor diffusion. The protein (pink) is layered with the mother liquor (blue) and placed on a pedestal above the reservoir of mother liquor as shown in the figure. The solutions mix immediately and are sealed, allowing the water to equilibrate causing an increase of the precipitant concentration in the drops of protein.

Phase Problem

Once diffraction quality crystals are obtained, diffraction data are collected. However, the next step in X-ray crystallography is a challenge that arises from the data collection process. The phase of the structure factor (the amplitude and phase representative of the overall scattering from a particular set of Miller planes) is lost. The amplitude (proportional to the square root of the reflection's intensity) remains measurable and is collected. This is known as the phase problem. To determine the lost phase information, different techniques must be applied. Molecular replacement (see below) is a popular solution if a homologous structure has been previously solved. For any *de novo* structure, two main strategies are utilized for phasing: multiple isomorphous replacement (MIR) and multiple-wavelength anomalous dispersion (MAD).

MIR relies on changing the crystal in such a way that the structure factors are perturbed. This perturbation allows the phases to be calculated, and can be caused by the introduction of a heavy atom. Heavy atoms such as xenon gas or uranium can be introduced into the crystal, with the goal of attaching them to a few sites with high occupancy, yet leaving the rest of the crystal contents unchanged. This is known as the isomorphous derivative. The differences in the scattering intensities show the placement of the heavy atoms, and give two possible solutions for each phase. The process is then repeated to distinguish which of the two possible phases is correct using a second derivative.

MAD techniques still require heavy atom derivatives, but instead of using multiple crystals, multiple wavelengths are used on a single crystal. The protein must contain an anomalous scattering atom, however, and one way to ensure this is to use a selenomethionine derivative (38). This derivative replaces the sulfur atom with selenium in the native methionine residues of a protein. To succeed a minimum of 1 selenomethionine residue for approximately every 75 amino acids present in the protein is required (86). Because anomalous scattering is maximal at the absorption edge of the heavy atom, this technique requires a tunable radiation source, such as can be found at a synchrotron. The heavy atom will then absorb the radiation and re-emit it with an altered phase. We attempted to use MAD techniques to solve the structure of beta toxin using a selenomethionine derivative. However, the crystals were twinned (see Twinning section below) making this impossible.

Traditional x-ray data collection involves x-rays from a copper κ_α radiation source (λ =1.54 Å) or a synchrotron source (usually λ= 0.9 Å) (65). If a chromium κ_α radiation source (λ =2.29Å) is used instead, the anomalous signal from elements such as selenium, calcium and potassium is enhanced compared to that of a copper source (98). This is also the case for sulfur, and generally the presence of 1 sulfur atom for every 40 residues can allow for successful phase determination (73).

Molecular Replacement

All beta toxin and mutant structures were obtained using molecular replacement techniques (see Materials and Methods sections for Chapters 3 and 4). Molecular replacement is a suitable technique to solve the phase problem if a model is available that has at least 40% sequence identity, though sequence identities of less than 40% have been known to work as well. This works by placing the unit cell of the phasing model into the same orientation and position as that from the collected data. The new protein structure is revealed during the process of phase improvement as the phases change from those of the phasing model to those of the new protein. This is accomplished by iterative rounds of model building and refinement (70), (27).

For a non-isomorphous phase model and/or new protein, the structure of the model must be placed on the structure of the new protein within the unit cell. Once both the orientation and the position of the new protein are known, phases can be calculated. A brute-force search to find the correct orientation and position is usually computationally impractical. Instead, separate searches are used to find the best orientation (rotation function) followed by the best position (translation function).

The rotation function determines the rotation matrix, which then allows the orientation to be determined. This relies on the Patterson function (Equation 1.1)

$$P(u,v,w) = 1/V \sum_h \sum_k \sum_l |F_{hkl}|^2 \exp[-2\pi i(hu + kv + lw)] \qquad \textbf{Equation 1.1}$$

The Patterson function contains the sum of all vectors within the unit cell. The Patterson map will show peaks at the end of vectors between atoms in the unit cell of the structure (1). These vectors start at the origin of the Patterson cell. The relative positions of the atoms are important, but the locations of the atoms are not. The rotation function works because intramolecular vectors are dependent only on molecular rotation, not molecular translation. Because of this, the phase model is rotated through a system of polar angles (27). When values of the Patterson function of the phasing model correspond to peaks in the new protein Patterson map, this orientation is placed in the new protein unit cell (70).

After the orientation of the new protein is found, the translation function is then used to determine the 3-D position of the molecule. The R factor (Equation 1.2) is used to judge the translation function.

$$R = \frac{\sum \| \mathbf{F}_{obs} | - | \mathbf{F}_{calc} \|}{\sum | \mathbf{F}_{obs} |} \qquad \textbf{Equation 1.2}$$

The translation function relates the expected structure-factor amplitudes from the phase model (F_{calc}) in a given trial location with the actual data derived amplitudes on the new protein (F_{obs}). A small R factor value indicates the best translation position. An R value of 0.3 to 0.4 is acceptable for initial estimates of phases (70).

Twinning

Twinning is a phenomenon that describes a growth disorder of a crystal. The crystal has distinct domains that differ, yet are related in a well-defined way (99). Twinning is common in small molecule crystals, but less so in macromolecular crystals. Merohedral twinning is a special case of crystallographic twinning where the lattices of different domains in a single crystal overlap in three dimensions (99). This means that instead of having the image of a single molecule, you see a double exposure of the molecule plus another rotated molecule (Figure 1.3).

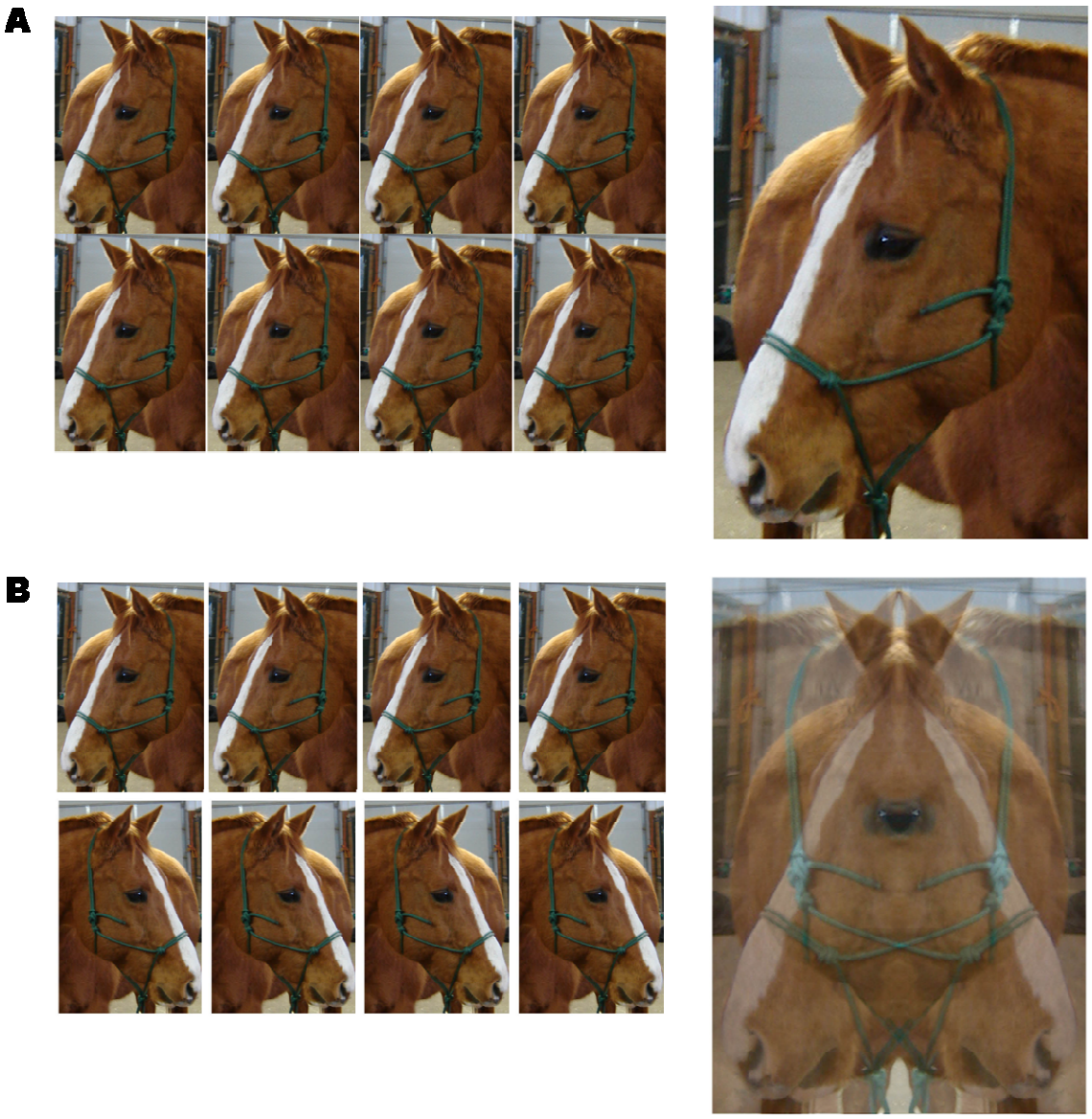

Figure 1.3 Normal vs. twinned crystal packing. (A) Normal crystal packing. The unit cell, represented by the horse looking to the left, is repeated by translation, but is not rotated. This crystal would result in the enlarged picture to the right. (B) Twinned crystal packing. The unit cell, as defined in part (A), is both translated and rotated (the horse is looking both to the left and the right). This would result in a merging of both orientations as depicted in the enlarged picture on the right.

Twinning can be described using two parameters; the twin factor, which is the fractional volume of the crystal that the smaller of the two domains occupies, and the twin operator, which is the symmetry operation that relates the orientations of the domains (16). The twin factor (α) has a value between 0.0 and 0.5. The twin operator is a mapping of reflection indices from hkl to h'k'l', where hkl and h'k'l' are the twin related indices. The twin operator can be deduced from the space group of the twinned crystal. The observed intensity of a twinned crystal is related to the intensities each domain (Equation 1.3)

$$I_{hkl}(\text{twin}) = \alpha\, I_{hkl}(\text{domain 1}) + (1-\alpha)\, I_{hkl}(\text{domain 2}) \qquad \textbf{Equation 1.3}$$

When α has a value of less than 0.5, the crystal is considered partially twinned. The data from a partially twinned crystal can be "detwinned" and the structure determined if α is significantly different from one-half and if α can be estimated accurately. The Merohedral Crystal Twinning Server (99), which statistically evaluates the similarity between twin-related observations, can be used for this purpose. An updated version of this server, the Merohedral Twin Detector: Padilla-Yeates Algorithm, is also available (67).

If α is equal to or very close to 0.5, the crystal is considered a perfect twin, and true untwined crystallographic intensities cannot be recovered from the observed measurements (99). This has been called "perfect twinning". Molecular replacement techniques can be used to solve the structure from a perfectly twinned crystal, and in theory, so can MIR techniques (99). Problems arise as additional symmetry is imposed by the twinning operation, and is seen in the diffraction pattern. Because of this, the data can be processed with false high symmetry. If the higher order symmetry is processed and refined, a false average of the two orientations of the actual structure is then obtained (33). In addition, most molecular replacement programs do not allow structures to interpenetrate as they must for a perfect merohedral twin.

Twinning prevents structure determination unless it is detected and corrected or avoided. Generally, twinning cannot be detected by visualizing the crystal. However, in some cases a microscope with crossed polarizers will show a twinned crystal that will

transmit light in some regions but remain dark in others. Non-twinned crystals should either transmit light or not, but not have a combination of both. Non-merohedral (epitaxial) twinning can generally be detected by the diffraction pattern, as two diffraction patterns are overlaid in a single image. Theoretically this type of twinning can be circumvented by indexing the two patterns separately (16).

Merohedral twinning can be detected several ways. Merohedral twinning is possible only in certain space groups. If the unit cell is calculated to be too small for the known molecule under the apparent space group symmetry, the crystal could be a perfect twin (99). Further indications of twinning are a physically impossible Patterson function for heavy atom searches, systematic absences inconsistent with the known space group, no structure solution, and problems with refinement (39), (80).

Native beta toxin and the active site mutants, H289N and H150N, crystallized as perfect merohedral twins. While attempting to crystallize native beta toxin and the two active site mutants in a non-twinned form, the structure of SmcL was published (66). SmcL is a neutral sphingomyelinase C from *Listeria Ivanovii* and has 55.7 % identity to that of beta toxin at the primary sequence level. SmcL was used as the search model for molecular replacement as described in the Materials and Methods section of Chapter 3.

The structure of beta toxin revealed a hydrophobic beta hairpin (see Chapters 3 and 4). Mutations of the beta hairpin (F277A P278A, 275-280 and 272-282) resulted in protein that did not form twinned crystals. All beta hairpin mutants crystallized under different conditions than that of native beta toxin, H298N, and H150N. Some of the mutants (F277A P278A and 275-280) crystallized in each other's conditions. It is interesting to speculate that the beta hairpin could have been interacting between unit cells to aid in the formation of twinned crystals. However, the reason why any crystal has a growth disorder, such as twinning, remains unknown.

Concluding Remarks

Crystallography remains a powerful tool to obtain three dimensional structures of large biomolecules. Though beta toxin was not the first neutral sphingomyelinase structure solved by crystallography (due to the twinned crystals), this work has identified key areas of beta toxin such as the active site (Chapter 3) and a hydrophobic beta hairpin (Chapter 4). Furthermore, the structure of beta toxin is very similar to that of DNase I. This observation led to the discovery that beta toxin binds DNA (Chapter 5). Because of this new activity, we discovered that beta toxin forms a nucleoprotein matrix of biofilms. From analyzing the crystallographic structure of beta toxin, we have uncovered novel roles for beta toxin in the virulence of *Staphylococcus aureus*.

CHAPTER 2
INTRODUCTION TO *STAPYLOCOCCUS AUREUS*

This chapter serves as an introduction to the pathogen *Staphylococcus aureus.* It details how virulence factor production leads to disease. It also provides an introduction to biofilms.

SUMMARY

Staphylococcus aureus is the leading cause of hospital acquired infections. It is considered the most virulent staphylococci. It becomes pathogenic by the coordinated expression of virulence factors, which allow it to attach to and invade host tissue, evade host immune surveillance, and damage host tissue for defense and nutritional purposes. Chronic *S. aureus* infections are associated with biofilm formation. Biofilms are communities of surface-attached microorganisms encapsulated within a matrix. Few components of this matrix have been defined. Biofilm infections are difficult to treat by conventional antimicrobials.

INTRODUCTION

Staphylococcus aureus is a gram positive bacterium that is the major cause of infections in the United States. Approximately 40% of healthy individuals are colonized by *S. aureus* typically in the nasal passages, vagina, or perianal area (6). In the United States, *S. aureus* is the major cause of nosocomial (acquired in a hospital) infections resulting in over 700,000 infections annually (according to the CDC). The emergence of antimicrobial-resistant strains, specifically to methicillin and vancomycin (MRSA and VRSA, respectively), highlights the importance of finding new antimicrobial targets. *S. aureus* becomes virulent when exposed to a stressor or new environment. This leads to the production of virulence factors, which are by definition the armada of extracellular and cell surface factors that aid in host invasion and attachment, immune system evasion, and nutrient scavenging.

Penicillin-resistant strains of *S. aureus* were reported as early as 1942 (59) . By 1997, 90% of *S. aureus* isolates were resistant to penicillin (51). Methicillin was first clinically used in 1960 to treat *S. aureus* infections. Today 40% of *S. aureus* isolates are methicillin resistant. Vancomycin is often the therapeutic of choice for MRSA infections. However, vancomycin-resistant isolates were first reported in 1997 (41), and are now clearly a global health threat. Virulence factors are key to pathogenesis, and therefore make excellent targets for new antimicrobial therapeutics.

DISCUSSION

Virulence Factors

S. aureus is regarded as the most virulent species of staphylococci due to its large variety of expressed virulence factors (36). Some virulence factors are tightly regulated by the accessory gene regulator, *agr* (61). *agr* is a quorum sensing system that responds to environmental signals during the course of an infection. The *agr* locus generates two primary transcripts, RNAII and RNAIII. RNAII is involved in generating the *agr*-sensing mechanism. RNAIII functions to increase the expression of secreted

virulence factors such as hemolysins and proteases (82). These products are then used to adhere to host cells, evade host defenses, and degrade host tissue for both nutrition and defenses (62).

When a pathogen is exposed to a new environment, for example during a surgical procedure, it will attempt to colonize the host. This is done by first expressing adhesion and defensive proteins (30). Adhesion proteins, such as protein A, coagulase, and fibronectin binding protein, are surface proteins that bind to host extracellular matrix components. Protein A and coagulase also function as defensive proteins using host molecules to disguise the pathogen from the immune system. Protein A inhibits phagocytotic engulfment by binding immunoglobulin Fcs, while coagulase binds fibrin, coating the *S. aureus* surface with the host molecule (87). After the pathogen has attached to the host, adhesion and defensive proteins are down regulated, and the hemolysins, cytotoxic proteins, and degradative enzymes are expressed (30).

The pathogen will further invade host tissue for nutrition and defense. This is accomplished on a local level by membrane damaging toxins known as hemolysins (Figure 2.1). There are four members of the hemolysin family; alpha, beta, gamma, and delta toxins. Beta toxin is the sole enzyme, and functions as a sphingomyelinase. Beta toxin is the focus of this thesis and is described in detail in the last three chapters. Alpha toxin is expressed as a monomer that binds to the membrane of susceptible cells, such as platelets and monocytes (87). The subunits oligomerize and form heptameric pores embedded in the host cell membrane (81). The host cell is lysed as its cellular contents leak out. Gamma toxin forms heterodimers with leucotoxins, which then form pores in the membranes of susceptible cells, leading to lysis (72). Delta toxin is a 26 amino acid peptide that forms an α helix. At low concentrations, delta toxin disrupts host cell membranes by inducing curvature strain on the membrane and causing ionic efflux (90). At high concentrations, delta toxin acts like detergent to induce solublization of the host cell membrane, which leads to cell lysis (90).

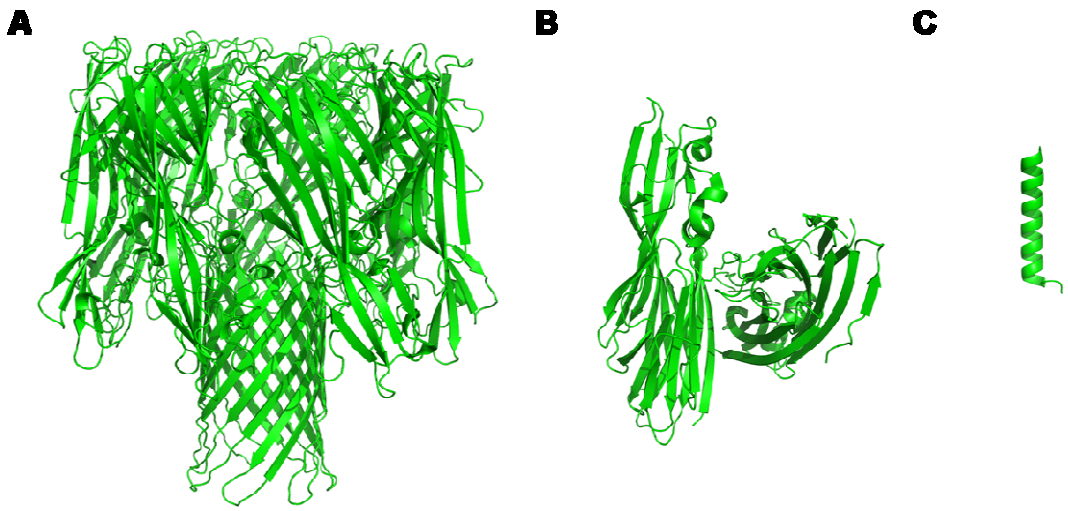

Figure 2.1 Cartoon representations of hemolysin structures. (A). Alpha toxin (81). (B) Gamma toxin (72). (C) Delta toxin (12). See text for mechanisms of action.

Superantigens are involved in a systemic mode of invasion. They do this by bypassing normal antigen presentation and instead induce strong T-cell mitogenic activity by locking MHC (major histocomapatibility) II molecules on antigen presenting cells to T-cell receptors on certain T cells (89). The result of this action is the massive release of cytokines, which can then lead to shock. This is how toxic shock syndrome toxin-1 and the staphylococcal enterotoxins function. Currently there are 17 well characterized superantigens produced by *S. aureus* (76).

Generally, a single virulence factor is not able to cause disease. However, when expressed in a coordinated fashion, virulence factors cause life threatening disease such as septicemia and shock. Virulence factors are excellent targets for new antimicrobial agents.

Biofilms

Many *S. aureus* infections are thought to involve the formation of biofilm, which are surface-associated communities of microbes encompassed by an extracellular matrix (Figure 2.2) (23), (24). As surveyed by scanning and transmission electron microscopy, many indwelling devices such as mechanical heart valves, neuronal shunts, and virtually all central venous catheters are colonized by staphylococci embedded in a biofilm (82). Once an indwelling device is colonized, it must be removed. This places a heavy cost burden on the health care system. NIH estimates that 80% of all bacterial infections involve biofilms. Biofilms can form on host tissues as well as indwelling devices.

Biofilms are populated with bacteria that have switched from a free floating, planktonic phenotype to an attached phenotype (Figure 2.3). Bacteria have different gene expression profiles depending on when they are planktonic or attached, as revealed by microarray analysis (82). Even within a biofilm, bacteria have different expression profiles; bacteria located deep within the biofilm behave very differently than those exposed near the surface.

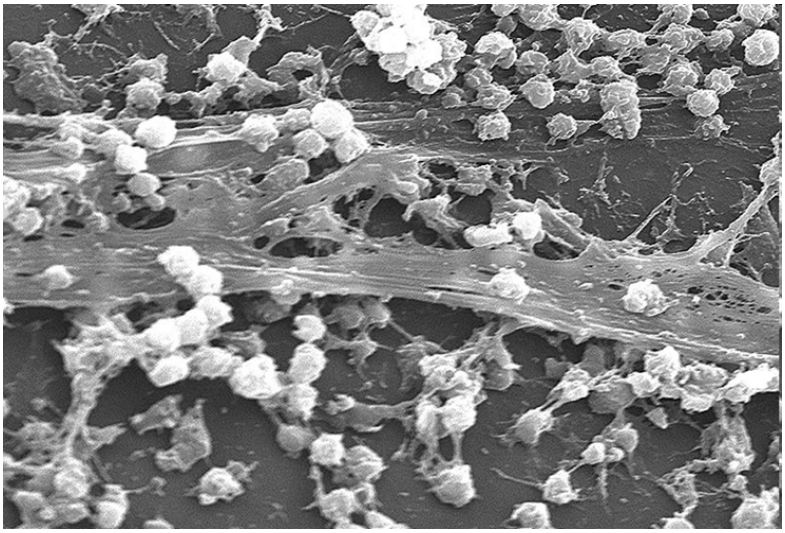

Figure 2.2 Image of a catheter colonized by *S. aureus* biofilm. Image provided by the CDC public health image library. Photo credit: CDC/ Rodney M. Donlan, Ph.D.and Janice Carr (PHIL #7488), 2005.[1]

The first step in biofilm formation is attachment to a surface. The pathogen can either attach to host proteins coating the surface, or directly to the surface itself (82). Once attached, the pathogen can proliferate and accumulate on the surface. It is during the proliferation phase that a polymeric substance is produced. The polymeric substance consists of high molecular weight compounds, mainly composed of polysaccharides, which the microorganisms secrete into their environment (83). The biofilm reaches maturation when the architecture contains several layers of cell with projecting structures known as towers. When the biofilm is subject to shearing forces such as blood flow or proteases, the towers dissociate. This dispersion can then seed new biofilms elsewhere (82).

[1]This image is in the public domain and thus free of any copyright restrictions and can be found at http://phil.cdc.gov/phil/home.asp image number 7488.

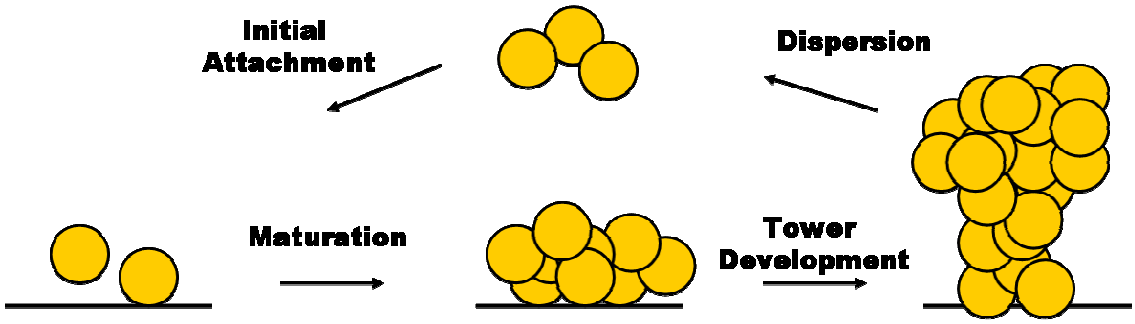

Figure 2.3 Process of biofilm formation. *S. aureus* (depicted as yellow circles) initially attaches to a surface, and then replicates/accumulates and secretes extracellular polymeric substance. Once maturation is reached, towers will develop, and the biofilm can then disseminate to a new site.

Some of the components of the polymeric substance are known. Polysaccharide intercellular adhesion (PIA) is a polysaccharide found in staphylococcal biofilms that functions both as an aggregation substance and as well as an adhesin molecule (50). However, staphylococcal biofilms can form independently of PIA. These biofilms are considered protein based, or PIA independent. Extracellular DNA is another major structural component of *S. aureus* biofilms (71). Few proteinacious biofilm components have been identified. BAP (biofilm associate protein) has been found to be crucial for initial adherence and intercellular accumulation during biofilm development in chronic bovine mastitis infections (25). SasG (surface associated *Staphylococcus* Protein G) is a surface protein that has been implicated in PIA independent biofilms (22).

Once a biofilm infection is established, it is very difficult to treat. Biofilms are resistant to traditional antimicrobial therapy due to impermeability of conventional drugs. Furthermore, treating a biofilm with antimicrobials can select for a sub population of antimicrobial resistant bacteria. Resistance could then be transferred to other microbes within the biofilm. Biofilms also sequester the microbe away from and ward off host defenses, due to impenetrability and other as of yet undefined factors (82).

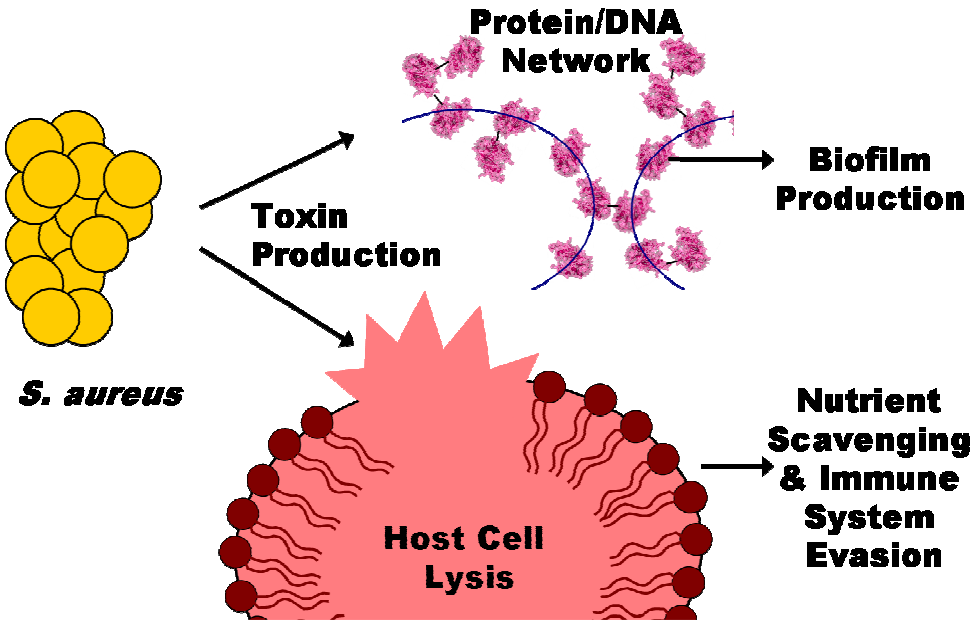

Figure 2.4 Model of beta toxin in pathogenesis of *S. aureus*. *S. aureus* (yellow circles, labeled) secretes toxins, such as beta toxin, following post exponential growth (arrows). Beta toxin lyses host cells (pink circle with simplified maroon lipid membrane) for nutrients and immune system evasion. Beta toxin forms a protein-DNA network (DNA represented by blue semi-circles, beta toxin by the magenta cartoon, and cross links are indicated by black lines) which is important in establishment of the biofilm matrix.

Concluding Remarks

Beta toxin functions at a local level to disrupt host immune cells (Figure 2.4). This is beneficial for *S. aureus* as it not only lyses the host cell trying to engulf it, but can also scavenge nutrients lost from the lysed cell. This is especially crucial in the case of iron, which is one way host defenses keep infections at bay. As will be shown in Chapter 5, beta toxin interacts with DNA and forms a nucleoprotein biofilm matrix. So not only does beta toxin attack host defenses, it also defends the pathogen by forming the biofilm matrix around it.

No virulence factor is able to cause disease by itself. Toxic shock syndrome toxin-1, staphylococcal enterotoxins, and exfoliative toxins is the exception to this (34). Because of the dual role beta toxin plays in pathogenesis, an antimicrobial targeted

towards it may prevent biofilm formation while alleviating lysis of host defense cells (Figure 2.4). This would be beneficial as the pathogen would remain planktonic, allowing the host cells to rid the infection. Indeed, the current antimicrobial trend is to target biofilm formation at the earlier stages before it can become mature and dissociate (82).

CHAPTER 3
STRUCTURE AND BIOLOGICAL ACTIVITIES OF BETA TOXIN

This chapter details the structure of beta toxin and active site mutants, H150N and H289N. Beta toxin is shown to lyse sheep erythrocytes and kill proliferating human lymphocytes in a sphingomyelinase dependent manner.[2, 3]

[2] Copyright © American Society for Microbiology. Huseby, M., Shi, K., Brown, CK., Digre, J., Mengistu, F., Seo, KS., Bohach, GA., Schlievert, PM., Ohlendorf, DH., Earhart, CA. Journal of Bacteriology, 189, 8719-26, 2007. The License agreement number is 2163121351686.

[3] Several people contributed to the work detailed in the chapter. Jeff Digre aided in mutation and primer design of the beta toxin mutants. Dr. Ke Shi was instrumental for structure determination from the twinned beta toxin crystals. Patrick Trogdon and Firkre Mengistu helped with protein purification and the sphingomyelinase activity assay. Dr. Patrick M. Schlievert offered reagents and laboratory space for the hemolytic and lymphotoxicity assays. Dr. Gregory Bohach provided the initial beta toxin clone.

SUMMARY

Beta toxin is a neutral sphingomyelinase secreted by certain strains of *Staphylococcus aureus*. This virulence factor lyses erythrocytes in order to evade the host immune system as well as to scavenge nutrients. The structure of beta toxin was determined at 2.4 Å resolution using crystals that were merohedrally twinned. This structure is similar to that of the sphingomyelinases of *Listeria ivanovii* and *Bacillus cereus*. Beta toxin belongs to the DNase I folding superfamily; in addition to sphingomyelinases, the proteins most structurally related to beta toxin include human endonuclease HAP1, *Escherichia coli* endonuclease III, bovine pancreatic DNase I, and the endonuclease domain of TRAS1 from *Bombyx mori*. Our biological assays demonstrated for the first time that beta toxin kills proliferating human lymphocytes. Structure-directed active site mutations show that biological activities, including hemolysis and lymphotoxicity, are due to the sphingomyelinase activity of the enzyme.

INTRODUCTION

Staphylococcus aureus produces a large number of cell surface and secreted virulence factors that allow the organism to cause a myriad of human illnesses, ranging from relatively mild boils and subcutaneous abscesses to highly severe toxic shock syndrome and necrotizing pneumonia (49),(56). The ability of the organism to cause human illnesses is thought to depend in part on three major activities: 1) colonization of mucosal and skin surfaces with concomitant surface immune evasion, 2) production of cytolysins that target large numbers of host cells locally for additional immune evasion and also nutrient acquisition, and 3) production of superantigens that become systemic and induce body-wide immune evasion (49), (56).

The majority of *S. aureus* infections begin with mucous membrane or skin colonization of the human host. Many of the cell surface virulence factors are thought to facilitate adherence of the organism to host tissue, and in addition to interfere with host phagocytic cell function, such as protein A binding to the conserved domain of IgG antibodies (49). *S. aureus* also secretes multiple toxins and leukocidins (cytolysins), many of which affect large numbers of epithelial, immune and red blood cells, primarily acting in the immediate area of infection (49). In addition to damaging the local immune system, these factors likely also provide nutrients to the organism in its efforts to expand the colonization/infection site. Finally, the organism may secrete a variety of superantigens which have limited local tissue receptors, but which cross-link MHC II molecules with the variable part of certain β chains of T cell receptors, and in doing so interfere with host immune function throughout the body (52),(56).

Among the cytolysins are alpha, beta, gamma and delta toxins (49). Of these, alpha toxin is a heptamer pore-forming exotoxin that lyses primarily rabbit erythrocytes but is toxic to human epithelial cells (37). Gamma toxin is a two component exotoxin, comprising at least 6 different combinations of proteins, one of which is also a leukocidin (28). Delta toxin is a low molecular weight exotoxin that forms multimeric structures with the ability to lyse many cell types. This toxin is also encoded by the gene that simultaneously makes RNA III which functions as a global regulator of both

cell surface and secreted virulence factors by being part of the accessory gene regulator (61).

The exotoxin we know the least about is beta toxin. This molecule has a molecular mass of 35 kDa and appears to function as a sphingomyelinase (SMase). The toxin is also known as the hot:cold toxin because of its unique activity on sheep blood agar plates (11). At 37° C, beta toxin interacts with sheep red blood cells, but does not lyse them. If the red cells are then placed at 4° C the cells then lyse; this is observed as a lack of hemolysis on blood agar plates at 37° C, and then complete hemolysis at 4° C. A survey by Aarestrup et al. (2) found beta toxin produced in 72% of bovine mastitis isolates, in 11% of healthy human nasal isolates, and in 13% of human septicemia isolates. Due to the likelihood of contamination from one or more cytolysins and the differential and species-dependent susceptibility to beta toxin, the literature has been rather variable regarding the effects of beta toxin on leukocytes. In addition, most prior work has studied beta toxin effects on neutrophils. However, Marshall et al. (54) demonstrated through biological assays and electron microscopy that both lymphocytes and neutrophils are susceptible to beta toxin, and the toxicity is enhanced by Mg^{+2}. However, both cell types are considerably less sensitive than sheep erythrocytes, presumably due to relatively less sphingomyelin.

This study was undertaken to determine the three dimensional structure of beta toxin as a SMase, characterize its active site amino acid residues, and to provide evidence that the toxin significantly affects human immune cell function.

MATERIALS & METHODS

Protein production

Beta toxin was produced from *S. aureus* strain RN4220 and from the beta toxin gene cloned into a pET28b vector containing an N-terminal His_6 tag and expressed in *E. coli* (referred to throughout this study as wild-type recombinant beta toxin). The resulting vector was chemically transformed and grown in BL21DE3 competent cells to

mid log phase and induced with 200 mM IPTG. Cells were harvested after 18 hr of induction at 25° C. The cells were cracked using lysis buffer consisting of 50 mM sodium dihydrogen phosphate and 0.5 M sodium chloride, pH 8.0, and ultrasonic treatment (Branson sonifier 450) followed by centrifugation for 30 min, 75,000 × g. Nickel resin (Novagen® His·Bind Resin 69670) was used to purify beta toxin.

The protein was incubated with the resin, washed extensively with lysis buffer, then eluted from the column by increasing the amount of imidazole from 25 mM to 250 mM over a gradient. Fractions were collected and assayed on a SDS PAGE gel, and the pure beta toxin was dialyzed into 0.1 M imidazole, 0.5 M sodium chloride, 1 mM β-mercaptoethanol (BME) (MP Biomedicals), and 1mM EDTA, pH 8.0 for 3 hr. The protein was concentrated using Centricon® tubes (Amicon) and the concentration assayed on a spectrophotometer (Beckman DU® 640). Alternatively, non-His_6-tagged beta toxin was produced in *S. aureus* RN4220 cultured in a dialyzable beef heart medium with purification by ethanol precipitation and thin-layer isoelectric focusing (14).

Active site mutations, H289N and H150N, were made via QuikChange® (Stratagene) site-directed mutagenesis and the mutants were purified and crystallized identically to that of the wild-type recombinant beta toxin.

Crystallization, data collection and data processing

Crystals were grown in sitting drops by vapor diffusion using 96 well plates (Emerald BioSystems plate type EBS-XJR). Initial crystallization conditions were obtained from Hampton Salt Rx screen condition 2, and crystals were further improved by using 0.1 M bis-Tris propane (Sigma) pH 6.8-7.4, 3.0-3.2 M sodium acetate (Fisher), and 1mM β-mercaptoethanol (MP Biomedicals) and stored at 18° C. Diffraction quality crystals appeared in 2-3 days and were found to be perfectly merohedrally twinned. Because of the difficulty in solving and refining structures from perfectly twinned crystals an extensive search of alternate crystallization conditions and of crystals obtained failed to produce nonmerohedrally twinned crystals.

Diffraction-quality crystals were placed in 3.2 M sodium acetate, 0.1 M bis-Tris propane, pH 7.0 solution with 20% glucose then frozen, stored, and diffraction data collected at -170° C. Data sets for the wild-type recombinant beta toxin were collected on Molecular Biology Consortium's beamline 4.2.2 at the Advanced Light Source synchrotron facility at the Lawrence Berkeley National Laboratory with a NOIR1 detector (29). The solution of the structure was found by molecular replacement using the coordinates of a previously solved SMase, SmcL, from *Listeria ivanovii(66)* as the search model. SHELXL (77) was used for initial structural model refinement followed by REFMAC (60).

The beta toxin, H289N, and H150N crystals were perfect merohedral twins. Data were processed with the *HKL2000* suite (HKL research, Inc.). We were able to attain the structural solution by molecular replacement using the program PHASER. Manually modeling the twinning and subsequent refinement using REFMAC lowered the Rwork from 42% to 35%.The structural refinement was subsequently done using program SHELXL, which can handle the twinning directly, with the twin law k, h, -l. Rigid body refinement followed by restrained refinement further lowered the Rwork/Rfree to 0.267/0.330. Subsequent refinement after manual modeling with program COOT and water addition gave a final Rwork/Rfree 0.195/0.228. The H150N and H289N data sets were refined directly from the wild type coordinates using program SHELXL.

Biological Assays

The SMase activity was measured as described by Dziewonsoka et. al (31). This involved spectrophotometrically assaying the amount of cleavage that occurs via a sphingomyelin analog. Hemolysis activity was assayed on agar plates containing sheep red blood cells kindly provided by the microbiology teaching lab of the University of Minnesota. Beta toxin was added in 1mg/mL, 0.1 mg/mL, 0.01 mg/mL, and 0.001 mg/mL concentrations and incubated at 37° C for 24 hr. The plates were then shifted to 4° C for 24 hr and the zone of lysis measured.

Human peripheral blood lymphocytes (PBLs) were obtained from heparinized venous blood samples after dilution in RPMI (BioWhitaker cat # 12-167F) and separation on Histopaque®-1077 (Sigma). The mononuclear cells were cultured with the superantigen toxic shock syndrome toxin 1 (TSST-1, from *S. aureus* strain RN4220 (pCE107)) in the absence and presence of simultaneously added variable concentrations of beta toxin, H289N, or H150N and analyzed in quadruplicate using the procedure described by Barsumian et al (7). Lymphocyte density was measured with a hemacytometer (Fisher Scientific) and diluted to 1×10^5 cells/experimental well. The plates were then incubated under a 5% CO_2 atmosphere in a humidified incubator 37°C for 3 days. The cells were labeled with 1 μCi of $_3$H methyl thymidine (PerkinElmer® NET-027Z) and incubated for 24 hr at 37° C. A multiwell semi-automated cell harvester (MASH) machine (Cambridge Technology, model 200A) was used to harvest the cells. Three milliliters of scintillation fluid (EcoLiteTM from MP, formerly ICN) was added and the CPM (counts per minute) read on a scintillation counter. Beta toxin isolated from *S. aureus* strain RN4220 was used for comparison to the recombinant protein. Cell counting was done in triplicate via a hemocytometer, and the average reported.

RESULTS AND DISCUSSION

Structural Overview

The 2.4 Å structural model (Figure 3.1) was determined and has statistics shown in Table 3.1. The Rwork and Rfree are somewhat higher than is typical due to the crystal twinning. The final model contains density for residues 6-297. The extreme amino terminal containing the His_6 tag is disordered and not observed in the electron density. Beta toxin folds into a 4-layer sandwich with two β sheets at the center. Sheet A consists of strands β11, β14, β1, β2, β5 and β3 with topology +1, +1, +1x, +2x, -1. Sheet B consists of strands β4, β6, β7, β8, β9, and β10 with topology +1x, +1, +1, +1x, +1, +1. In the outer layer on top of Sheet A are helices α1 and α2, a 25 Å β duplex formed by strands β12 and β13 and a W loop connecting helix α4 and strand β10. In the

outer layer on top of Sheet B are helices α3 and α4 and a W loop connecting strands β6 and β7.

In the known genomic sequences of *S. aureus* the amino acid sequences of the beta toxin gene (*hlb*) are essentially identical. The exceptions are strains in which phages φ42 and φ13 recombine with the 5'end of the beta toxin producing *hlb*$^{-}$ phenotypes (18), (20). In strains 8325, USA300, MSSA476, MRSA252, and MW2, this results in the deletion of the first 24 residues of the amino terminus of the mature beta toxin sequence. The effects of this change include deletion of an export signal as well as strand β1 which is an internal strand of Sheet A thereby explaining the negative phenotype. It should be noted that strain 8325-4 produces functional beta toxin because it has been cured of phages φ11, φ12 and φ13 (18-20). In strains N315 and Mu50 the insertion results in replacing residues 1- 24 with sequence RDSKPNKYCCYKVS. This sequence is long enough to replace strand β1. However, this would replace the buried hydrophobic residues L10 and V13 with arginine and lysine, respectively. Not only is there insufficient space for these larger residues but these changes result in the burying of unpaired charges which is extremely destabilizing (26) again producing the negative phenotype.

Two orthologs of *S. aureus* beta toxin are found in *Staphylococcus schleiferi* and in *Staphylococcus epidermidis* that are 72% and 52% identical, respectively. These sequences are presented in Figure 3.2. An examination of the positions of the sequence differences in light of the structure reveal that the significant changes are either on the surface or away from the active site. This suggests that these proteins should be active if they are expressed. In addition there are 4 open reading frames in *Leptospira interrogans* which show significant (37-47%) sequence homology to beta toxin (69) that have β-hemolytic and SMase activity (101).

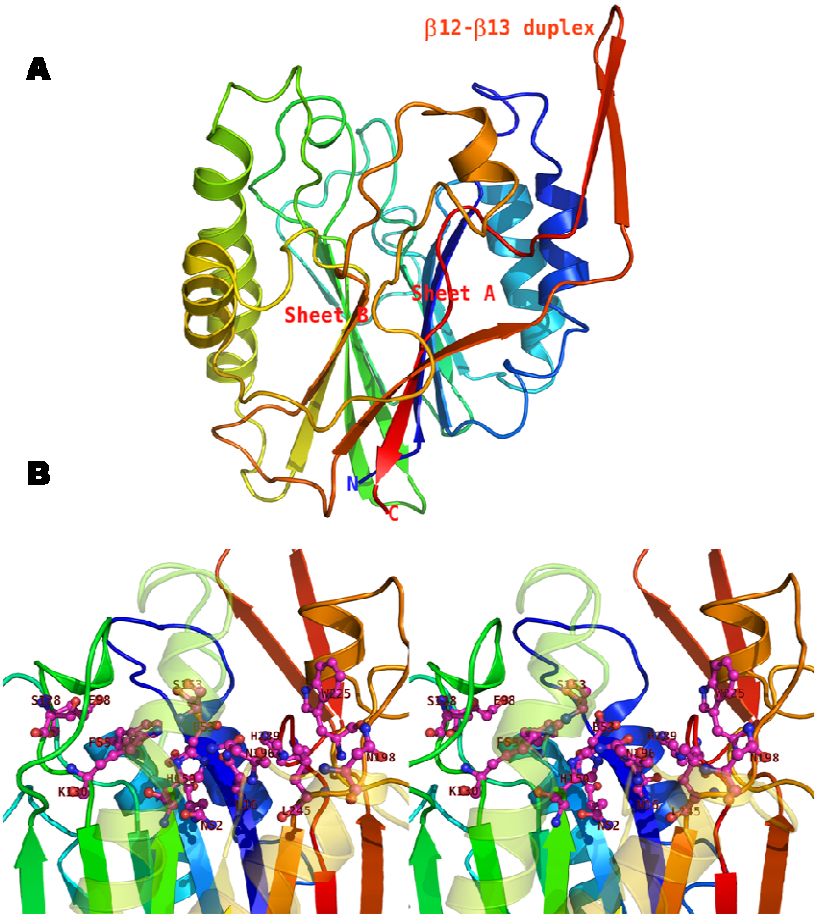

Figure 3.1 (A) Beta toxin secondary structure. Residue colors range from blue (N terminal) to red (C terminal). N and C termini, sheets A and B, and secondary structural elements are labeled. (B) Stereo drawing of active site. The view is roughly from the left of the view in panel A.

	Wild-type	H289N	H150N
Data Collection			
Space Group	F23	F23	F23
Unit cell dimension	a = 174.1 Å	a = 174.4Å	a = 174.3Å
Data resolution (Å)	2.4	2.3	3.2
Completeness (%)	93 (94)	94 (93)	100 (100)
Redundancy	4.4 (2.3)	4.7 (3.0)	3.6 (3.5)
$<I/\sigma_I>$	21.3 (2.3)	17.5 (2.1)	12.1 (2.4)
R_{sym}	0.084 (0.537)	0.082 (0.554)	0.081 (0.49)
Molecules/asymmetric unit	1	1	1
Refinement			
R_{work} (R_{free})	0.195(0.228)	0.226(0.318)	0.228(0.285)
# of non-H protein atoms	2330	2328	2328
# solvent molecules	40	40	40
Ramachandran regions			
% in core	71.5	68.4	58.6
% in allowed	26.9	28.9	36.5
% in generously allowed	1.6	2.8	4.4
% in disallowed	0	0	0
RMSD from ideal geometry			
Bond distance (Å)	0.006	0.006	0.007
Bond angles (°)	1.84	1.55	1.26

Table 3.1 Data collection and refinement statistics for native, H150N, and H289N beta toxin.

The primary sequence of beta toxin is 55.7% identical to SmcL, a neutral SMase from *Listeria ivanovii (66)* and 59.2% identical to the SMase from *Bacillus cereus (3)*. Its structure is also homologous to those of these proteins (PDB entries 1ZWX and 2DDR, respectively) with RMSD's of 1.21 Å and 1.07 Å, respectively, for all common Cα's and 1.37 Å and 1.39 Å, respectively, over all common atoms.

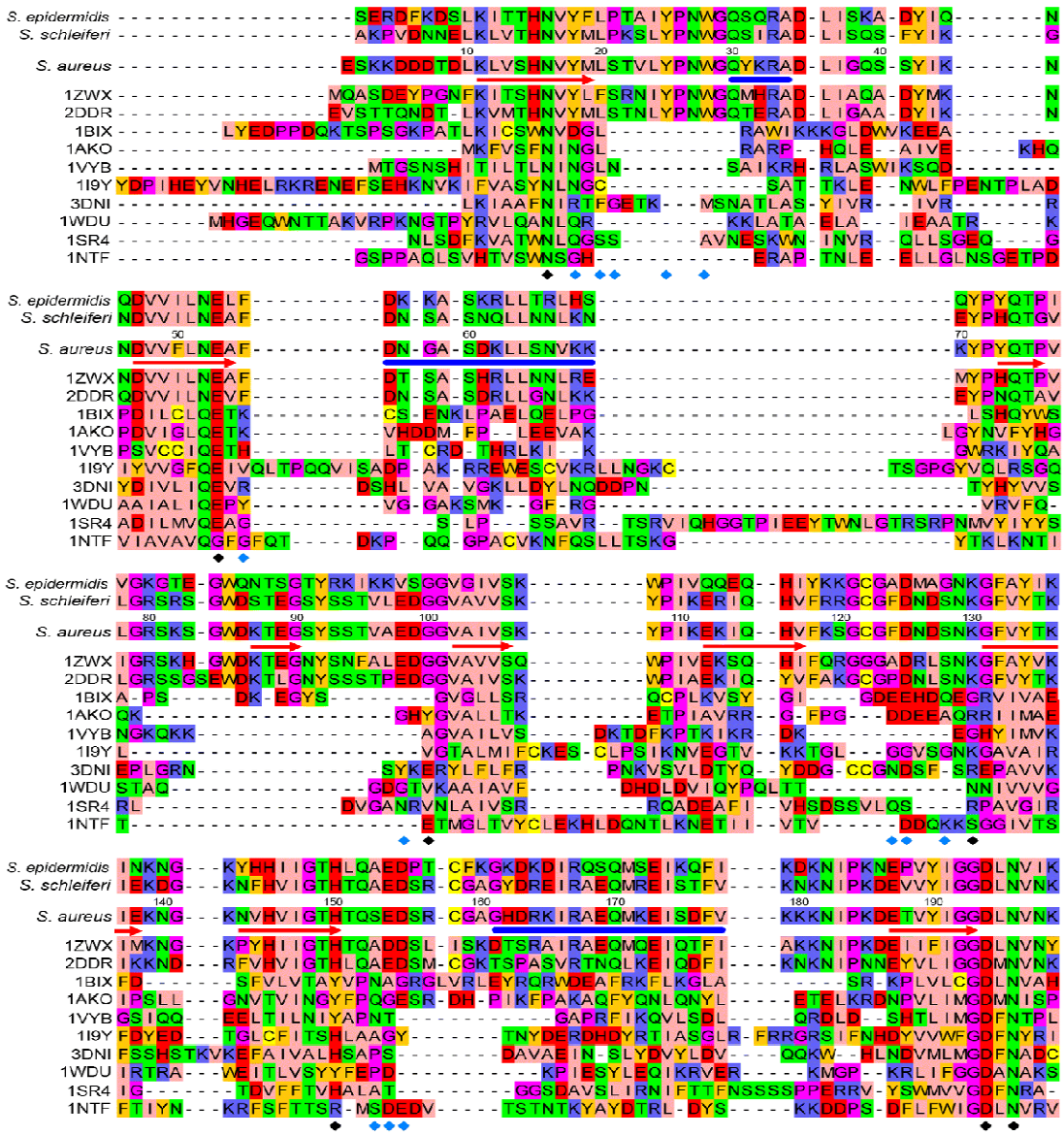

Figure 3.2. See next page for second half of figure and legend.

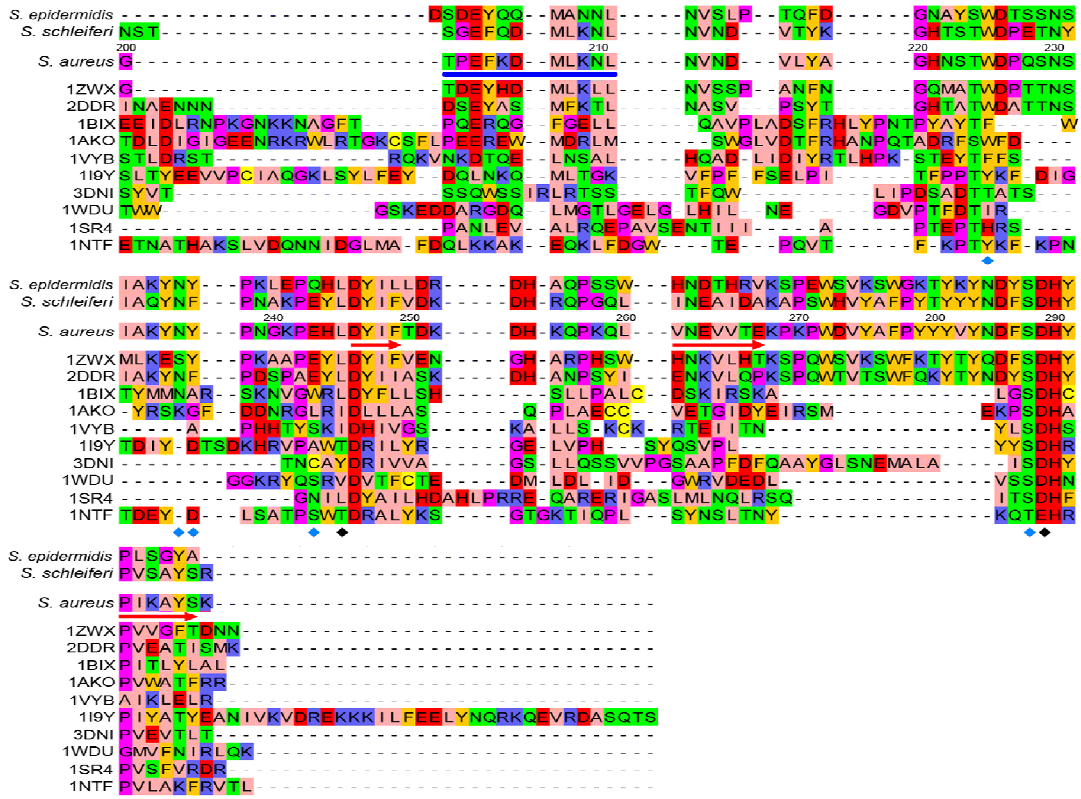

Figure 3.2. Alignment of beta toxin homologs. The first three sequences are the sequences of three species of *Staphylococcus*; the last 10 sequences are the sequences of structural homologs found by a DALI (42) search of the Protein Data Bank in order of decreasing similarity. 1ZWX is a neutral SMase from *L. ivanovii*, 2DDR is the SMase from *B. cereus*, 1BIX is human endonuclease HAP1, 1AKO is *E. coli* endonuclease III, 1VYB is the endonuclease domain of human Line-1 retrotransposon, 1I9Y is inositol polyphosphate 5-phosphatase from *S. pombe*, 3DNI is bovine pancreatic DNase I, 1WDU is the endonuclease domain of TRAS1 from *B. mori*, 1SR4 is *H. ducreyi* cytolethal distending toxin, and 1NTF is salivary nitrophorin from *C. lectularius.* The colors used to indicate amino acids are as follows: blue, R and H; red, D, E, and H; yellow, C; orange, Y, W, and F; green, T, N, Q, and S; violet, G and P; and pink, I, V, L, A, and M. β Strands and α helices of *S. aureus* beta toxin are indicated by red arrows and blue bars, respectively. The numbers are the positions in *S. aureus* beta toxin. Residues at the bottom of the active site are indicated by solid black diamonds, and residues along the sides of the active site are indicated by solid blue diamonds.

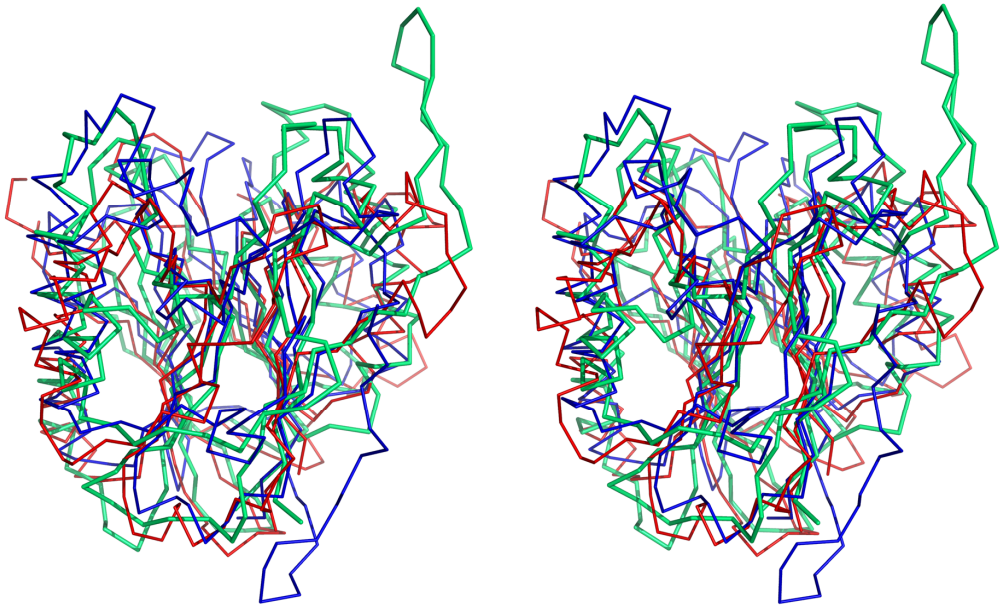

Figure 3.3 . Stereo drawing of superposition of Cα's of beta toxin (green), Bovine DNAse I (red) and human HAP1 endonuclease (blue).

Beta toxin belongs to the DNAse I folding superfamily (CATH (68) class 3.60). The proteins that are most structurally homologous to beta toxin, aside from the SMases, as revealed by a DALI (43) and SSM (47) search, are human endonuclease HAP1 (PDB entry=1BIX; RMSD = 3.3 Å over 221 Cαs), *E. coli* endonuclease III (PDB entry = 1AKO; RMSD = 3.5 Å over 221 Cαs) endonuclease domain of human Line-1 retrotransposon (PDB entry =1VYB; RMSD = 3.0 Å over 207 Cαs), inositol polyphosphate 5-phosphatase from *Schizosaccharomyces pombe* (PDB entry= 1I9Y; RMSD = 3.2 Å over 214 Cαs), bovine pancreatic DNAse I (PDB entry = 3DNI; RMSD = 3.3 Å over 220 Cαs), endonuclease domain of TRAS1 from *Bombyx mori* (PDB entry = 1WDU; RMSD = 2.9 Å over 193 Cαs), *Haemophilus ducreyi* cytolethal distending toxin (PDB entry = 1SR4; RMSD = 3.0 Å over 208 Cαs) and salivary nitrophorin from *Cimex lectularius* (PDB entry = 1NTF; RMSD = 3.3 Å over 210 Cαs). Figure 3.3 shows a superposition of the Cα traces of human HAP1 endonuclease and bovine DNAse I onto beta toxin. Despite the structural homology the amino acid identity between beta toxin and these proteins is only 10-19%.

Active Site

As found in all the DNAse superfamily members, the active site of beta toxin is at the bottom of the central sheets in a deep cleft (Figure 3.1). Comparing the active sites of beta toxin with the 2 other SMase structures show a strong conservation of the 27 residues whose side chains line the site (RMSD over all common atoms of these residues is 1.06 Å). The 9 residues lining the bottom of the active site are 100% conserved (Figure 3.2). For the other active site residues the changes are conservative except for F124 (alanine in *Listeria* and proline in *Bacillus* enzymes) and N236 (serine in *Listeria* enzyme) at the opening of the active site and S153. S153 is immediately above N196; it is an alanine in both reported SMase structures and in the putative beta toxins from *S. epidermidis* and *S. schleiferi*.

Ago *et al.*. (3) report 3 metal ions in crystals of Co^{2+}, Ca^{2+} and Mg^{2+}complexes of *B. cereus* SMase. All the reported metal ligands are conserved in beta toxin. In the *B. cereus* SMase edge metal-binding site a metal in bound between E98 and D99 (beta toxin numbering). In the purification of beta toxin, metal ions were removed through dialysis so as to not interfere with the metal affinity chromatography. In the absence of metal in beta toxin the E98 side chain is pointing away from D99. In the central metal binding site Ago *et al.*. (3) report the Co^{2+} and Mg^{2+} ions sit between E53 and H289 (beta toxin numbering). In beta toxin no metal is seen and the E53 side chain is rotated 66° making an interaction with a metal untenable without side chain rotation. This side chain may rotate if a metal were present, however.

As all proteins in the DNAse I superfamily cleave phosphodiesterase bonds it is not surprising that the 9 absolutely conserved residues presented in Figure 3.2 either line the bottom of the active site (H16, D194, N196, and H289) or are critical in positioning residues there. Specifically, D246 makes hydrogen bonds with the side chains of T224 and H289. G193's unusual main chain conformation (φ = 135°, ψ = -74°) allows the D194 nitrogen and oxygen to form hydrogen bonds with the T159 oxygen and the T151 nitrogen, respectively, positioning the D194 side chain in the active site.

H150 and H289 (beta toxin numbering) have been identified as residues crucial for activity in the *B. cereus* SMase, as well as in DNase 1. To verify the importance of H150 and H289 in beta toxin, they were separately mutated to asparagine for analysis. Both mutants crystallized isomorphously with the His-tagged recombinant beta toxin (see data collection and refinement statistics in Table 3.1). The RMSD's over Cα's between the 2 mutant structures and wild type are 0.44 Å and 0.60 Å and the F_{obs} mutant – F_{obs} wild type maps have no significant features other than the mutations. These data indicate that the structures of these mutants and the native beta toxin are identical within experimental error.

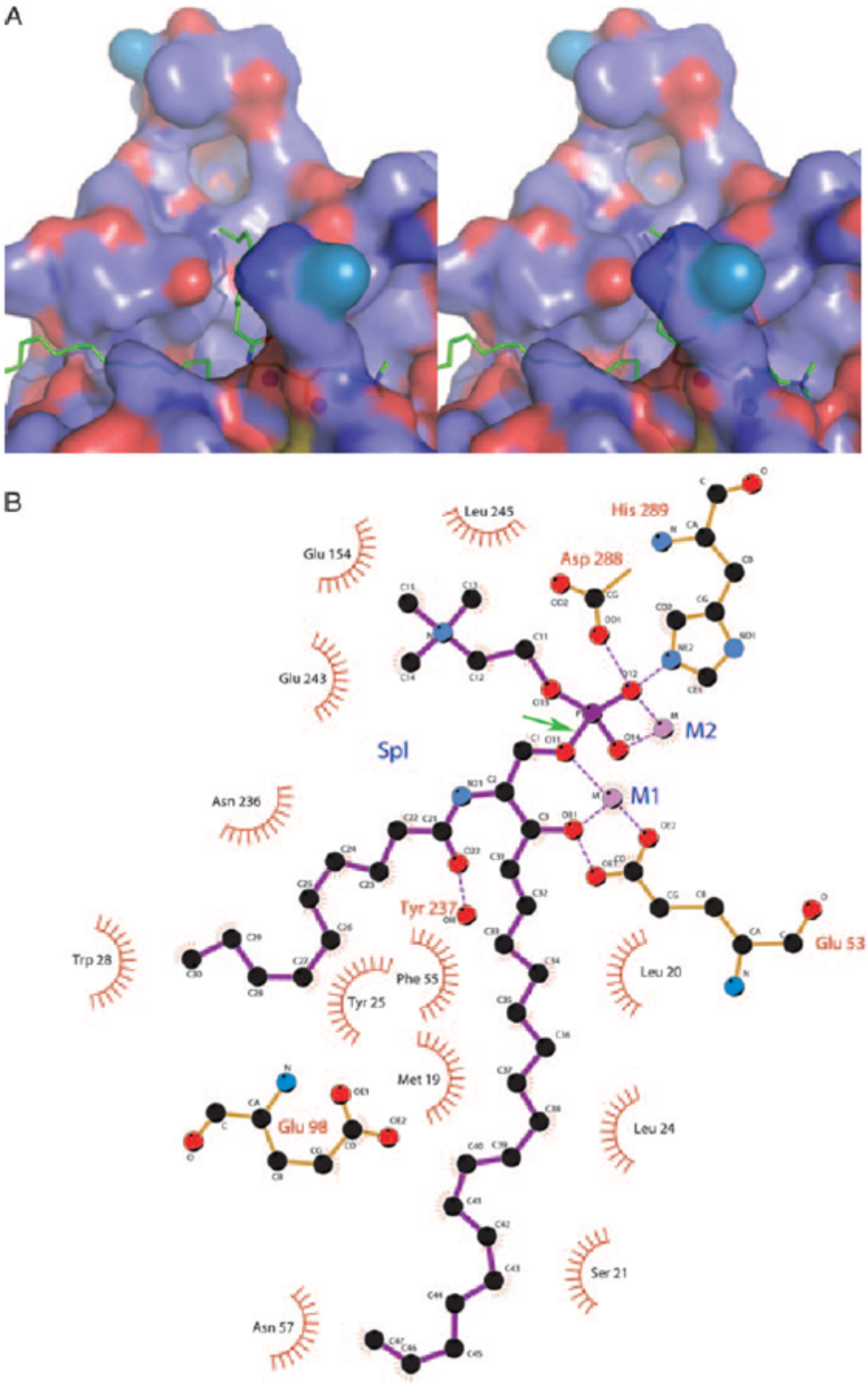
A
B
Leu 245
His 289
Glu 154
Asp 288
Glu 243
M2
Spl
M1
Asn 236
Tyr 237
Trp 28
Phe 55
Tyr 25
Met 19
Glu 98
Leu 20
Glu 53
Leu 24
Ser 21
Asn 57

Figure 3.4. (A) Stereo drawing of a model of beta toxin-sphingomyelin complex. SMase is shown in space filling with oxygen atoms red, carbon atoms light blue, nitrogen atoms navy, and sulfur atoms cyan. The two metals found by Ago *et al.*. (3) are indicated by small magenta spheres. (B) LIGPLOT (94) drawing of a model of the complex of beta toxin with sphingomyelin (Spl) metal sites reported by Ago *et al.*. (3). Dashes indicate hydrogen bond interactions. Red semicircles indicate hydrophobic interactions. The bond cleaved is indicated by a green arrow. All residues labeled are conserved between beta toxin and the SMase from *B. cereus.*

Models of SMases have been made using the structures of nucleases (55, 79). Matsuo et al. (55) predicted that E53 (beta toxin numbering) would interact with the C1 hydroxyl of glycerol and the carbonyl oxygen of the ceramide. Obama et al. (63) predicted that E53 interacts with the phosphate through a bound Mg^{+2}. Ago *et al.*. (3) modeled a complex and proposed a similar role for Glu 53. Using the structure of beta toxin as a starting point, the complex with sphingomyelin was modeled and energy minimized (Figure 3.4). The sphingosine chain lies in a cleft formed by the β1-α1, β2-α2, and β4-β5 loops. Its hydroxyl and a phosphate oxygen are proposed to be coordinated by a metal ion (M1 in Figure 3.4) (3). The N-acyl chain of the substrate lies in a cleft between the β1-α1 and α4-β10 loops and against the β12-β13 duplex. The carbonyl of the amide is recognized by Y237 (beta toxin numbering) (Figure 3.4) which in conserved in *Listeria* SMase and *S. epidermidis* beta toxin. In the *B. cereus* SMase and the *S. scheiferi* beta toxin this residue is a phenylalanine (Figure 3.2). In other structural homologs this residue is not conserved. The cationic choline projects between the β8-α3 and α4-β10 loops and is recognized by the side chains of E154 and E243 (beta toxin numbering) (Figure 3.4). These residues are conserved in the beta toxins and SMases (exceptions = D154 in *Listeria* SMase and Q243 in *S. epidermidis* beta toxin) but not in other structural homologs (beta toxin numbering) (Figure 3.2).

Sphingomyelinase Activity

The ability of native recombinant beta toxin and the H150N and H289N mutants to cleave sphingomyelin were assayed. As shown in Figure 3.5A mutation of either His 150 or His 289 abolished SMase activity. In addition, the ability to perform hot:cold lysis of sheep erythrocytes was also assayed using native recombinant beta toxin and the H289N and H150N mutants. The activity of these mutants was reduced 60- and 200-fold, respectively (Figure 3.5B and 3.6).

A unique structural feature of the SMases relative to other members of the DNAse I superfamily is the long beta hairpin (strands β12 and β13). As mentioned above, this hairpin interacts with the N-acyl chain of sphingomyelin. The residues facing sphingomyelin are W272, V274, A276, P277, Y280 and Y283 (beta toxin numbering). All of these residues are absolutely conserved except for 276 and 277 which are serine and tryptophan in *S. epidermidis* and 280 which is threonine in *S. epidermidis* and *S. schleiferi*. None of the other residues in the exposed end of the beta hairpin is conserved in all 3 species. Openshaw et al. (66) proposed the hairpin to play a significant role in interacting with the membrane in preparation for cleaving sphingomyelin. This appears to be unlikely in *S. epidermidis* since residues 275, 279 and 282 (beta toxin numbering) are lysines. Ago *et al.*. (3) reported the binding of the buffer 2-morpholinoethanesulfonic acid adjacent to the beta hairpin region in the crystal form of *B. cereus* SMase containing bound Mg^{+2}. The relevance of this structural change is uncertain as 2-morpholinoethanesulfonic acid is over 13 Å from the active site metals and bears little resemblance to substrate. Ago *et al.*. also mutated W279 and W290 (*B. cereus* numbering) to alanine and reported reduced binding to sphingomyelin liposomes and loss of ability to disrupt these liposomes or to lyse sheep erythrocytes. Verification of a regulatory role for the beta hairpin of beta toxin from *S. aureus* awaits further study.

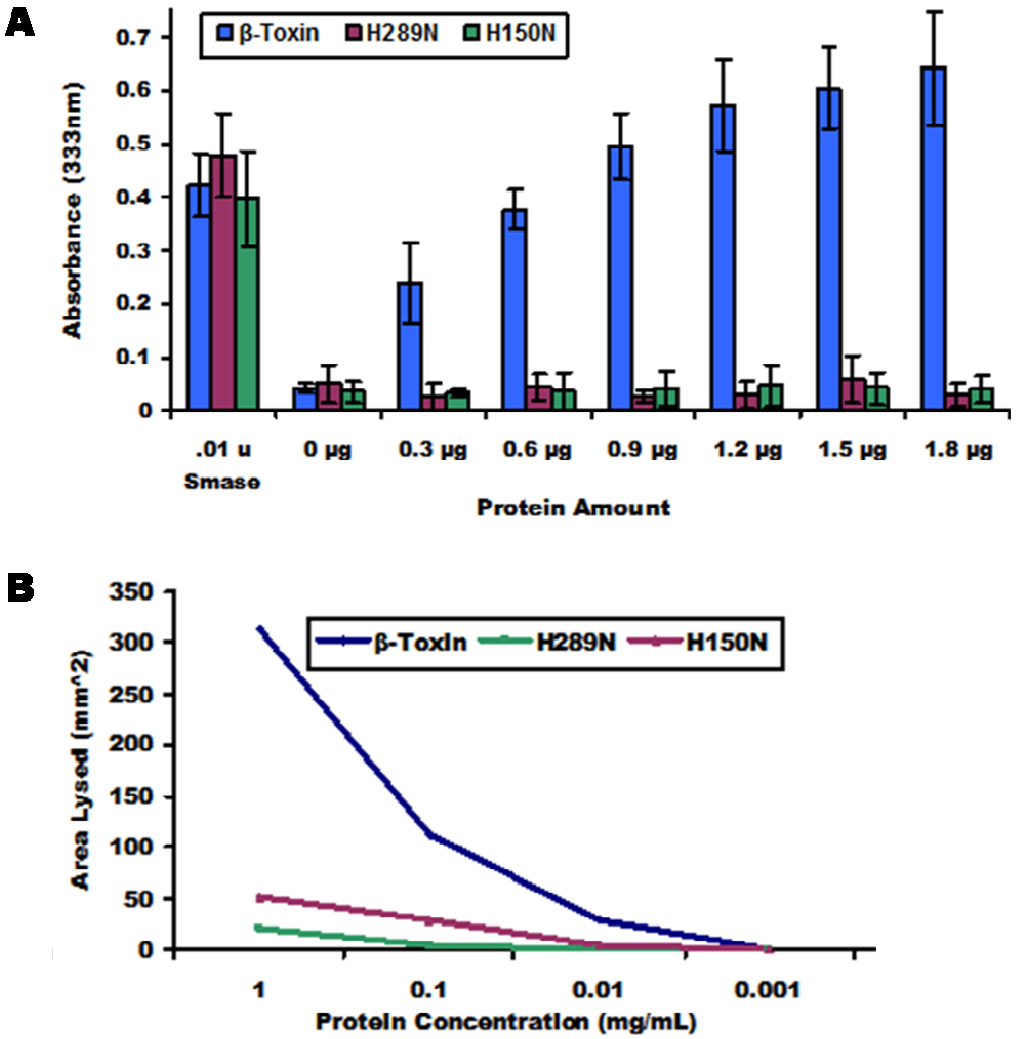

Figure 3.5. SMase and hemolytic activities of beta toxin and the H289N and H150N mutants. (A) SMase activity as described by Dziewanowska et al. (31). The positive control (Smase) was a neutral SMase purchased from Fisher Scientific and isolated from *S. aureus*. (B) Hemolytic assay performed with sheep erythrocytes (see Figure 3.6).

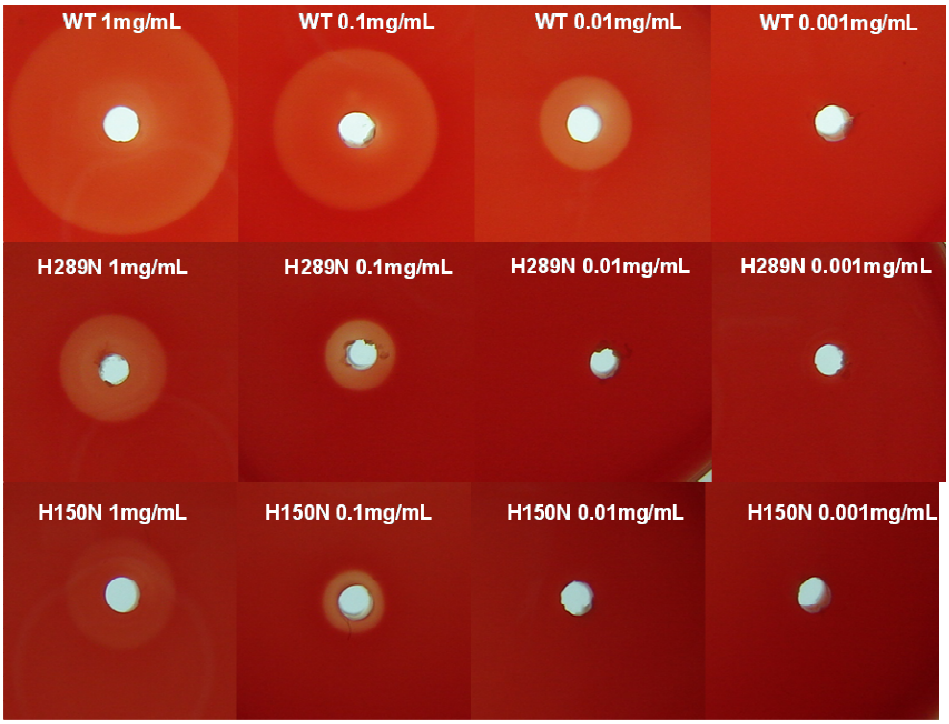

Figure 3.6 Photographs of beta toxin, H289N, and H150N induced hemolysis. After the addition of various concentrations of beta toxin, H289N, and H150N, the plates were incubated at 37° C for 24 hr. The plates were then shifted to 4° C for 24 hr, after which time the zone of lysis was measured (Figure 3.5B) and photographed. WT indicates recombinant His_6 tagged beta toxin.

Lymphocyte Proliferation

The response of lymphocytes to superantigens such as TSST-1, and the cytotoxicity of beta toxin for resting lymphocytes has been documented (52, 54). However, the effect of beta toxin on proliferating lymphocytes is unknown. When lymphocytes are incubated with TSST-1 and beta toxin, a decrease in the amount of tritium incorporation into the DNA is observed (Figure 3.7A). The experiment was repeated twice and the same results seen.

To ensure that it was beta toxin protein that was inhibiting incorporation of $_3H$ thymidine, two active site mutations, H289N and H150N were made. As stated above, both active site mutants show no sphingomyelin cleavage *in vitro* (Figure 3.5A). When

tested for hemolysis on sheep erythrocytes, very little lysis is observed after 48 hr of incubation (Figure 3.5B, Figure 3.6) although the structures of H150N and H289N are virtually unchanged from native beta toxin. However, these two mutants failed to interfere with TSST-1 induced lymphocyte proliferation.

To differentiate between lymphocyte death induced by beta toxin and interference with the TSST-1 mitogenic signal, cells were counted and photographs were taken of representative experimental wells (Figure 3.8). In these assays, there was significant autostimulation of lymphocytes in the absence of added superantigen, or in the presence of beta toxin mutants, as shown by incorporation of $_3$H-thymidine into lymphocyte DNA (Figure 3.9). However, beta toxin significantly reduced incorporation of thymidine in proliferating cells (Figure 3.9). TSST-1 causes proliferation of lymphocytes, as can be seen in TSST-1 only well of Figure 3.8, in the form of large numbers of colonies, presumably due to proliferation of T lymphocytes containing Vβ-2 bearing T cell receptors. Lymphocytes incubated without TSST-1 lack these colonies. The proliferative (colony forming) effect is negated in the presence of beta toxin, either isolated from *S. aureus* or expressed in *E. coli* (Figure 3.9). These results also show that the N-terminal His_6-tag does not affect biological activity.

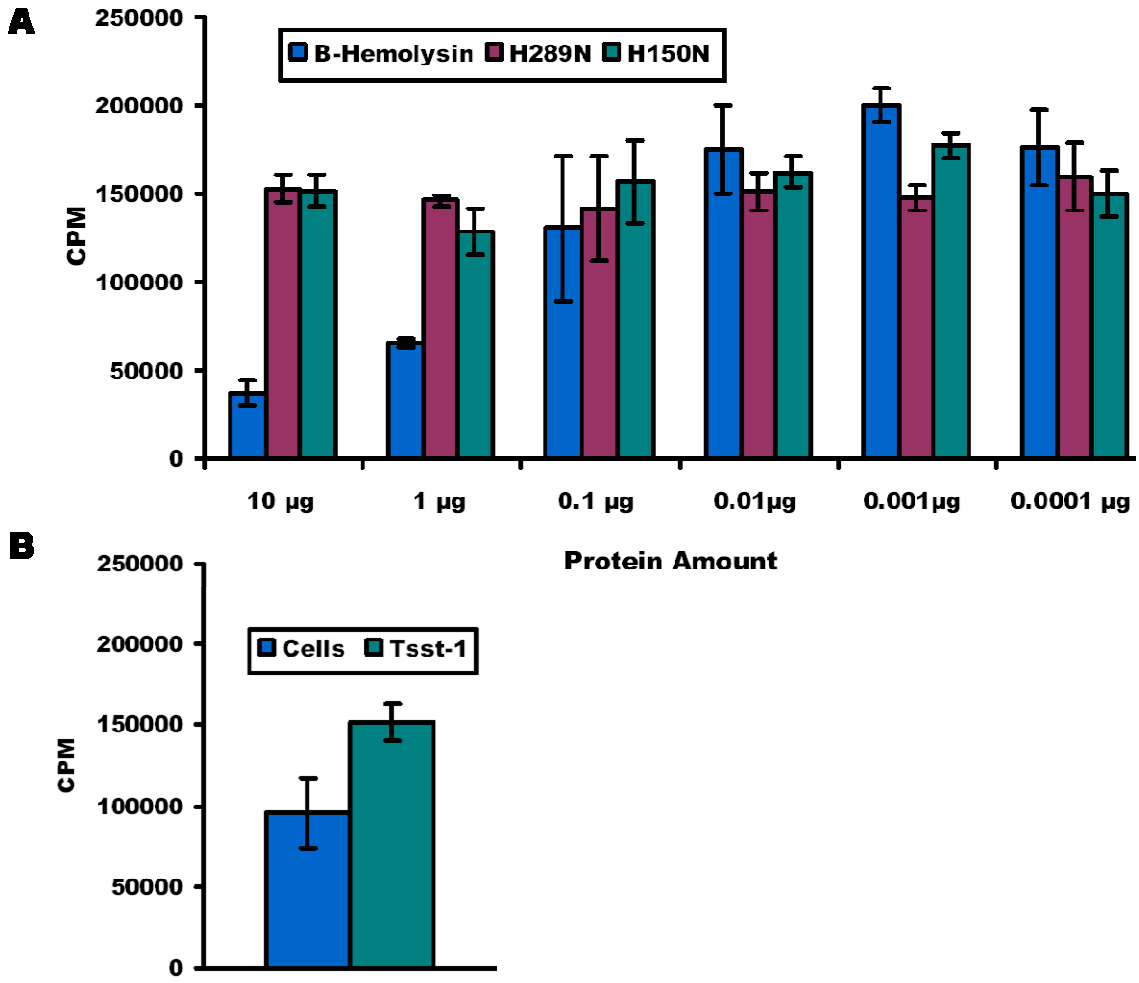

Figure 3.7. Beta toxin lysis of TSST-1-induced lymphocytes. (A) Tritium incorporation into induced lymphocytes in the presence of different concentrations of beta toxin and the H289N and H150N mutants. The experiment was performed in quadruplicate, and averages are shown. Three experiments were done on three different days. (B) Tritium incorporation into lymphocytes in the absence of beta toxin and in the absence (lymphocytes only) or presence (TSST-1) of TSST-1.

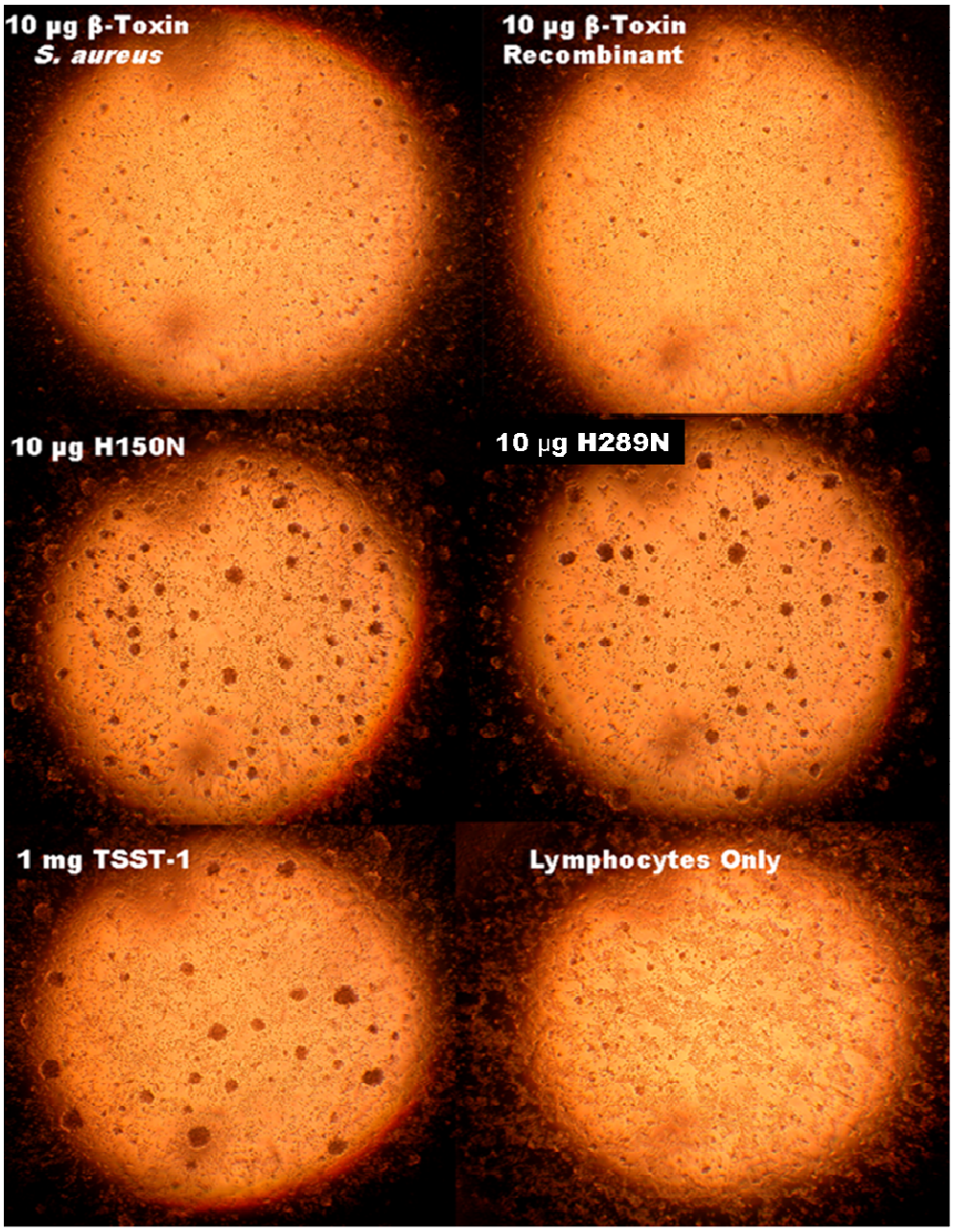

Figure 3.8 Photographs of representative experimental wells containing 10 µg of beta toxin or the H289N or H150N mutant. The brown clumps are colonies of proliferating lymphocytes. Some autostimulation of the lymphocytes was observed (lymphocytes only).

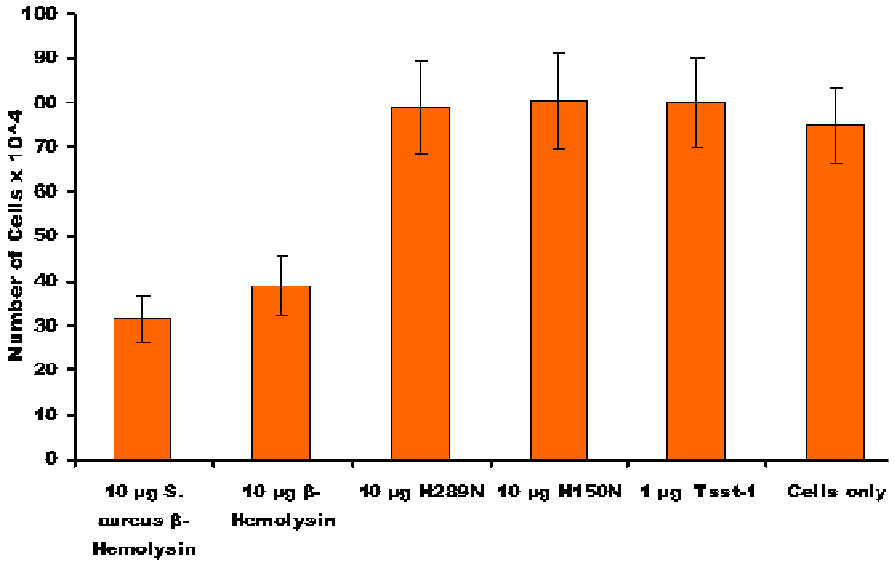

Figure 3.9 Cell counts of Figure 3.8 obtained with a hemocytometer. Counting was done in quadruplicate and the averages after 4 days of incubation are shown. The error bars indicate standard deviations. 10 µg β-Hemolysin refers to recombinant beta toxin. 10 µg S. aureus β-Hemolysin refers to beta toxin purified from *S. aureus.*

Conclusion

Iron is a limiting nutrient for all organisms and is necessary in many biological processes. *S. aureus* has a multicomponent heme scavenging system, which imports heme from host heme proteins and extracts the iron (88). A potent source for heme is hemoglobin and myoglobin, which can be found in erythrocytes. Erythrocytes may be an early host defense cell encountered during infection, specifically during the clotting process. One role long proposed for bacterial hemolysins, such as beta toxin, is their potential to endow the organisms with the ability to acquire iron in the form of heme.

Our results suggest that beta toxin may also contribute to immune modulation of the host in the presence of accessory virulence factors such as superantigens. Strains of *S. aureus* such as RN6390 (NCTC8325-4, RN4220) have been known to secrete large amounts (up to 500 µg/mL) of beta toxin. These strains are important pathogens in animals but were thought not to be important in humans. This study shows conclusively that beta toxin affects human PBLs, specifically by killing proliferating T lymphocytes.

Other human cells that are susceptible to beta toxin are monocytes (92), resting lymphocytes, and polymorphonuclear leukocytes (54). This action on human lymphocytes is most likely done in order to evade the host machinery, as well as to scavenge nutrients.

The activities of beta toxin are shown to be tied to its SMase activity. This cleavage of a phosphodiester bond uses the structural framework found in DNAse I and an extended hydrophobic binding site for the fatty acid chains and specific recognition for the choline head group. Whether activities are due to changes in the physical properties of the membrane or to production of ceramide as a progenitor of apoptosis requires further study.

CHAPTER 4

THE ROLE OF A HYDROPHOBIC BETA HAIRPIN OF BETA TOXIN IN VIRULENCE OF *STAPHYLOCOCCUS AUREUS*

This chapter examines the purpose of a solvent exposed hydrophobic beta hairpin found on beta toxin and other neutral sphingomyelinases. A substitution (F277A P278A) and two deletions (275-280 and 272-282) were created and assayed for sphingomyelinase, hemolytic, lymphotoxicity, and liposome disruption abilities. All mutants were crystallized and the structures solved by molecular replacement. The F277A P278A mutation was also crystallized with Ca^{2+} and Mg^{2+} ions.[1]

[1] Several people contributed to the experiments detailed in the chapter. Jeff Digre aided in cloning and primer design of all beta toxin mutants. Fikre Mengistu discovered the crystallization conditions for 275-280 mutant. Andrew Kruse discovered the crystallization conditions for the F277A P278A and 272-282 mutants, and attempted to co-crystallize F277A P278A with sphingomyelin, as well as aided with sphingomyelinase activity assays. Dr. Ke Shi and Andrew Kruse aided with the structure determination for all mutants and metal soaks. Dr. Patrick M. Schlievert allowed the use of laboratory space and reagents for the hemolytic and lymphotoxicity studies. Dr. David D. Thomas allowed the use of the circular dichroism spectrometer, and David Kast helped with CD analysis.

SUMMARY

In the previous chapter, I reported the structure of beta toxin from *Staphylococcus aureus* and linked its lymphotoxity to its enzymatic sphingomyelinase activity. This chapter examines the role of a solvent exposed hydrophobic beta hairpin unique to beta toxin and some bacterial neutral sphingomyelinases. Mutational analysis showed that altering the length but not the content attenuated the biological activities associated with beta toxin. In addition, the hydrophobic beta hairpin is a stabilizing structure for the protein as shown by altered melting temperatures. X-ray crystallographic analysis of the mutants revealed very minimal structural changes. We also show for the first time diacylglycerol bound in the crystal structure of the 275-280 deletion mutant to the hydrophobic beta hairpin region. Furthermore, we report either Ca^{2+} ions or Mg^{2+} and phosphate bound to the active site of the F277A P278A mutant.

INTRODUCTION

Beta toxin is a virulence factor from *Staphylococcus aureus* and is a member of the neutral sphingomyelinase (SMase) C family of enzymes. We have previously reported its structure and linked its SMase activity to its toxicity towards proliferating human lymphocytes (44). Beta toxin is also toxic to monocytes (93), T cells (21), and resting lymphocytes, (53) presumably due to its SMase activity.

Neutral SMases are found in bacteria, yeast, and humans. Though sequence homology is low at the protein level, the known active site residues are well conserved. Neutral SMases C act on sphingomyelin (SM) at the phosphodiester bond, hydrolyzing the phosphorylcholine polar head group from the ceramide tail moiety. They act at an optimum pH of 7.4 and are dependent on Mg^{2+} ions for activity, though Co^{2+} and Mn^{2+} can be substituted (17). Eukaryotic SMases are predicted to be anchored to the plasma membrane; prokaryotic SMases are secreted virulence factors (17).

Beta toxin folds into a four layer sandwich of α helices flanking two β sheets (44). The active site sits atop the β sheets in a deep, solvent exposed cleft. The active sites of beta toxin, the neutral SMase C from *Bacillus cereus*, and Sml C from *Listeria Ivanovii* (PDB entry 1ZWX) have been well characterized (44), (3). The structure of the *L. ivanovii* enzyme reveals phosphate bound at the active site, but metal ions are not present (66). Ago *et al.*. report three structures from the *B. cereus* enzyme co-crystallized with either Co^{2+} (PDB entry 2DDS), Mg^{2+} (PDB entry 2DDT) or Ca^{2+} (PDB entry 2DDR) (3). The Co^{2+} structure reveals two water-bridged metals in the active site arranged in bi-pyramidal geometry. However, in the Mg^{2+} structure, only one metal ion is present in the active site, while a water molecule replaces the site where the second Co^{2+} ion occupies. In the Ca^{2+} structure, a sole Ca^{2+} ion is found with five water molecules bound to form a hepta-coordinate system. In all three *B. cereus* structures, another metal binding site is found away from the active site and bound to an outer loop, but the purpose of the third metal site is unknown. To date no complex of a SMase with SM has been shown structurally.

A unique structural feature of the bacterial neutral SMase family is a solvent exposed, hydrophobic beta hairpin. *Openshaw et al.*. first hypothesized that the beta hairpin is important in initial membrane recognition of Smc L to a susceptible host cell (66). Ago *et al.*. further investigated the *B. cereus* SMase by mutating the two outermost aromatic residues separately to alanine (W248A and F285A) (3). They conclude that the hydrophobic residues were necessary for relocation of the enzyme to the cell membrane.

We previously showed that the lymphotoxicity and hemolytic abilities of beta toxin are tied to its SMase activity (44). The native structure reveals a solvent exposed hydrophobic beta hairpin. Here we report that the length but not the content of the beta hairpin is functionally important. Furthermore, the beta hairpin has a stabilizing role in the structure of the beta toxin. We also report two structures with Ca^{2+} or Mg^{2+} and phosphate bound. The purpose of this study was to elucidate the role of the beta hairpin of beta toxin to host cell toxicity.

MATERIALS & METHODS

Mutation Design

Native beta toxin was used for the template in all mutation design. F277A P278A was made using QuikChange (Stratagene) site directed mutagenesis. The 275-280 truncation and 272-282 deletion were made using cassette mutagenesis. A silent BrsgI restriction digest site was introduced into the wild type vector, and then BrsgI and Nco1 restriction enzymes were used to cut the plasmid. Oligos were purchased from Integrated DNA Technologies, and restriction enzymes and ligase was purchased from New England Biolabs. The 275-280 oligos were 5'- CAT GGG ATG TAG ACG GAT ACG T-3' and 5'- GTA CAC GTA TCC GTC TAC ATC C-3' and were annealed by boiling for 3 min in 0.01 M Tris-HCl pH 7.5 and 1 mM EDTA then cooled in a hood. Double cut vector DNA (0.1 μg) and annealed oligos (0.5 μg) were ligated with T4 DNA ligase, transformed in to XL1 blue competent cells, and the mutation verified by sequencing. To create the Δ272-282 mutation, the wild type vector was digested with

NcoI and EcoRI restriction enzymes. The oligos were 5'- CAG GGA ATG ATT TTT CAG ATC ATT ACC CAA TCA AAG CCT ATA CTA AAT AGG -3' and 5'- AAT TCC TAT TTA CTA TAG GCT TTC ATT GGG TAA TGA TCT GAA AAA TCA TTC -3', and were annealed, ligated and the mutation verified as described above.

Protein Expression and Purification

All beta toxin mutants were purified as previously published (44). Briefly, the cloned gene in a pET28b vector containing an N-terminal His_6 tag was chemically transformed into BL21(DE3) competent cells, grown to mid-log phase, induced with isopropyl-β-D-thiogalactopyranoside (IPTG), then harvested. Cells were lysed by alternating freeze/thaw cycles and ultrasonic treatment. Crude lysate was incubated with an affinity column, and the proteins eluted by increasing the amount of imidazole in the washes. The washes were checked via SDS-PAGE, and pure fractions combined and dialyzed into 0.1 M imidazole pH 8.0, 0.5 M NaCl, 1 mM β-mercaptoethanol (BME) (MP Biomedicals), and 1 mM EDTA.

Crystallization, Data Collection and Data Processing

Prior to crystallization, all beta toxin mutants were concentrated to 12 mg/mL using Centricon® tubes (Amicon), and the final concentration of BME brought to 2 mM. All chemicals were purchased from Hampton Research unless otherwise noted. Sitting drop vapor diffusion was used to crystallize all mutants with a "2+2" drop of protein to mother liquor in a 96 well plate (Emerald Biosystems). Initial crystals of F277A P278A were found in a grid scan, and the crystallization conditions refined to 0.1 M MES (Sigma) pH 6.0-7.0 and 28-30% PEG 4K. The truncation mutant, 275-280, crystallized initially in the Hampton Research PEG/Ion Screen condition 1. This initial condition was optimized to 0.15-0.25 M NaF and 28-34% PEG 3350. 272-282 crystallized initially in the Hampton Research Index screen condition 77, and the conditions optimized to 0.1 M Tris-HCl pH 7.0-8.5 and 26-32% PEG 3350, and 0.2 M Li_2SO_4 (J. T. Baker Inc.), with the addition of 0.4 μL of 0.1M betaine hydrochloride to the final drop.

F277A P278A was co-crystallized with stearoyl SM (Avanti Polar Lipids) in 0.1 M MES pH 6.5 and PEG 4K and 5 mM $MgCl_2$ (Fisher Scientific). The SM was dissolved in 100 % ethanol (AAPER) to 20 mg/mL and then diluted with a small volume of 0.1 M n-octyl-β-D-glucopyranoside (Sigma) dissolved in the protein buffer. At this point the SM precipitated, but redissolved with stirring. This solution was further diluted with protein buffer and then mixed with protein such that the final concentration of ethanol was less than 5% (v/v) and the concentration of detergent was approximately 20 mM.

Prior to data collection, all crystals were cryoprotected with the mother liquor and the addition of 20% PEG 400 for F277A P278A, and 20% glycerol for Δ275-280 and Δ272-282. F277A P278A crystals were then soaked in a solution containing mother liquor and 10% 100 mM $CaCl_2$ for 5 minutes, followed by flash freezing in liquid nitrogen. Diffraction quality crystals appeared after 3 days of growth at 18 °C in all cases. Data were collected at beam line 14 BM-C at the Advanced Photon Source, Argonne National Laboratory on an ADSC Quantum-315 detector. Data were processed with the *HKL2000* suite (HKL research, Inc.). We were able to attain the structural solution by molecular replacement using the program PHASER and the coordinates of wild type beta toxin (44). Subsequent refinement after manual modeling were accomplished using the program COOT. REFMAC was used for structural refinement (60).

Biological Assays

The SMase, hemolytic, and lymphotoxicity assays were preformed as previously published (44). SMase activity was assayed spectrophotometrically using a SM analog (31). Hot:cold hemolysis was analyzed by measuring the zone of lysis on sheep red blood cell agar plates kindly provided by the microbiology teaching lab at the University of Minnesota. Lymphotoxicity of the beta toxin mutants was analyzed as previously published (7). Briefly, different amounts of beta toxin mutants were incubated with human peripheral blood lymphocytes and toxic shock syndrome toxin-1

then labeled with tritium. The cells were harvested, washed, and the counts per minute read to assay the amount of labeled DNA left.

The liposome disruption assay is based on the protocol by Ago *et al.*. (3). Lipid and cholesterol were purchased from Avanti Polar Lipid. Each protein concentration was tested on three independent experiments. Stearoyl SM (18:0) (1.4 μmol) and ovine wool cholesterol (1.2 μmol) were dissolved individually in chloroform, mixed together, and then dried over night under a gentle stream of air. The lipid cake was hydrated with 100 μL TBS (20 mM Tris-HCl pH 7.5 and 0.9% w/v NaCl) and 200 μL of 1 mM 5'carboxy fluorescein in 0.9% NaCl in a 58 °C water bath for 1 hr. The suspension was sonicated (Branson Sonifier 450) 3 times for 10 min in a water bath heated above 60 °C with brief vortexing in between. The liposomes were further diluted with 400 μL TBS, and then centrifuged at maximum speed in a tabletop centrifuge for 10 min. This step was repeated 4 times, removing the supernatant and gently resuspending the liposomes in 550 μL TBS to remove all non-encapsulated fluorescein. The liposomes were resuspended in 3.6 mL TBS, and 400 μL of mixture was used per reaction with the addition of 5 mM $MgCl_2$. Triton X100 (50 %) was used as a positive control. Beta toxin mutants were incubated with the liposomes in a 37 °C water bath for 30 min, and then centrifuged for 10 min. The supernatant was assayed on a fluorimeter (Varian Cary Eclipse Fluorescence Spectrophotometer), using λ=490 nm and λ=516 nm as the excitation and emission wavelengths, respectively. The supernatant of the 10 μg samples was monitored for the presence of the His_6 tag using an ELISA system (Novagen). The ELISA experiment was performed in 96 well plates (NUNC) and performed according the manufactures instructions. Samples were read on a plate reader (Spectra MAX plus, Molecular Devices) and the absorbance at λ=450 nm reported.

Melting temperature analysis of the beta toxin mutants was performed using circular dichroism spectroscopy (Jas.co J-815 CD Spectrometer model J-815-1505). Protein was dialyzed into 10 mM NaF, 1 mM NaH_2PO_4, and 10 mM Na_2HPO_4 and then diluted to 0.4 mg/mL. The spectrum was analyzed every 30 seconds with three data accumulations between λ=240 and λ=190 nm. The data were measured at 2 degree increments from 30 °C to 70 °C. We reported the data as percent of denatured protein

present, or by subtracting the value at 30 °C from the current value and dividing by the value at 70 °C. The values reported were at λ=215 nm as the largest changes in the secondary structure of beta toxin and mutants were seen there.

RESULTS & DISCUSSION

Beta Hairpin Analysis

The hydrophobic beta hairpin is composed of the amino acids 272DVYFAFPYYY282. Three mutants were created in order to test the beta hairpin's role in host cell toxicity. The F277A P278A substitution was made such that the outermost hydrophobic amino acid F277 was substituted for nonpolar alanine residues, and P278 changed to alanine to alter the size and flexibility of the residue. The 275-280 truncation was created to shorten the length of the hairpin while replacing one of the hydrophobic amino acids at the tip with a charged aspartic acid residue, followed by glycine to ensure that a hairpin would still form (272DVYDGYY282). The reverse orientation of the aspartic acid residue and glycine residue was also created (272DVYGDYY282) and tested with identical results for all assays detailed in this chapter to that of the DG orientation (data not shown). However, the GD orientation was not crystallized. The third mutation, 272-282, was made such that the entire hydrophobic beta hairpin was eliminated. These mutants were then tested for SMase activity, hemolytic activity, lymphotoxicity, ability to disrupt liposomes composed of SM, and melting temperature sensitivity. The F277A P278A, 275-280, and 272-282 mutants were crystallized, and their structures solved by molecular replacement.

Biological Activities

Altering the hydrophobic content of the beta hairpin did not significantly affect the SMase or hemolytic activity of beta toxin, as evident in the F277A P278A mutation (Figure 4.1A and 4.1B). When the beta hairpin is truncated, as in the 275-280 protein, the SMase and hemolytic activities are attenuated. However, complete removal of the

beta hairpin severely cripples the SMase activity, and decreases the hemolytic activity 100-fold compared to the native enzyme.

The same trend is evident in the liposome disruption assay (Figure 4.2), which is an *in vitro* mimic of the SM content of a sheep erythrocyte. Briefly, this assay is performed by incubating beta toxin with fluorescein encapsulated by the liposome. After the incubation, the reaction components are separated by centrifugation, and the fluorescence of supernatant is measured. At all concentrations tested, the F277A P278A mutation did not have significantly different liposome disrupting capabilities than that of native protein. The 275-280 truncation mutant loses an approximately 100-fold liposome disruption ability. The 272-282 deletion demonstrates very little disruption ability over that of the background (liposomes only). Two active site mutants, H150N and H289N, both of which lack SMase and hemolytic activity (44) do not disrupt the liposomes (see Chapter 3, and results not shown). The active site mutants and 272-282 deletion similarly lack the ability to disrupt liposomes.

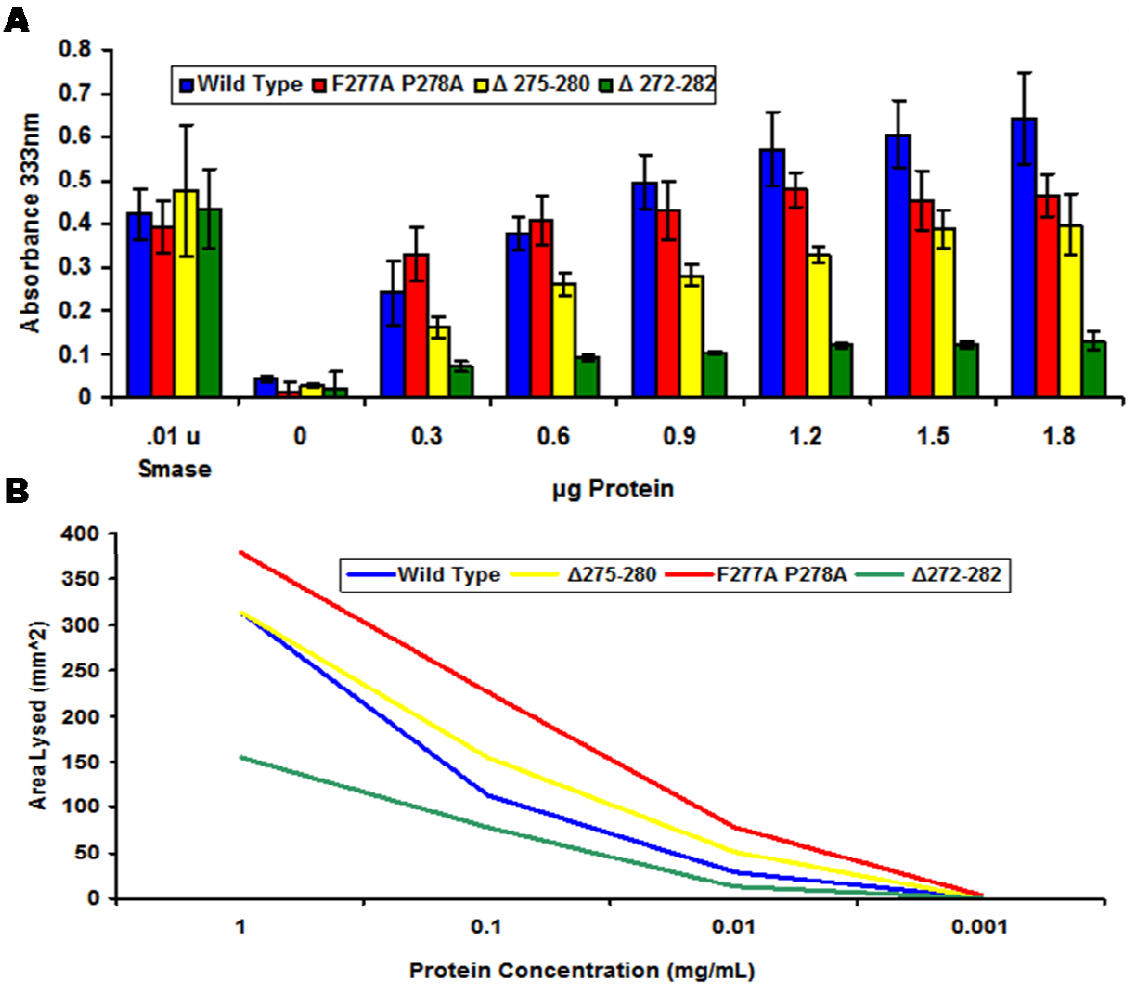

Figure 4.1 SMase and hemolytic activities of beta toxin and beta hairpin mutants. (A) SMase activity was analyzed as previously published (31, 44). The positive control was a neutral SMase purchased from Fisher isolated from *S. aureus* (Smase). The error bars denote standard deviation. (B) Hemolytic assay performed with sheep erythrocytes. The area lysed was measured and reported above.

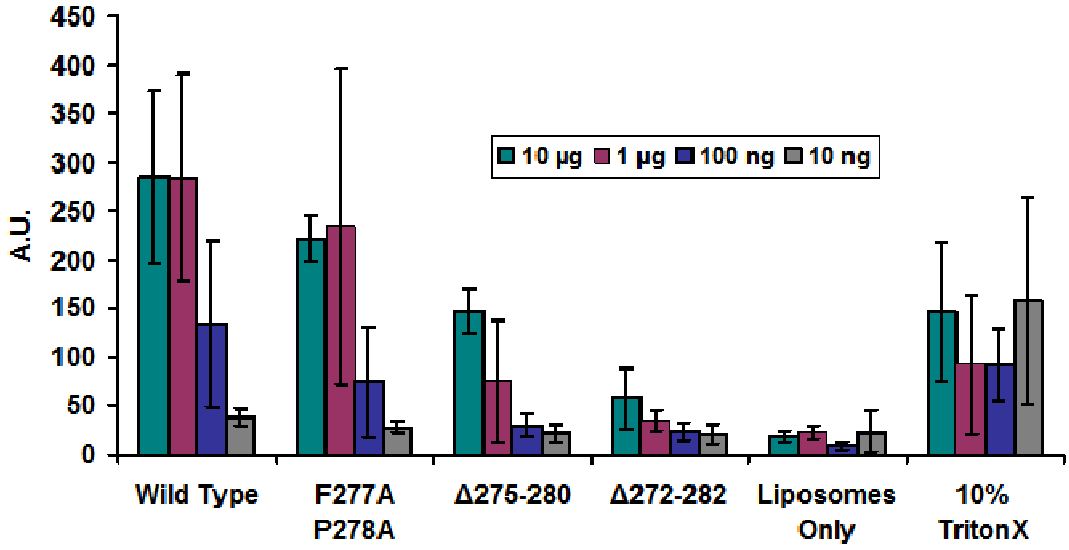

Figure 4.2 Liposome disruption activities of beta toxin and beta hairpin mutants. Liposomes were composed of approximately 50% SM to mimic the contents of a sheep erythrocyte. Each concentration of protein was done in triplicate. The error bars denote standard deviation. The liposomes only sample consisted of liposomes reacted without enzyme. 10% Triton X100 served as the positive control.

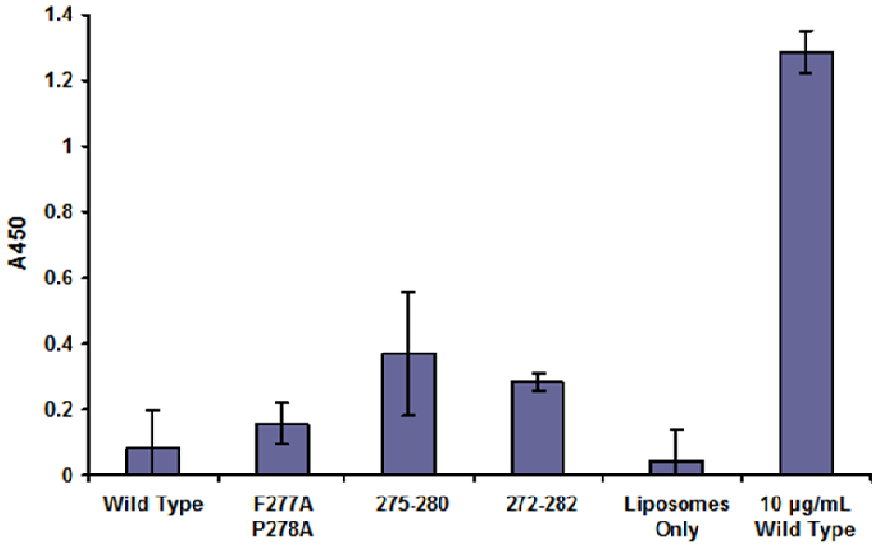

Figure 4.3 ELISA of supernatants from liposome disruption assay of beta toxin and beta hairpin mutants. The liposomes only sample represents the background level of absorbance at λ=450 nm. The positive control (10 µg/mL Wild Type) is native beta toxin not reacted with the liposomes. Error bars denote standard deviation.

When the liposome disruption assay was complete, the insoluble lipid fraction was separated from the soluble fraction of the reaction. To ascertain which fraction the beta hairpin mutants located to, we employed an ELISA system, taking advantage of the His_6 tag used to purify each protein. The native protein is present in the soluble portion in significant quantities above that of the background level (Figure 4.3), however this is most likely due to the fact that most of the liposomes are disrupted, and hence native beta toxin has little to bind to. This is in contrast to the catalytically inactive mutants, H150N and H289N, which are not detected in the supernatant, and hence are bound to the liposome (data not shown). The F277A P278A mutant is present in the soluble fraction, but at similar levels to the native protein, and most likely for the reason stated previously. Both the 275-280 and 272-282 deletion samples have significantly more protein in the supernatant of the reaction. This finding suggests that the beta hairpin may be necessary for beta toxin to anchor in the membrane. Once anchored in place, the protein can then find SM to hydrolyze. However, it could be that the beta hairpin is only

used for membrane recognition, and is not used to attach beta toxin to the membrane. Further experimentation is necessary to know which mechanism, or if both, is correct.

We previously showed the toxicity of beta toxin towards proliferating lymphocytes by measuring tritium incorporation into TSST-1 stimulated cells (44). As beta toxin lyses the stimulated lymphocytes in a SMase dependent manner, less tritium is incorporated into dividing cells and measured. When this experiment is repeated with the beta hairpin mutants, deletions of the beta hairpin have the most severe effects. Compared to native beta toxin, the 275-280 truncation has 1,000-fold less toxicity, and the 272-282 deletion has approximately 5,000-fold less (Figure 4.4A and 4.4B). Surprisingly, the substitution mutation, F277A P278A, shows a 100-fold decrease in the lymphotoxicity at lower amounts of protein. At the highest protein concentration tested, F277A P278A has nearly wild type toxicity. It is unclear why this substitution causes a dose-dependent effect not seen in the SMase, hemolytic, and liposome disruption assays. One reason could be the length of the experiment. Beta toxin is incubated with proliferating lymphocytes for a total of 4 days. However, as the hemolytic assay involves a 2 day exposure of beta toxin to sheep erythrocytes, this is unlikely.

Ago *et al.*. analyzed the function of the outmost hydrophobic amino acids, W284 and F285 (*B. cereus* numbering), in the beta hairpin of the *B. cereus* neutral SMase. This enzyme shares 59.2% identity at the protein level to beta toxin. The RMSD values for beta toxin and the SMase from *B. cereus* are 1.07 Å for all common Cαs and 1.39 Å over all common atoms. Ago *et al.*. mutated W284 and F285 separately to alanine (3). In contrast to our corresponding double substitution, F277A P278A, Ago *et al.*. found 100- and 1000-fold decreased binding to liposomes for the W284A and F285A mutants, respectively. Furthermore, they report a 1000-fold decreased hemolytic activity towards sheep erythrocytes for both substitutions (3). It should be noted that a different hemolytic activity assay was used by Ago *et al.*., but the liposome disruption assay was based on the same protocol. It is unlikely that a single alanine substitution would cause more severe effects than a double alanine mutation to the outermost hydrophobic amino acids of the beta hairpin.

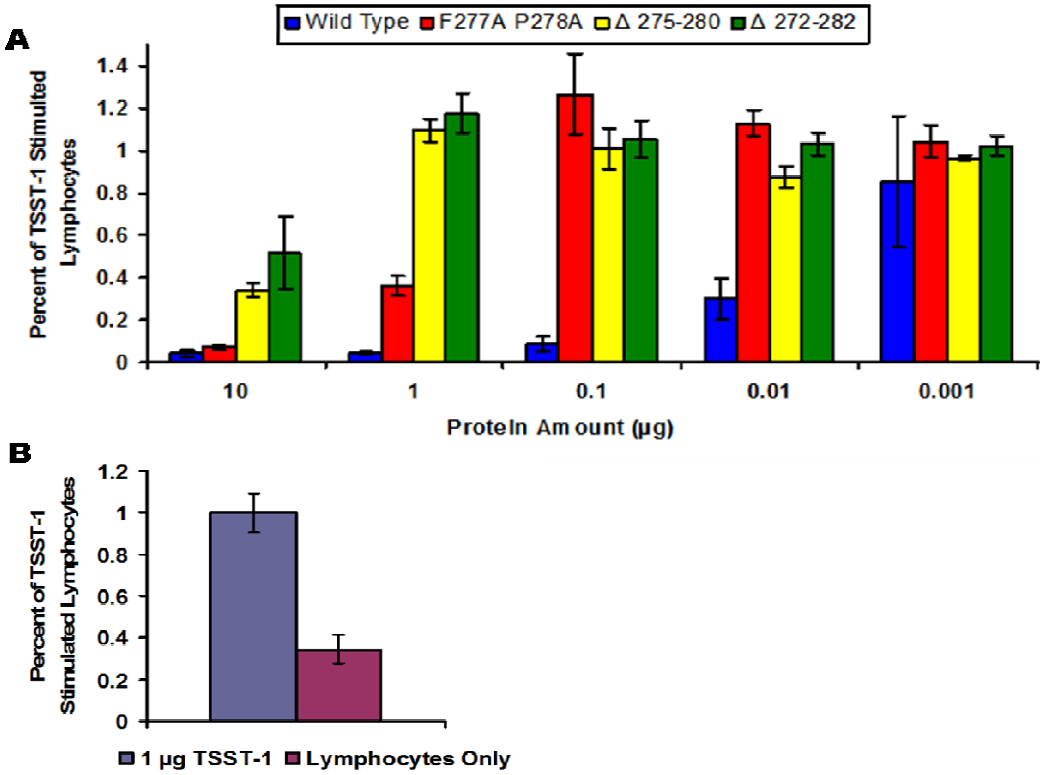

Figure 4.4 Toxicity of beta toxin and beta hairpin mutants towards proliferating human lymphocytes. (A) Tritium incorporation into induced lymphocytes in the presence of different concentrations of beta toxin, F277A P278A, 275-280, and 272-282. The experiment was performed in quadruplicate, and averages are shown. The percent of TSST-1 stimulated lymphocytes is reported. The data were normalized to the TSST-1 stimulated lymphocytes. Error bars denote standard deviation. (B) Tritium incorporation into lymphocytes in the absence of beta toxin and in the absence (lymphocytes only) or presence (1 µg TSST-1) of TSST-1.

Sequence analysis of the neutral SMases from *Leptospira interrogans* and *Pseudomonoas sp* strain TK4 do not reveal residues that could form a beta hairpin (78), (84). Instead, these enzymes have an additional 186 amino acids in their C terminus that are not present in beta toxin, Smc L, or the *B. cereus* enzyme. The extra amino acids are predicted to form a different, unknown membrane interacting structure. Indeed, deletion

of the 186 amino acids causes loss of hemolytic activity, presumably because the enzymes are no longer able to associate with the plasma membrane (17). Consistent with this hypothesis is the finding that the 272-282 deletion results in protein that can no longer lyse cells, even though it has an intact active site. Furthermore, the 272-282 deletion is found predominately in the supernatant of the liposome disruption assay (i.e. not bound to the liposome), similar to that of the 275-280 truncation. This suggests that the beta hairpin is necessary for anchoring beta toxin to the plasma membrane for SM hydrolysis to occur.

We have shown the hydrophobic beta hairpin is important in SMase, hemolytic, liposome disruption, and lymphotoxicity activities of beta toxin. To show that the beta hairpin is structurally as well as functionally important, we used circular dichroism spectroscopy to test the melting temperature of the mutants. Native beta toxin has a melting temperature of 46 °C (Figure 4.5). F277A P278A has a slightly lower melting temperature of 44 °C. The 272-282 deletion has a significantly reduced melting temperature of 40 °C, indicative that the hydrophobic beta hairpin is necessary for structural integrity of the protein even in the absence of substrate. Surprisingly the 275-280 truncation has a slightly higher melting temperature of 48 °C. This increase may be explained by the charge from the aspartic acid residue acting as a stabilizing force in solution, allowing the enzyme to withstand higher temperatures. Another option is that the 275-285 protein is prone to aggregation, and the aggregation may cause the increase in melting temperature.

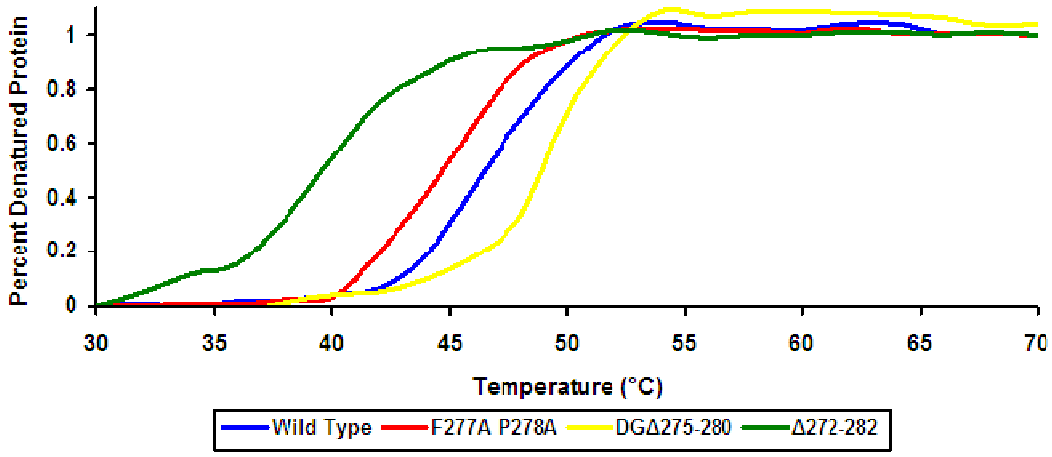

Figure 4.5 Melting curve analysis of wild type beta toxin and beta hairpin mutants λ= 215 nm. Percent denatured protein calculated as stated in material and methods section. The melting temperature was determined by the value where 50% of the protein was unfolded.

Structural Analysis

Surprisingly, altering the content or the length of the hydrophobic beta hairpin did not significantly change the structure of the proteins from that of native beta toxin. Native beta toxin folds into a four layer sandwich with the active site located between the beta sheets (44). When superimposed on the native beta toxin structure, the RMSD are calculated as 0.96 Å over 286 residues for the F277A P278A substitution, 0.85 Å over 282 residues for the 275-280 truncation, and 0.88 Å over 277 residues the 272-282 deletion, with the only change seen in the beta hairpin where the substitution or truncations were introduced (Figure 4.6, Table 4.1). This data, in context with the biological data, further highlights the mechanistic importance of the hydrophobic beta hairpin.

Figure 4.6 Cartoon representation and supposition of native beta toxin and beta hairpin mutant structures. Native beta toxin is in blue, F277A P278A is in red, 275-280 is in yellow, and 272-282 is in green. Hydrophobic beta hairpin is on the upper right.

Data Collection	**F277A P278A**	**275-280**	**272-282**
Space Group	$P2_12_12_1$	P1	$P2_1$
Unit cell dimension (α) (Å)	63.18, 68.67, 127.84	55.18, 69.05, 75.64, 93.06, 94.6, 92.13	151.38, 134.47, 161.46, 90,119.9, 90
Data Resolution (Å)	1.75	2.78	3.17
Completeness (%)	95.35	81.4	82.2
Redundancy	4.5 (3.0)	2.1 (1.8)	3.7 (2.2)
$<I/\sigma I>$	22.66 (1.99)	9.42 (2.28)	15.4 (2.3)
Rsym	0.042 (0.441)	0.082 (0.175)	0.097 (0.517)
Molecules/asymmetric unit	2	4	16
Refinement			
Rwork (Rfree)	0.212 (0.2642)	0.22 (0.285)	0.172 (0.303)
No. of non-H protein atoms	5223	9256	35705
No. of solvent molecules	567	115	0
Ramachandran regions			
% in core	87.7	84.2	67.7
% in allowed	11.7	15.8	27.8
% in generously allowed	0.4	0.0	3.2
% in disallowed	0.2	0.0	1.3
RMSD from ideal geometry			
Bond distance (Å)	0.008	.002	0.056
Bond angles (°)	1.165	.451	4.339

Table 4.1 Crystallographic statistics for F277A P278A, 275-280, and 272-282 beta toxin structures.

Metal Binding to F277A P278A

We attempted to co-crystallize F277A P278A with SM in the presence of Mg^{2+} (Table 4.2). Though this attempt was unsuccessful, we do see Mg^{2+} and a phosphate molecule in this structure at 1.75 Å resolution (Figure 4.7C). When the extra density in this structure was first discovered, we modeled phosphorylcholine, the product of SM hydrolysis, into the active site (Figure 4.7A). Though phosphorylcholine fits the

density, it was found to be the incorrect molecule. One reason for this is the presence of phosphorylcholine allows no space for the two metals hypothesized to SM hydrolysis. Another indication is that the Mg^{2+} ion in the *B. cereus* structure (PDB entry 2DDT) is in the same position as that of the F277A P278A structure when Mg^{2+} is modeled in (Figure 4.7F).

As phosphate is not present in the crystallization conditions, it may have been carried by the protein through the purification process, or a contaminating species from another source. It is possible this density represents a molecule other than phosphate. For example, it could be water molecules exhibiting distorted geometry. However, in structure of Smc L (PDB entry 1ZWX), a phosphate group is also present in the active site, though not in the identical position as seen in the F277A P278A structure (Figure 4.7B). This, coupled with the tetrahedral geometry, makes phosphate the most likely candidate.

Ago *et al.*. describes the Mg^{2+} ion to be in a centered octahedral bi-pyramid coordinated by water and E53 (beta toxin numbering). Another water molecule occupies the site where the second Mg^{2+} ion is predicted to be (3). The Mg^{2+} ion in the F277A P278A structure is also coordinated by E53 and water molecules in an octahedral configuration (Figure 4.7E and 4.7F). Other interacting residues are H289 and D288. However, the second metal binding site cannot be water as in 2DDT, nor is it likely to be another Mg^{2+} ion. Instead, the second site exhibits tetrahedral geometry, consistent with a phosphate group. The phosphate molecule appears to have ligand-like characteristics, and is coordinated by H150, H289, and D194 (Figure 4.7E).

We soaked F277A P278A crystals with $CaCl_2$ to further identify metal binding sites. This structure reveals two Ca^{2+} ions bound to the active site residues (Figure 4.7C, Table 4.2). The Ca^{2+} ions are coordinated by H150, H289, E53, D194, and D288. This is different than the structure solved by Ago *et al.*., where a lone Ca^{2+} ion is present bound to five water molecules in a hepta-coordinate system (PDB entry 2DDR) (3). We do not see the five water molecules that are found in the 2DDR structure, as observed by superposition of both structures, though the Ca^{2+} ion is in the same location (Figure 4.7 D). The *B. cereus* structure co-crystallized with Co^{2+} has two ions bound to the active

site coordinated by a bridging water molecule (3). Only one Co^{2+} is found in the 2DDS PDB, however, and is coordinated by the same residues as one of the Ca^{2+} ions in the F277A P278A structure (superposition not shown). Based on the literature, both ions are located at the same sites and coordinated by the same active site residues, though no analogous bridging water is apparent in the F277A P278A Ca^{2+} structure. It should be noted that both beta toxin and the *B.cereus* SMase have reduced activities when reacted with Ca^{2+} compared to their activities with Mg^{2+} or Co^{2+}.

Ago *et al.* also report an edge binding site for all three metal bound *B. cereus* structures (3). We do not find a corresponding metal binding site in either the Mg^{2+} or Ca^{2+} bound F277A P278A structures. We do see two ions bound to a different edge of F277A P278A in the Ca^{2+} structure, but they are most likely artifacts of the soaking process. Ago *et al.* hypothesizes that the edge metal binding site is solvent exposed, and may be regulated by Ca^{2+} binding. The Ca^{2+} binding to this site would then regulate how the enzyme interacts with the plasma membrane (3). Such a mechanism remains to be determined, however.

The model for SM hydrolysis we propose is in agreement with that of Ago *et al.* (see Chapter 3). The structures of F277A P278A bound with both Ca^{2+} and Mg^{2+} and phosphate also agree with our prior hypothesis. Ago *et al.* hypothesize that Co^{2+} binds very strongly to the *B. cereus* SMase compared to that of Mg^{2+}, and much more strongly than that of Ca^{2+} as a function of the ions relative Lewis acid strengths (3). They also report that the binding site associated with the second metal ion has slightly less affinity than the first binding site. However, as they performed the co-crystallization experiments in large excess of metal ions, it is still unclear as to why the Mg^{2+} and Ca^{2+} structures have only one metal ion bound.

Data Collection	**F277A P278A Mg^{2+}**	**F277A P278A Ca^{2+}**
Space Group	$P2_12_12_1$	$P2_12_12_1$
Unit cell dimension (α) (Å)	63.06, 69.12, 127.68	68.09, 70.19, 129.58
Data Resolution (Å)	1.61	2.6
Completeness (%)	75.22	98.72
Redundancy	5.0 (2.3)	5.7 (5.6)
$<I/\sigma I>$	13.9 (2.76)	14.73 (4.86)
Rsym	0.066 (0.374)	0.057 (0.357)
Molecules/asymmetric unit	2	2
Refinement		
Rwork (Rfree)	0.205 (0.252)	0.207 (0.298)
No. of non-H protein atoms	5170	4717
No. of solvent molecules	5115	4661
Ramachandran regions		
% in core	86.7	84.5
% in allowed	12.7	14.3
% in generously allowed	0.4	0.4
% in disallowed	0.2	0.8
RMSD from ideal geometry		
Bond distance (Å)	0.013	0.038
Bond angles (°)	1.472	2.605

Table 4.2 Crystallographic statistics for F277A P278A co-crystallized with Mg^{2+} and F277A P278A soaked with Ca^{2+} structures.

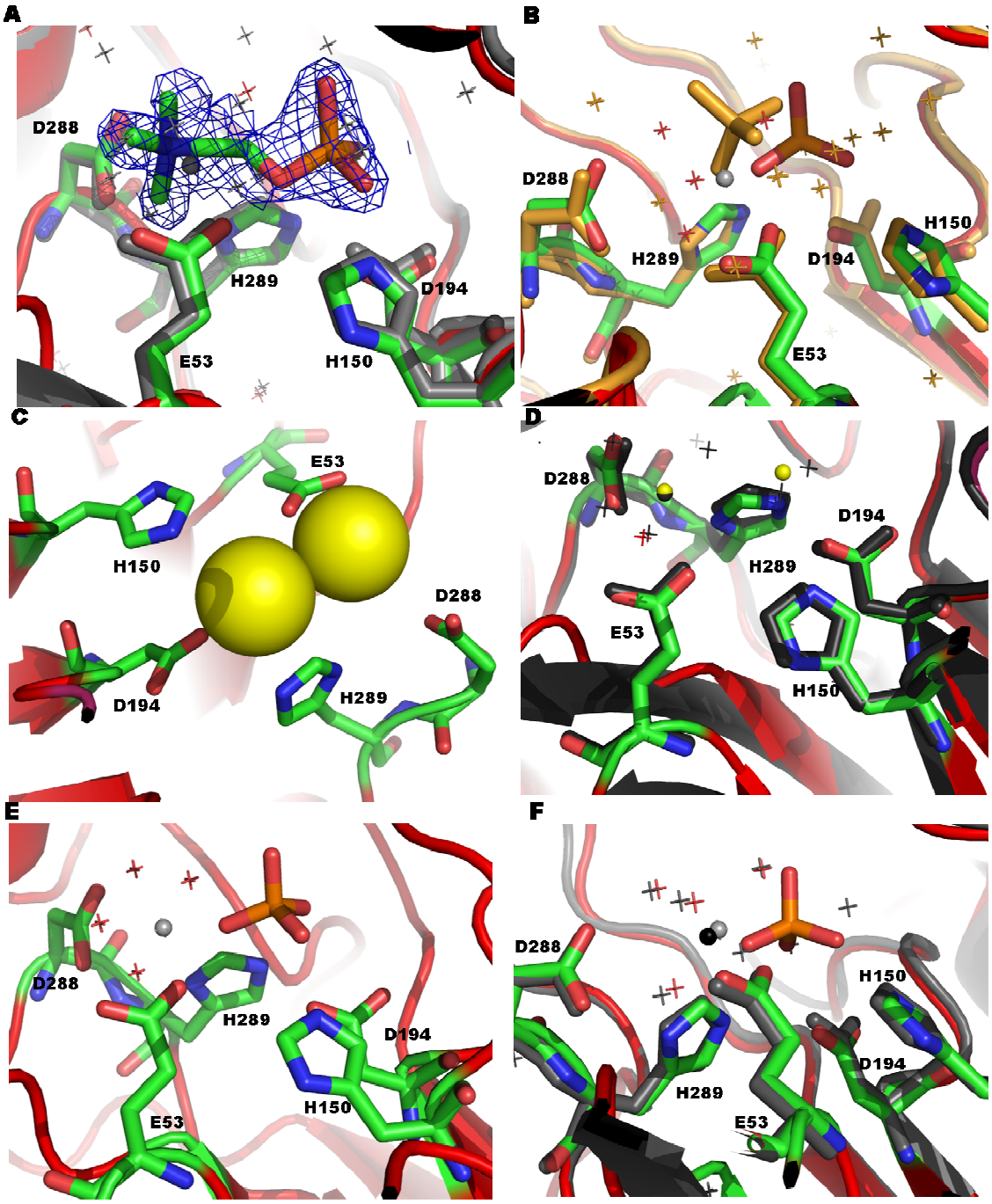
A
D288
H289
D194
E53
H150
B
D288
H289
D194
H150
E53
C
E53
H150
D288
D194
H289
D
D288
D194
H289
E53
H150
E
D288
H289
D194
H150
E53
F
D288
H150
D194
H289
E53

Figure 4.7 Mg^{2+} and Ca^{2+} binding to F277A P278A. (A) Initial model of phosphorylcholine in the active site of F277A P278A (red cartoon) superposed with 2DDT (gray cartoon). Active site residues (green sticks for F277A P2778A and gray sticks for 2DDT) that interact with phosphorylcholine (green sticks with blue mesh contoured at 1σ) are labeled. Water molecules (F277A P278A red crosses and 2DDT gray crosses) are shown. Magnesium (gray sphere) is from the 2DDT structure. (B) Active site of F277A P278A (red cartoon) with phosphate and magnesium superposed with 1ZWX (orange cartoon). Active site of F277A P278A (green sticks) and 1ZWX (orange sticks) are labeled. The phosphates (F277A P278A red stick and 1ZWX orange stick) are shown along with magnesium (gray sphere) from F277A P278A. Waters (F277A P278A red crosses and 1ZWX orange crosses) are shown. (C) Active site of F277A P278A with Ca^{2+} (red cartoon) with Ca^{2+} bound (yellow van der Waals radii). Active site residues (green sticks) that coordinate the Ca^{2+} ions are labeled. (D) Superposition of 2DDR (gray cartoon) and F277A P278A (red cartoon). Active site residues (green sticks for F277A P278A and grey sticks for 2DDR) are labeled using F277A P278A numbering. Water from 2DDR (gray crosses) and F277A P278A (red crosses) are shown. The overlapping Ca^{2+} ion from both structures is represented as half grey, half yellow sphere. The Ca^{2+} ions from F277A P278A are yellow spheres. (E) F277A P278A co-crystallized with Mg^{2+} (red cartoon) with active site residues (green sticks, labeled). Phosphate (orange stick) and Mg^{2+} (gray sphere) are shown with coordinating waters (red crosses). (F) Overlay of 2DDT (gray cartoon) with F277A P278A with Mg^{2+} (red cartoon). Active site residues for 2DDT (gray sticks) and F277A P278A (green sticks) are labeled using F277A P278A numbering. Mg^{2+} for F277A P278A (gray sphere) and water molecules (red crosses) are shown with 2DDT (black sphere) and water molecules (gray crosses).

Structural Properties of the 275-280 Truncation

We discovered unexpected density on the D chain of the 275-280 truncation structure. The density interacts with residues W28, N27, D275 (the introduced mutation), Y277, and Y235. After several rounds of refinement, we modeled diacylglycerol into the density (Figure 4.8). Diacylglycerol can be the cleavage product of lipases acting on phosphatidylethanolamine, the major component of the *E. coli* biological membrane though we cannot rule out that the 275-280 enzyme cleaved the precursor lipid (91). The mother liquor contents do not fit the density. Sphingolipids, including sphingomyelin, are not found in the *E. coli* biological membrane, nor in the membranes of bacteria that secrete neutral SMases (84). The diacylglycerol is bound close to the mutations at the tip of the truncated beta hairpin, and forms a hydrogen bond to Y235 at a distance of 3.26 Å. There is no obvious charged area where the diacylglycerol is bound that would indicate hydrophobic interactions.

This is the first example of a SMase bound to a lipid, and for the first time shows a role for the hydrophobic beta hairpin in lipid recognition. Ago *et al.* showed a molecule of buffer 2-morpholinoethanesulfonic acid adjacent to the beta hairpin in the crystal form of *B. cereus* SMase containing bound Mg^{+2} (PDB entry 2DDT) (3). As the 2-morpholinoethanesulfonic acid is over 13 Å from the active site metals and bears little resemblance to a lipid, the relevance of this structure is uncertain.

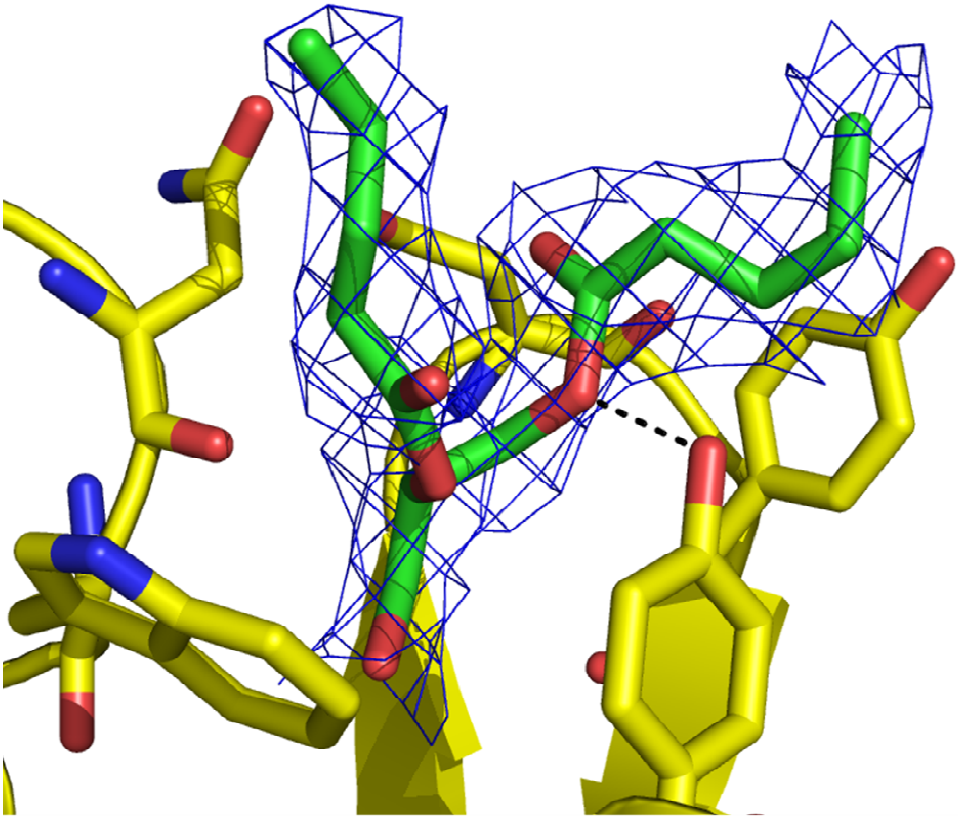

Figure 4.8 Cartoon representation of diacylglycerol density in the 275-280 structure. Diacylglycerol portrayed as green stick figure. The top of hydrophobic beta hairpin (where the DG mutation is) is directly behind the diacylglycerol and is colored yellow. Oxygen atoms are portrayed in red, and nitrogen atoms in blue. The electron density map is represented as blue mesh at 1 σ. Residues predicting to interact with the diacylglycerol are W28, N27, E275 (the introduced mutation), Y277, and Y235 (naming starts on lower left and continues clockwise). Y235 formed a hydrogen bond (dashed line) to the oxygen on the diacylglycerol.

Structural Properties of the 272-282 Deletion

The 272-282 deletion protein was difficult to crystallize, and once crystals were obtained, it was difficult to find one that diffracted to resolutions better than 8 Å. The poorly diffracting crystals correlate with the lower melting temperature, and hence decrease in stability of the 272-282 deletion. The 272-282 deletion crystallized with 16 molecules in the asymmetric unit showing domain swapped mediated dimer interactions (Figure 4.9).

The structure was solved by molecular replacement using *Phaser* with the coordinates of wild type beta toxin as a search template. Even after optimizing search parameters, an initial search with *Phaser* could identify only nine monomers, not the 15-20 monomers expected based on Matthews coefficient calculations. This partial solution yielded a map that showed density corresponding to several other monomers, which were placed by fitting the template monomer structure to the F_o-F_c map with *MOLREP*. Repeating this procedure afforded a nearly complete solution with 15 monomers, and it was only at this point that density corresponding to the last monomer became visible. Following refinement it became apparent that this monomer has a significantly higher B-factor than any other in the structure, accounting for the difficulty in locating it during molecular replacement.

The density clearly shows how the C terminus of one monomer enters into the neighboring monomer to form domain swapping dimers (Figure 4.9A) The domain swapping may be due to insufficient flexibility of the hinge region (where the beta hairpin is normally located) necessary to achieve a complete turn. With the C terminus extended into another molecule, this need for a sharp turn is avoided. The C terminus of the 272-282 deletion is composed of 15 amino acids (271-WNDFSDHYPIKAYSK-286). Domain swapping was the only way the 272-282 deletion structure could be modeled, as the region where a turn should have been located would not fit due to steric hindrance from its partnering dimer (Figure 4.9B).

There is variation within the dimers (Figure 4.9C), as one monomer is rigid, with the other monomer showing more disparity. Some dimer chains have high B factors which could also explain the higher R_{free} value of the 272-282 deletion structure

(Figure 4.10). For instance, the dimer formed by chains O and P exhibit substantially higher B factors than other dimers. Choosing a new origin for the unit cell and repeating the refinement gave no difference in the B-factor distribution, indicating that the unit cell parameters are correct. This can be rationalized because there are less extensive intermolecular contacts within the crystal lattice at these chains. However, the dimer formed by chains A and B shows lower B factors than most other dimers as it forms more contacts with molecules within crystal lattice. In native beta toxin, the beta hairpin is located between residues 271-286. By replacing this motif with W271 N272, as in the 272-282 deletion, the protein sequence is not sufficient to form a turn. Perhaps a W271G mutation may have allowed for the formation of a loop, and hence a more stable protein.

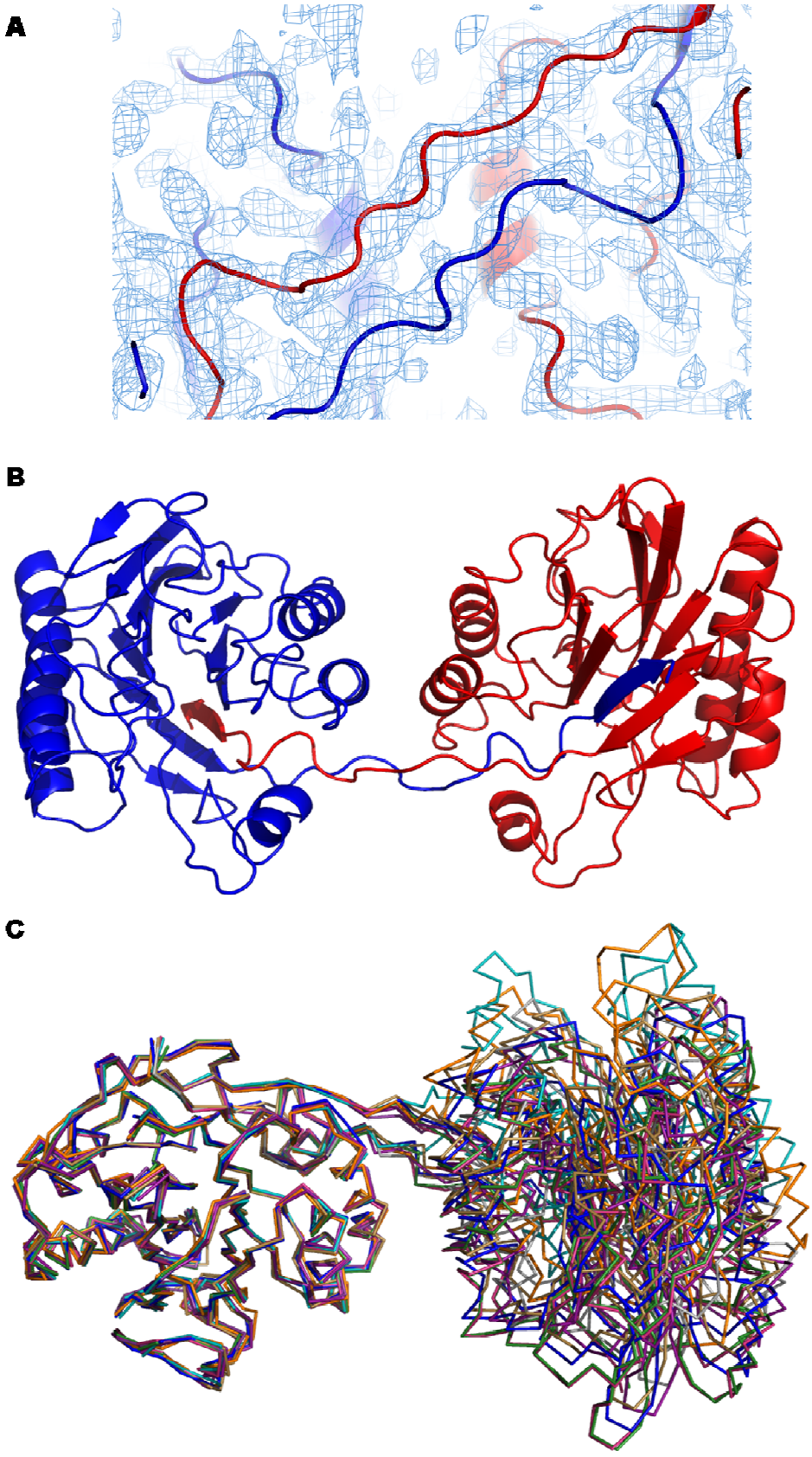
A
B
C

Figure 4.9 Domain swapping of the 272-282 deletion and superposition of all dimers in the unit cell. (A) Electron density of domain swapping region of 272-282 deletion structure. 2Fo-Fc map contoured at 1 sigma. One dimer is portrayed as the red cartoon; the other dimer is portrayed as the blue cartoon. (B) Cartoon representation of domain swapping. Coloring the same as in Figure 4.8A, showing the C terminal 15 amino acids interact to form dimers. (C) Ribbon diagram and superposition of 8 dimer interactions in unit cell.

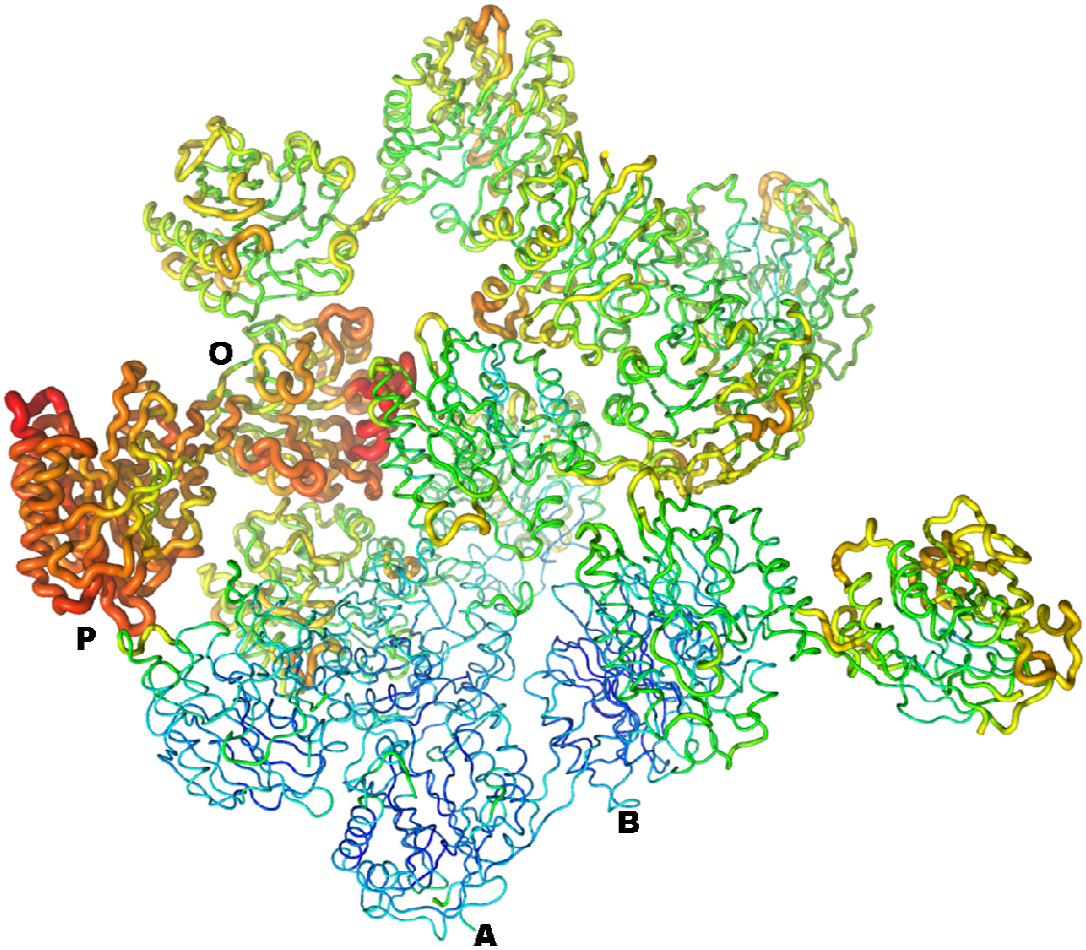

Figure 4.10 B factor analysis of the 272-282 deletion. Ribbon diagram of 272-282 unit cell dimer interactions. Chain A and B form a dimer with low B factors (blue, labeled) while chains O and P form a dimer with high B factors (red/orange, labeled). Higher B factor is also indicated by a thicker ribbon.

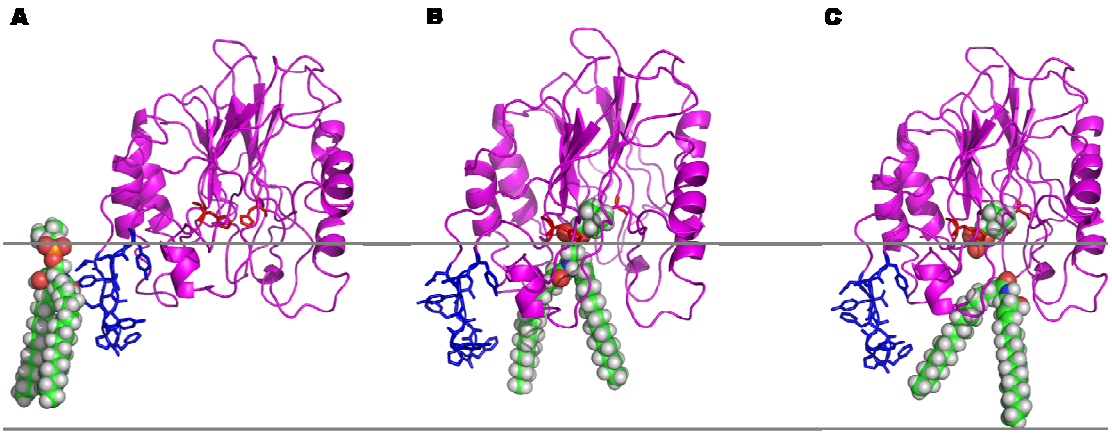

Figure 4.11 Model of beta toxin bound to a host cell membrane. (A) Beta toxin recognizes SM via the hydrophobic beta hairpin insertion into the outer leaflet of the plasma membrane. (B) Beta toxin binds and hydrolyzes SM. (C) Phosphorylcholine and ceramide are expelled as beta toxin searches the membrane for another SM molecule. Beta toxin is represented as magenta cartoon. Active site histidines, H289 and H150 are portrayed as stick figures in red. The hydrophobic beta hairpin is shown as stick figures in blue. SM is shown as green spheres, with green indicating carbon, blue indicating nitrogen, red indicating oxygen, orange indicating phosphorous, and white indicating hydrogen. The outer leaflet of the plasma membrane is represented by two grey lines, with beta toxin in the extracellular portion.

Given the data, we propose the following mechanism for beta toxin and other neutral SMases binding to susceptible host cell membranes (Figure 4.11). Beta toxin is secreted after exponential growth by *S. aureus* (61). The hydrophobic beta hairpin interacts with the charged phospholipids of the host cell membrane, and further sinks in to interact with lipid fatty acid chains. The beta hairpin anchors beta toxin to the membrane, and membrane dynamics shift beta toxin within the membrane until it encounters a molecule of SM. There are hydrophobic residues on the loops located at the top of beta toxin which can further interact with the membrane. We believe the beta hairpin functions as an anchor, holding the enzyme to the outer leaflet of the membrane. When the beta hairpin is removed, as shown by the 272-282 deletion data, the protein

no longer disrupts liposomes, presumably because it cannot initially attach or stay attached to the liposome (Figures 4.2 and 4.3). With the enzyme anchored in the membrane, the active site is poised for SM to bind. After SM hydrolysis, the products ceramide and phosphorylcholine are expelled and beta toxin is free to encounter the next SM molecule.

Conclusion

The mechanism of beta toxin and other SMases induced cell lysis is unknown. One possible mechanism could be physical disruption to the membrane. Beta toxin driven hydrolysis of SM could cause ions and cellular content to leak into the extracellular matrix. Human lymphocytes can have as little as 6.2 % SM content in the plasma membrane (45). Such a low value makes it unlikely that physical membrane disruption would be the method of cell lysis. However, this cannot be ruled out, as membranes with high cholesterol content can sequester SM in concentrated areas, known as rafts (95). If beta toxin were to act on a SM rich raft, the membrane dynamics could be disrupted and result in cell lysis.

Ceramide is the product of SM hydrolysis, and is a potent signal for apoptosis (64). Ceramide has been implicated in cellular processes in response to stress, as well as a source of other lipid secondary messengers such as sphingosine and sphingosine 1-phosphate (17). Mammalian neutral SMases are predicted to be tethered to inner leaflet of the plasma membrane. These SMases are the major source of ceramide for the stress induced ceramide production pathway, which then leads to apoptosis.

Several pathways are involved in mammalian SMase-mediated apoptosis. Increases in intracellular ceramide levels lead to the activation of c-Jun N-terminal Kinases (JNKs) (75). JNKs are also activated in response to stress stimuli, which can then lead to apoptosis. Ceramide activates Ceramide-Activated Protein Phosphatases (CAPPs) (29). CAPPS in turn cause cell cycle arrest at the G1 phase, indicating a role for ceramide in cell cycle progression (74). Ceramide also activates caspases, which cause cells to undergo apoptosis.

The most likely explanation is that bacterial neutral SMases cause cell lysis due to apoptosis. Indeed, Zhang et al. showed that *B.cereus* SMase, when expressed using a mammalian expression vector in Molt-4 leukemia cells does induce apoptosis (100). However, this was expressed intracellularly, so only SM on the inner leaflet was hydrolyzed to ceramide. Zhang et al also report that exogenously added *B. cereus* SMase did not induce apoptosis in Molt-4 cells. However, the mechanism of cell lysis due to exposure of bacterially secreted extracellular SMases is unknown.

As eukaryotic cells tightly regulate intracellular ceramide levels, it is logical that the JNK, caspase, or CAPP pathway would be activated in response to bacterial SMases mediated release of ceramide, leading to cell cycle arrest, apoptosis, or both. Cell lysis would then be caused by apoptosis, not due to physical membrane disruption. However, further experimentation is necessary to determine which mechanism is correct.

Bacterial SMases are important virulence factors. In strains of *L. ivanovii* where Smc L is knocked out, the bacteria are no longer able to escape from the host cell phagosome into the cytoplasm (35). This results in decreased virulence in the mouse model, as lower concentrations of intracellular bacteria are present. When beta toxin is knocked out of *S. aureus* in a mouse mammary gland infection, fewer bacteria are recovered than in a wild type infection (15). Furthermore, the beta toxin knock out strain showed less damage in a rabbit corneal infection model (15).

Because bacterial SMases are important in virulence of pathogens, it is crucial to understand the molecular underpinnings of their actions. The active sites of beta toxin, Smc L, and the *B. cereus* enzyme are well characterized. However, the action of neutral SMase binding to a host cell membrane, as well as the residues of the SMase associated with this event, had been poorly characterized. This study reveals that the length, but not the content, of the beta hairpin on the SMase from *S. aureus* is important in anchoring beta toxin to the membrane. Armed with this knowledge, this mechanism of pathogen-induced host cell lyses could be prevented with the development of new antimicrobial therapeutics.

CHAPTER 5
BETA TOXIN STIMULATES FORMATION OF NUCLEOPROTEIN BIOFILM MATRIX

This chapter details the mechanism of biofilm formation in the *Staphylococcus aureus hlb*$^{+}$ strain COL. Beta toxin shares structural homology with DNase I, but does not function as a DNase. Beta toxin oligomerizes and forms cross-links with itself and other proteins in the presence of DNA, forming the skeleton of the biofilm matrix.[1]

[1] Several people contributed to the experiments detailed in this chapter. Dr. Reuben Harris provided the oligomers used for the gel motility experiment. Dr. Kylie Walter shared reagents and knowledge for urea gel analysis. Andrew Kruse helped test the DNA-beta toxin pellet linkage. Dr. Patrick M. Schlievert designed the experiment to inactivate beta toxin, and provide the Newman and COL strains of *S. aureus*. Dr. Kenneth W. Bayles provide reagents and laboratory space to perform the adherence assay and biofilm studies, as well as provided the pCN51 plasmid and bacteriophage 11. Ethan Mann helped perform the adherence and biofilm studies.

SUMMARY

Beta toxin is a key virulence factor in the human pathogen *Staphylococcus aureus*. We have shown that in addition to the ability to lyse erythrocytes, beta toxin kills proliferating human lymphocytes. Here we demonstrate that beta toxin forms cross-links to other proteins in the presence of nucleic acids resulting in a profound effect on biofilm formation *in vivo*. We hypothesize that cross-links between beta toxin molecules and other proteins bound to extracellular DNA (eDNA) and extracellular polysaccharides produces the skeletal framework at the core of staphylococcal biofilms.

INTRODUCTION

Biofilms are communities of microorganisms within a polymeric matrix that are attached to a surface. This surface can vary from rocks in the oceans to plaque on teeth. Biofilms also form on the surfaces of medical devices and on damaged heart valves. The matrix of a biofilm typically contains extracellular polymeric substance consisting of extracellular DNA (eDNA) (71, 96) plus carbohydrate, e.g., in pseudomonas lung infections, or protein, e.g., in staphylococcal infections. Formation of a biofilm protects the organism from the effects of detergents and antibiotics. It has been estimated that nearly 80% of all cases of bacterial infections involve formation of a biofilm.

Beta toxin of *Staphylococcus aureus* is a neutral sphingomyelinase (SMase). The ability to lyse erythrocytes and kill proliferating human lymphocytes is linked to this SMase activity (44). Its structure (44) shows it to be a member of the DNAse I superfamily (CATH class 3.60) (68). When superposed, beta toxin and DNase I have an RMSD of 3.3 Å over 220 Cαs, and 7 of the 9 active site residues are identical (Figure 5.1). This homology led us to hypothesize that beta toxin retained the ability to bind DNA. These studies have led to the unexpected finding that beta toxin plays a key role in the establishment of biofilms.

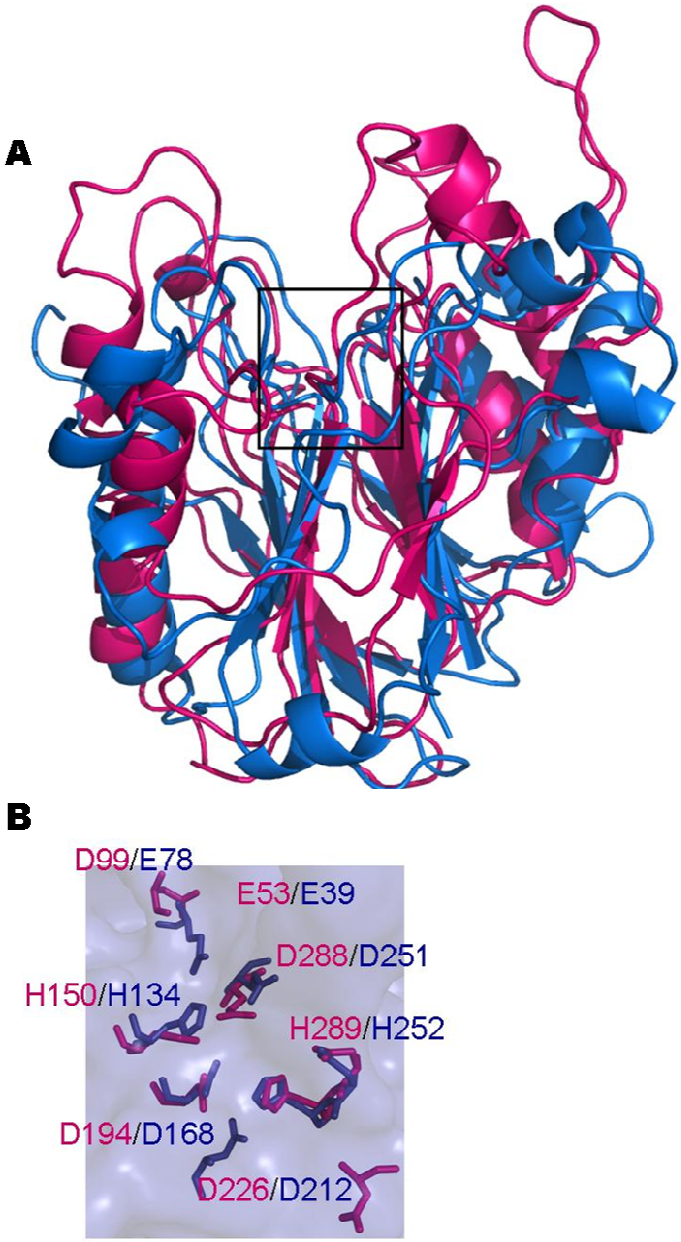

Figure 5.1 Beta toxin and DNase I share a similar overall structure. (A) Cartoon representation of beta toxin (in magenta) and DNase I (in blue) superposed. The black box represents the location of the active site. (B). Superposition of conserved active site residues. Residues important in either sphingomyelinase activity (magenta sticks) or DNase activity (blue sticks) are displayed and colored according to which molecule they belong to. The background is a surface model of beta toxin (light blue).

MATERIALS & METHODS

DNA Binding Studies

Beta toxin, H150N, and H289N were purified and expressed as previously published (44). Pure protein (10, 25 or 50 µg) or 1 U DNase-I (New England Bioscience) was combined with single stranded (Biotin-ATTATTATTATTCCAATGG ATTTATTTATTATTTATTTATTT-Fluorescein) or with annealed double stranded ATTATTATTATTCCGUGGATTTATTTATTTATTTATTTATTT-Fluorescein and AAATAAATAAATAAATAAATAAATCCGCGGAATAATAATAAT 0.02 nmol oligos (generously shared by the Harris laboratory at the University of Minnesota). The entire reaction was mixed with sample buffer (Invitrogen) and ran on on Novex® 6.0 % TBE gels (Invitrogen) for 1 hr at 150 volts after pre-running in 0.5 X TBE buffer (Invitrogen) for 20 min. The gel shifts were visualized using a Fujifilm FTA-5000 phosphoimager.

Beta toxin was combined with 12 µg Qiagen maxi prep purified pUC18 plasmid DNA in 1X DNase I buffer (New England Biosciences) and 12 µg ethidium bromide then incubated at 37° C for 30 min. The reaction was stopped by incubation on ice for 10 min, followed by centrifugation for 10 min in a microcentrifuge. The pellet was separated from the supernatant and washed twice with water, then resuspended in 10 µL water. Half the pellet was run on a NuPAGE Bis-Tris gel (Invitrogen NP0322) then stained and destained according to the manufacturer's directions. The other half of the pellet was run on an 0.8% agarose gel made with 1X TAE and ran at 100V for 1.5 hr. The supernatant was assayed identical to that of the pellet.

To treat the pellet, the reaction was scaled up 10 fold, and the protocol followed as stated above. The pellet was split equally and treated with 0.05, 0.25. 0.5, or 2.5 M BME; 2, 10, or 20 U DNase I (NEB); 2, 20, or 100 µg proteinase K (Sigma). The treated pellets were reacted and run on gels as stated above.

Inactivation of COL *hlb*$^+$

Phage were isolated from *S. aureus* strain Newman by diluting a saturated culture (1/500) into fresh Todd Hewitt broth, shaking for 1.5 hr at 37° C followed by the addition of 1.0 µg mitomycin C. The cells were shaken for 3 hr, pelleted, and the supernatant sterile filtered. COL *hlb*$^+$ was diluted 1/500 from a saturated culture in Todd Hewitt broth and shook at 37° C for 3 hr, then placed on ice for 1.5 hr. COL *hlb*$^+$ was plated (100 µL) onto Todd Hewitt agar plates and left upright for 30 min at room temperature. The Newman supernatant was then spotted onto the COL *hlb*$^+$ plate and left upright for 15 min at room temperature, then inverted and incubated at 37° C overnight. Colonies with a zone of lysis were picked and streaked on blood agar plates. Lysogens that have the phage inserted into the beta toxin gene (COL *hlb*$^-$) no longer lysed red blood cells and were picked for further analysis.

Biofilm Studies

Adherence was measured as previously published (8). Briefly, cultures were grown overnight in TBS (tryptic soy broth) supplemented with 3% sodium chloride and 0.5 % glucose. The cultures were diluted to OD600, and 200 µL was placed in a 96 well plate (Costar 3596) previously coated in 20% human plasma diluted in carbonate buffer pH 9.6 in quadruplicate. The cultures were incubated statically at 37° C overnight. The cultures were removed from the plate, and the plate washed twice with 1X PBS (phosphate buffered saline), followed by 2 min room temperature incubation in 100 µL 100% ethanol. To the ethanol, 100 µL stain solution (0.41% crystal violet in 12.0 % ethanol) was added and allowed to sit for 2 min at room temperature. The stain was removed, and the wells washed with 1 X PBS three times. The absorbance was read on a plate reader at λ=595 nm.

COL *hlb*$^+$ and COL *hlb*$^-$ (4) were grown overnight in TSB (tryptic soy broth), and diluted to 5 x 10^6 bacteria in TSB, then injected into flow cells for biofilm formation analysis as previously published (71). The reaction was monitored for 3 days, after which the biofilm was stained with Syto-9 and Toto-3 (Invitrogen) and the average thickness calculated.

Creation of COL *hlb*$^{-}$ pCN51 *hlb*$^{+}$

The native beta toxin gene was kindly provided by the Bohach laboratory at The University of Idaho. The native promoter and signal sequence were cloned along with the ORF and inserted into the pCN51 plasmid (kindly given by the Dr. K Bayles, University of Nebraska Medical Center). The primers used were 5'GCATCTATTTTGTTGCATCCT ATATAAAAGGAGTC-3' and 5'GTTATTAGTTAGTGAATTCCTATTTACTATAG GCTTTG-3'. The native gene was PCR amplified and then cut with EcoRI and BamHI (both NEB). The digest was ran on an 1.5 % Agarose gel, and the corresponding band cut out and gel purified, and ligated into the pCN51 plasmid, cut with the same restriction digest enzymes. The ligates were then transformed into *E. coli* XL-blue cells, and ampicillin resistant clones were picked for further DNA isolation.

Either pCN51 with the beta toxin insert or with the pCN51 empty vector were transformed into competent *S. aureus* strain RN4220 (generously provided by Dr. P Schlievert, University of Minnesota). The cells were made competent by diluting overnight cultures grown in TSB to an OD600 of 0.05 and shaking for 1 hr at 250 RMP 37° C. The OD600 was assayed again and the cells used only if it had reached a minimal value of 0.4. The cells were spun down at 10,000 X g, the supernatant discarded, and resuspended in 15 mL sterile room temperature ddH_20. This step was repeated, and the cell resuspended in 2.5 mL room temperature 10.0% sterile glycerol, and then spun down at 10,000 X g. The cells were resuspended in 1.25 mL 10.0% sterile glycerol, transferred to eppendorf tubes, and incubated without shaking at room temperature for 15 min, then spun down 10,000 X g for 2 min. The supernatant was discarded, and the cells resuspended in 325 µL 10% sterile glycerol and 80 µL of cells were immediately transformed.

Prior to transformation, 1.0 µg DNA was drop dialyzed against ddH_20 with a Millipore 0.025 µm membrane for 15 min, and then added to 80 µL fresh competent cells. The cells were electroporated at 100 ohm, 25 µf, 200 kV, followed by the immediate addition of 390 µL B2 media (1.0% Casein Hydrolysate, 2.5% Yeast

Extract, 0.1% K2HPO4, 0.5% Glucose, 2.5% NaCl pH 7.5). The reaction was incubated at 37° C without shaking for 110 min, then 100 µL of the transformation was plated onto TSA with 10 µg/mL erythromycin, and incubated at 37° C overnight.

Transformants resistant to erythromycin were grown overnight in TSB at 37° C, 250 RMP. The following day the cultures were diluted 1:100 in TSB and incubated at 37° C, 250 RMP for 1.5 hr. Bacteriophage Φ11 (kindly provided by Dr. K Bayles, University of Nebraska Medical Center) was added to the culture such the MOI (multiplicity of infection) was 0.1. To this 1 mL of freshly made 10 mg/mL $CaCl_2$ was added. The cultures were incubated at room temperature without shaking for 30 min and then slowly rotated at 30° C for 5 hr or until the cells were lysed. The cultures were then placed at 4° C overnight. The phage was filtered through a sterile 0.45 µm filter, and tittered in duplicate by diluting 10^{-6} though 10^{-9} in phage buffer (6.47 g glycerol-2-phosphate, 60 mg $MgSO_4$, 2.4 g NaCl, 0.5 g gelatin dissolved in 475 mL ddH_2O, autoclaved, cooled, followed by the addition of 22.5 mL of freshly made 10 mg/mL $CaCl_2$). RN4220 was used for titering.

COL *hlb*$^-$ were grown overnight in TSB at 37° C with shaking at 250 RMP, then diluted 1:100 and incubated at 37° C with shaking at 250 RMP for 1 hour. The cells were pelleted at 13,200 RPM for 5 min. The supernatant was discarded, and the cells washed with 5 mL TSB, and then pelleted 13,200 RPM for 5 min. The cells were resuspended in 1 mL TSB, and 40 µL of fresh 10 mg/mL $CaCl_2$ and the appropriate amount of phage to give an MOI of 0.1 were added, and incubated at room temperature for 10 min and then at 30° C for 35 min without shaking. To this, 5 mL TSB was added, and the cells pelleted at 13,200 RPM. The cells were resuspended in 10 mL TSB, transferred to a Falcon tube, and incubated at 37° C, 250 RPM, for 1.5 hr. The cells were pelleted at 13,200 RPM, the supernatant discarded, and resuspended in 1 mL TSB, and 0.1 mL of cells were plated on TSA and 10 µg/mL erythromycin, and then incubated at 37 ° C overnight. Colonies that were resistant to erythromycin and non-lysogenized were chosen for further analysis.

Growth Curve Analysis

Growth curve analysis was done by diluting overnight cultures of COL *hlb*$^{+}$ and COL *hlb*$^{-}$ grown in TSB 1:100 in fresh TSB. The OD600 was assayed every 15 min for 3 hr, and the results reported. The experiments were done in triplicate and repeated twice.

RESULTS AND DISCUSSION

Beta Toxin and DNA Analysis

Beta toxin binds DNA but is not a DNase. We proved this by looking for an increase of the absorbance at 260 nm due to liberated nucleic acids and for a decrease in the fluorescence of intercalated ethidium bromide (Figure 5.2). Beta toxin binds to both single-stranded and double-stranded oligomers as evident by gel shift analysis (Figure 5.3). Mutations of the active site of beta toxin, H289N and H150N, which negate SMase activity and lymphotoxicity (44) yield protein that is are still able to bind DNA.

Though beta toxin and DNA belong to the same superfamily, differences in the enzymes exist such that each has substrate specificity towards either DNA or SM. Beta toxin is a larger enzyme, and has extra loops at the top of the central cleft (Figure 5.1A) Comparison of the active site residues shows differences, as well (Figure 5.1B). Beta toxin residue D99 is changed to E78 in DNase I. Also, beta toxin residue D226 does not align well with corresponding DNase I residue D212. These differences account for the lack of DNase I like activity displayed by beta toxin.

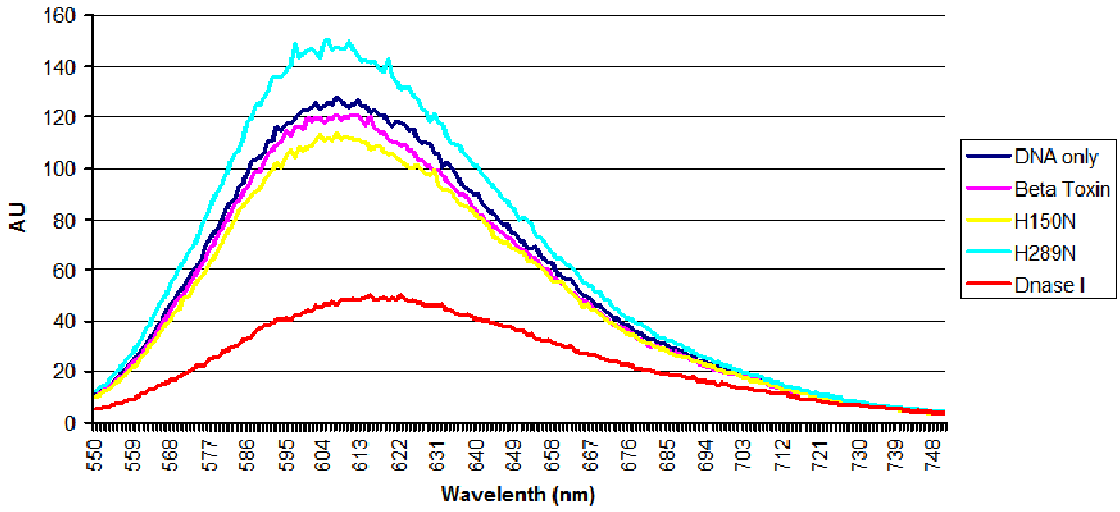

Figure 5.2 Beta toxin is not a DNase. Beta toxin and inactive SMase mutants incubated with ethidium bromide and pUC 18 DNA do not cause a decrease in fluorescence as seen with DNase I.

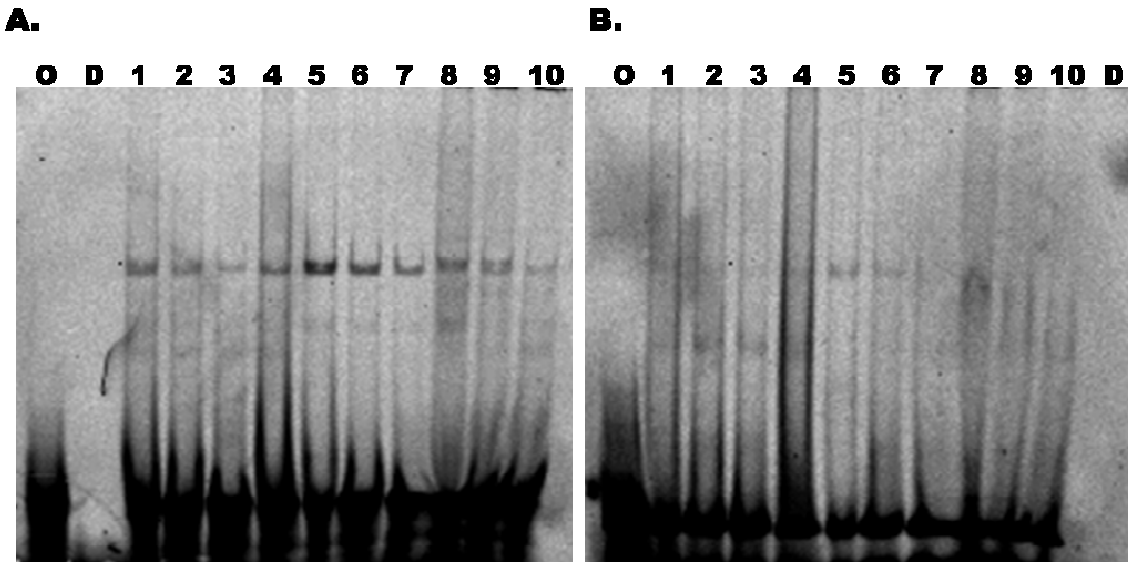

Figure 5.3 Beta toxin binds single and double stranded DNA oligomers. (A) Gel shift of single stranded DNA. Lane O is oligos only. Lane D is oligos combined with 1 unit DNase I. Lanes 1, 2, and 3 contain oligos with 50, 25 and 10 μg native beta toxin, respectively. Lane 4 contains 50 μg native beta toxin with oligos in the absence of $MgCl_2$. Lanes 5, 6 and 7 contain oligos with 50, 25 and 10 μg H289N, and lanes 8, 9 and 10 contain oligomers with 50, 25, and 10 μg H150N, respectively. (B) Gel shift of double stranded DNA. Lane indications the same as in Figure 5.3A.

Beta toxin precipitates DNA. When beta toxin is added to pUC18 DNA, the immediate effect is the production of a precipitate whose amount was strictly proportional to the amount of beta toxin added. SDS PAGE of the precipitate reveals the presence of additional peptide bands with molecular weights corresponding to dimers, trimers and tetramers of beta toxin (Figure 5.4). Furthermore, agarose gel analysis shows that the pUC18 DNA aggregates in the presence of beta toxin (Figure 5.5). This experiment was repeated in 8M urea with identical results (data not shown). These high molecular weight bands remain after treating the precipitate with DNase I (Figure 5.6). Agarose gel electrophoresis of the precipitate shows that the DNA is unable to enter the gel unless the precipitate is treated with proteinase K (Figure 5.7).

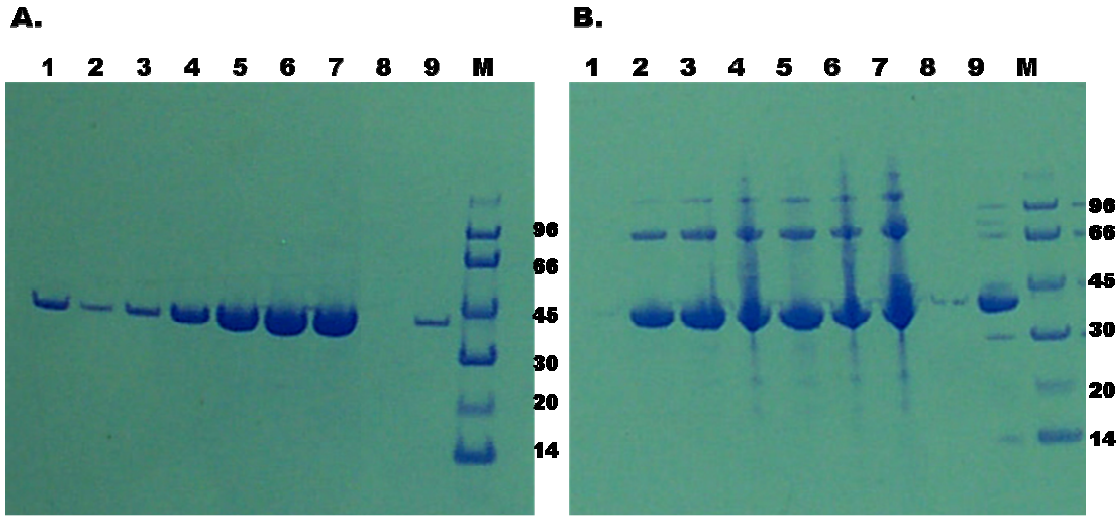

Figure 5.4 DNA induces oligomerization of beta toxin monomers. (A) SDS-PAGE analysis of the supernatant of the reaction of beta toxin with pUC 18 DNA. Lane 1 contains 50 μg beta toxin in the absence of DNA. Lanes 2 through 7 contain 12, 50, 100, 200, 300, and 400 μg beta toxin reacted with pUC 18 plasmid DNA, respectively. Lane 8 contains DNA only. Lane 9 is a duplication of lane 3 in the absence of ethidium bromide. M indicates the low molecular weight marker used, and bands are labeled (kDa). (B) SDS-PAGE analysis of the pellet of the reaction of beta toxin with pUC 18 DNA. Lane contents are identical to that of Figure 5.4A.

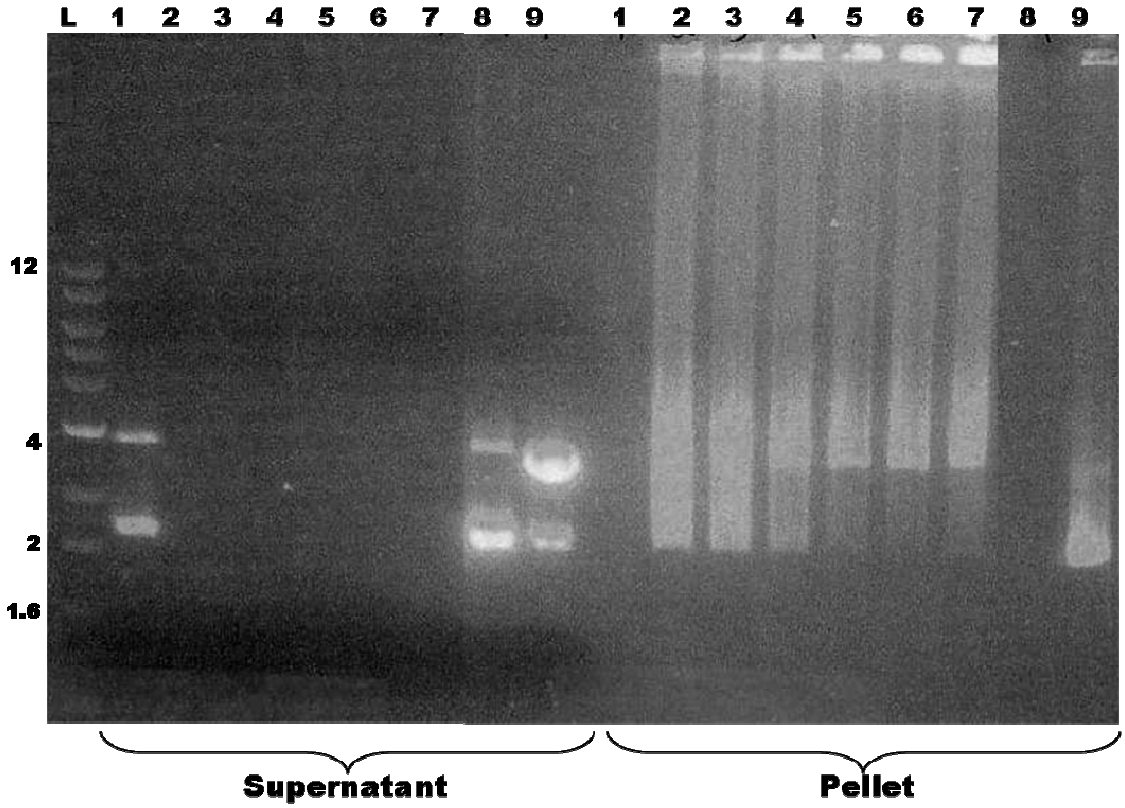

Figure 5.5 Agarose gel analysis of pUC 18 DNA reacted with beta toxin. The pellet (right lanes 1-9) and supernatant (left lanes 1-9) were run on a 0.8% agarose gel. Lane L indicates the 1 KB ladder with select bands labeled (kbs). Lanes 1-7 are 12, 50, 100, 200, 300, 400 and 500 μg native beta toxin reacted with pUC 18 plasmid DNA, respectively. Lane 8 is DNA reacted in the absence of beta toxin. Lane 9 is identical to lane 2 in the absence of ethidium bromide.

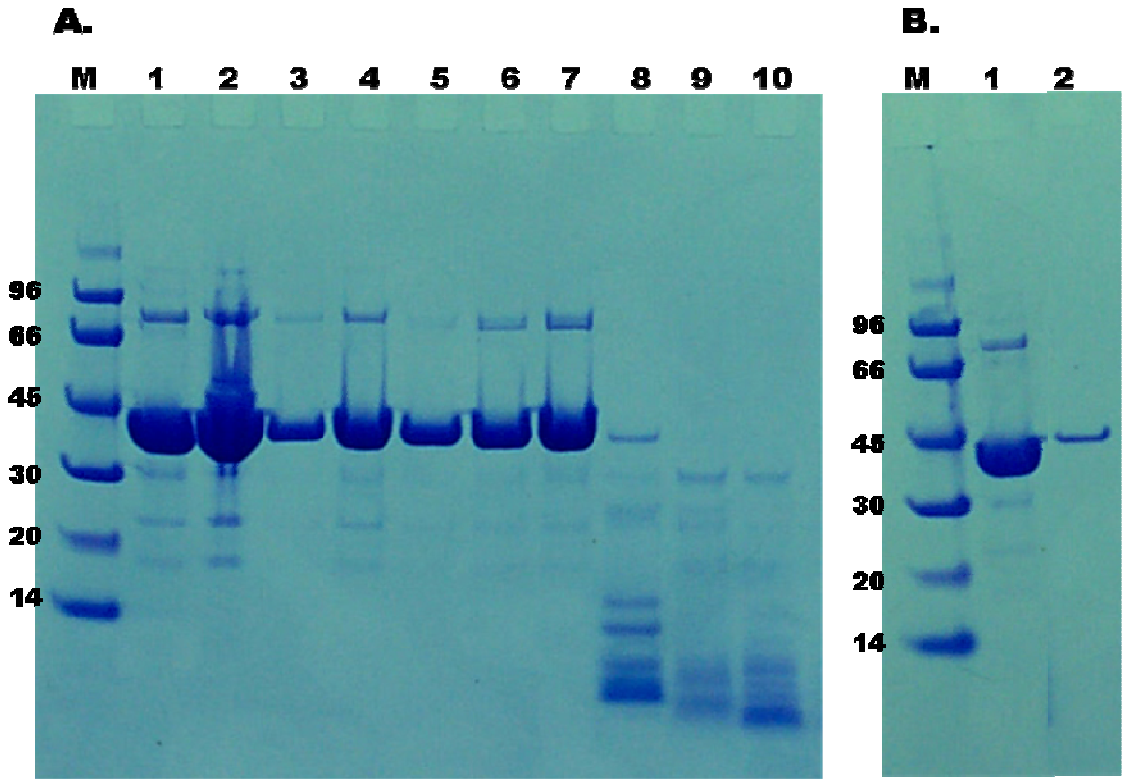

Figure 5.6 Beta toxin covalently oligomerizes in the presence of DNA. (A) SDS-PAGE analysis of the beta toxin-DNA reaction pellet treated with 0.05, 0.25. 0.5, or 2.5 M BME (lanes 1-4), 2, 10, or 20 U DNase I (lanes 5-7); 2, 20, or 100 µg proteinase K (lanes 8-10). Lane M contains the low molecular weight marker and bands are labeled (kDa). (B) SDS-PAGE analysis of the pellet of the beta toxin-DNA reaction which was not treated. Lane 1 contains the pellet, lane 2 contains the supernatant of the reaction. Lane M contains the low molecular weight marker

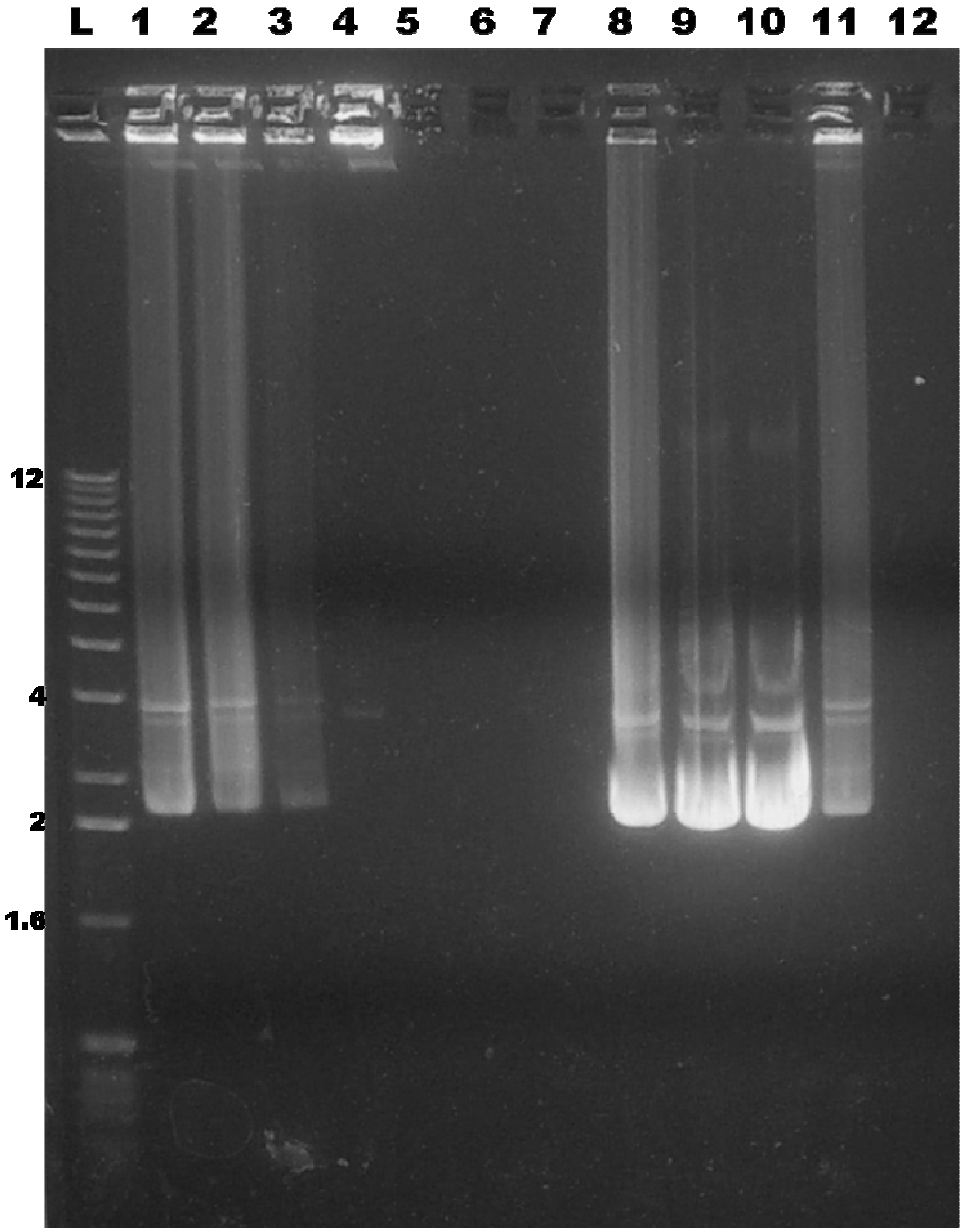

Figure 5.7 Agarose gel analysis of the beta toxin-DNA reaction pellet treated with 0.05, 0.25. 0.5, or 2.5 M BME (lanes 1-4), 2, 10, or 20 U DNase I (lanes 5-7); 2, 20, or 100 µg proteinase K (lanes 8-10). Lane L contains the 1 KB ladder and select bands are labeled (kb). Lane 11 contains the untreated pellet, and lane 12 contains the untreated supernatant.

"Inactive" beta toxin precipitates DNA. From the homology between beta toxin and DNase I, H150 and H289 were identified as residues required for SMase activity. Mutating these residues individually to asparagine abolishes both SMase activity and lethality toward proliferating human lymphocytes (44). However, neither of these mutations has any detectable effect upon DNA-binding (Figure 5.3) or precipitation (Figure 5.8). This suggests the reactive residue producing cross-linking is distinct from those producing SMase activity.

Beta toxin is cross-linked only in the presence of DNA. In the PAGE analysis bands corresponding to oligomers of beta toxin are observed in the precipitate but not in the supernatant. Nor are they seen in control incubations without DNA (Figure 5.4 and Figure 5.5). Addition of a soluble protein that does not bind DNA produces additional bands in SDS-PAGE corresponding to beta toxin cross-linked to the quenching protein (Figure 5.9). We hypothesize that the activated residue can attack any target residue creating a covalent bond. This could be another protein, or a carbohydrate, or a sugar with the proper moiety to perform the chemistry.

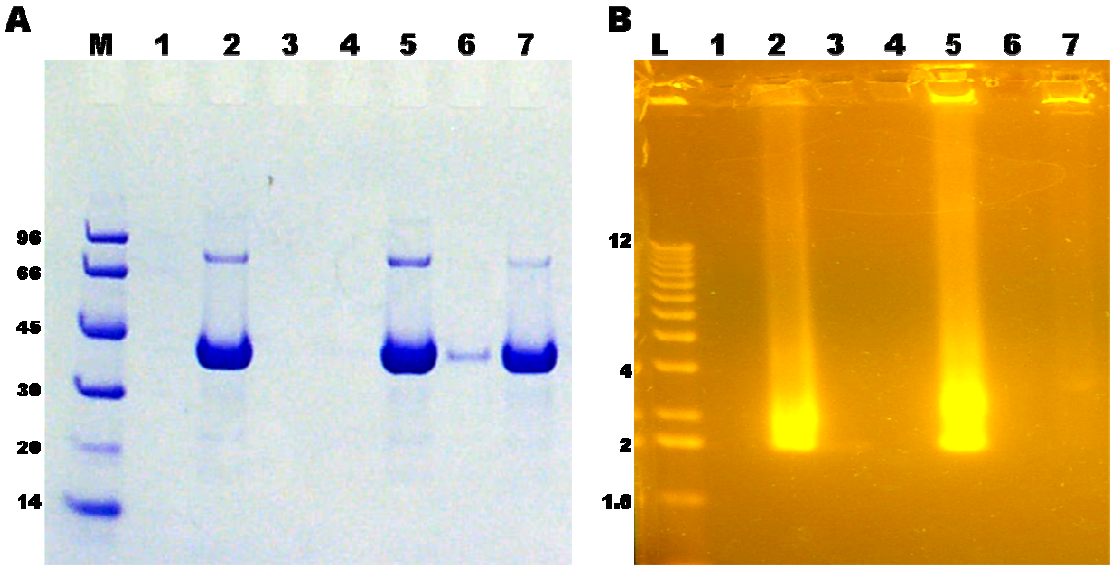

Figure 5.8 Inactive SMase mutants oligomerize in the presence of DNA. (A) SDS PAGE analysis of native beta toxin, H150N, and H298N pellets reacted with pUC 18 DNA as described in the materials and methods section (supernatants not shown). Lane M denotes the low molecular weight marker and bands are labeled (kDa). Lane 1 contains native beta toxin only. Lane 2 contains native beta toxin with 12 μg pUC18 DNA, while lane 3 contains DNA only. Lanes 4 and 5 contain H150N without and with 12 μg pUC18 DNA, respectively. Lanes 6 and 7 are identical to 4 and 5 except using H289N. For all experiments 100 μg of protein was used. (B) Agarose gel analysis of native beta toxin, H150N, and H289N. Lane L contains a 1Kb ladder and select bands are labeled (kb). Lanes 1-7 are identical to those listed in Figure 5.8A.

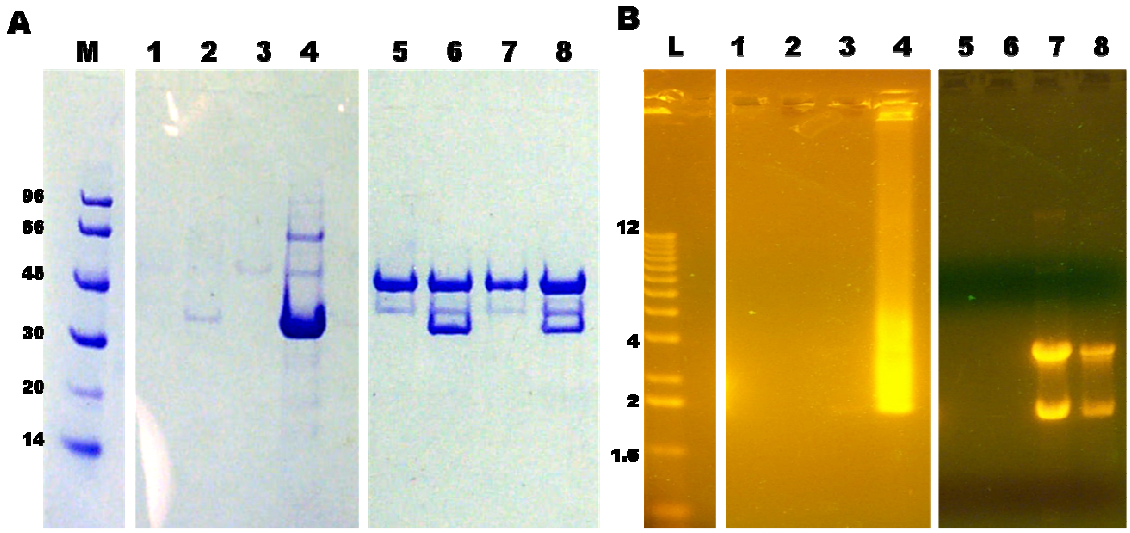

Figure 5.9 Beta toxin cross-links and precipitates other proteins. The reactions were reacted as described previously. Results for both the precipitate (lanes 1-4) and the supernatant (lanes 5-8) are shown. (A) SDS-PAGE analysis of beta toxin precipitated with DNA and C5A peptidase. Lane M is the low molecular weight marker and bands are labeled (kDa). Lane 1 contains C5A peptidase only. Lane 2 contains C5A peptidase and 12 μg DNA. Lane 3 contains C5A peptidase and beta toxin. Lane 4 contains C5A peptidase, beta toxin and 12 μg DNA. Lanes 5-8 contents are the supernatants of the reactions of lanes 1-4. (B) Agarose gel analysis of beta toxin precipitated with DNA and C5A peptidase. Lane L contains the 1 kb ladder and select bands are labeled (kb). Lanes 1-8 are identical to that in Figure 5.9A.

Cross-Link Analysis

These data have led us to hypothesize that beta toxin binds DNA and that DNA catalyzes cross-linking of beta toxin. This oligomerization requires DNA because the oligomers do not form unless beta toxin has been incubated with DNA. Although we cannot rule out oligomers joined by short pieces of tightly bound DNA that might be protected from digestion (as in a DNase I protection footprint), regions of DNA between the bound beta toxins will be digested. Therefore it is likely that the oligomers are not linked by DNA as digestion by DNase I does not eliminate them. The linkage is

covalent because it is not disrupted by SDS and 8M urea. It is not from disulfide formation as an additional incubation in 100mM β-mercaptoethanol does not eliminate the oligomerization.

The band on the SDS gel for the beta toxin dimer was cut out, the protein extracted and digested with immobilized trypsin, and the result subjected to electrospray mass spectrometry. Four of the predicted 24 peptides with masses greater than 500 Daltons are not seen (Figure 5.10). Since the reaction depends upon DNA binding, the cross-linking active site needs to contact bound DNA. Given this constraint, tryptic peptides Asn143-Arg157 or Cys158-Arg164 may include the reactive residue.

MS revealed no new larger fragment(s) as might be expected if there were an isopeptide cross-link. However, we believe that the reactive residue is rather indiscriminate in its target. Thus a large number of unique isopeptide-linked fragments would be produced exacerbating identification of the reaction product. The observation that other soluble proteins are able to react with the reactive residue and block DNA precipitation is supportive of this hypothesis.

If the linkage is an isopeptide bond then either the reactive residue or its target is a carboxylate. There are several possible residues that could be involved in cross-linking. We can eliminate cysteine because (1) the crosslink is not subject to reductive cleavage, and (2) there are only 2 cysteines in beta toxin and they form an internal disulfide linkage. It is unlikely to be a tyrosyl hydroxyl as the product has no color unlike many tyrosyl adducts. We hypothesize that the oligomerization is through isopeptide bonds between lysine and acidic or amide side chains. Such linkages are seen when proteins are ubiquitinated (40). Although crosslinks via a serine or threonine are possible, we believe an amino group (lysine), a carboxylate (aspartate or glutamate), or a glutamine to be involved (32). However, the chemistry remains to be determined.

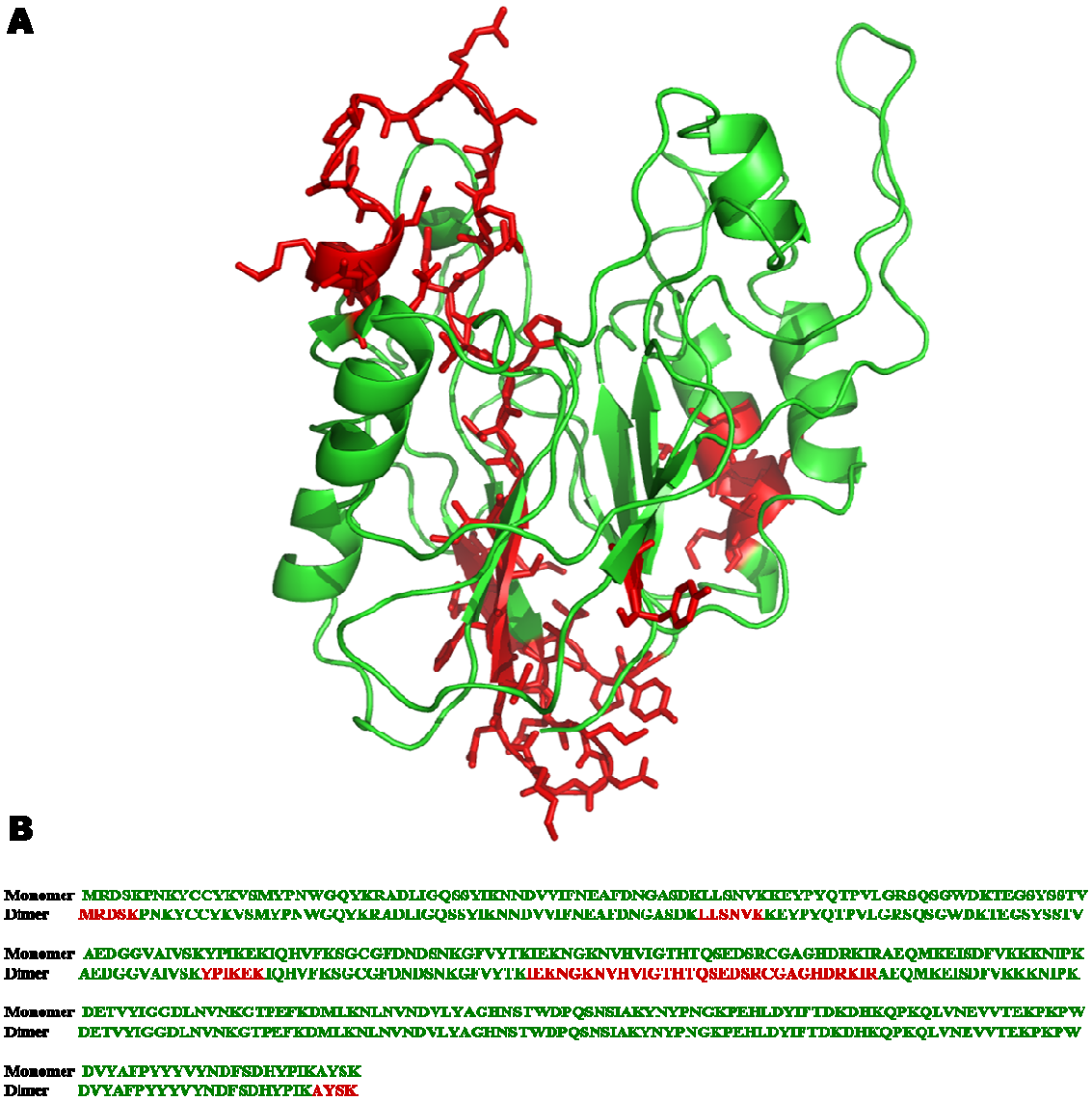

Figure 5.10 Cartoon representation and sequence of beta toxin dimer as revealed by electrospray mass spectrometry. Beta toxin was reacted with plasmid pUC 18 DNA, and the precipitant ran on an SDS gel. The bands corresponding to the dimer and monomer were cut out and analyzed. (A) Cartoon representation of beta toxin monomer. Hydrophobic beta hairpin is on the upper right of the molecule. The sequence which was detected in both the monomer and dimer is in green cartoon. Sequence not found in the dimer is in red and represented as sticks. (B) Sequence comparison of the reacted beta toxin monomer and dimers. Coloring is the same as Figure 5.10A.

Adherence and Biofilm Studies

Beta toxin stimulates adherence and growth of biofilms. The *hlb* gene for beta toxin in *S. aureus* COL (*hlb*$^{+}$) was disrupted by insertion of phage Φ11 to produce *S. aureus* COL *hlb*$^{-}$. As eDNA is an important component of biofilms (71), these organisms were compared to reference strain *S. aureus* UAMS-1 for the effect of beta toxin on adherence and biofilm growth.

Figure 5.11 reports the effect of the presence of beta toxin on cell adherence to 96 well plates coated with human plasma. *S. aureus* COL (*hlb*$^{+}$) showed 2-fold higher adherence than *S. aureus* UAMS-1 (13), (9), (71). It should be noted that *S. aureus* UAMS-1 does have the phage insertion into the *hlb* gene and, consequently, lacks the active beta toxin gene product. *S. aureus* COL *hlb*$^{-}$ shows decreased adherence compared to *S. aureus* UAMS-1 and a 2 fold difference from *S. aureus* COL (*hlb*$^{+}$). Supplying beta toxin on plasmid pCN51 into *S. aureus* COL *hlb*$^{-}$ nearly restores adherence to that of native *S. aureus* COL (*hlb*$^{+}$).

Figure 5.12 shows the effect of the presence of beta toxin on the growth of biofilms in flow cells over 3 days. *S. aureus* COL (*hlb*$^{+}$) has a much more robust (faster growing, thicker) biofilm when compared to *S. aureus* COL *hlb*$^{-}$. Indeed, when the biofilms are stained and the average thickness calculated after three days of growth, *S. aureus* COL (*hlb*$^{+}$) is on average 60 nm thicker (Figure 5.13). A growth defect of *S. aureus* COL *hlb*$^{-}$ is not the cause as growth curve analysis shows *S. aureus* COL *hlb*$^{-}$ grows at a slightly faster rate than *S. aureus* COL (*hlb*$^{+}$) (Figure 5.14). And, finally, supplying *hlb* on pCN51 to *S. aureus* COL *hlb*$^{-}$ partially restores the phenotype.

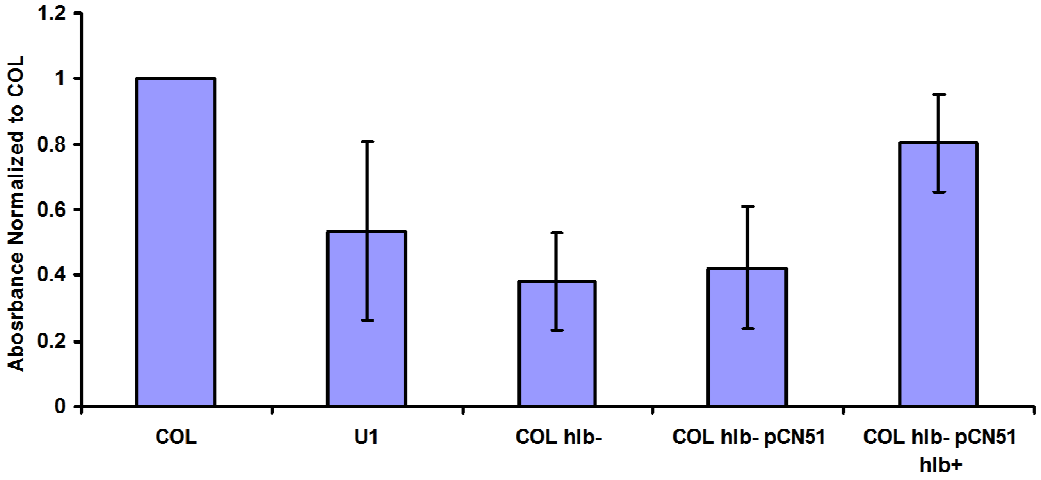

Figure 5.11 Adherence of COL was compared to that of UAMS1 (U1) and COL *hlb*$^{-}$. Expression of beta toxin on the pCN51 plasmid in the COL *hlb*$^{-}$ background rescued the phenotype (COL *hlb*$^{-}$ pCN51 *hlb*$^{+}$). The empty plasmid (COL *hlb*$^{-}$ pCN51) expressed in showed slightly higher levels of adherence than that of COL *hlb*$^{-}$.

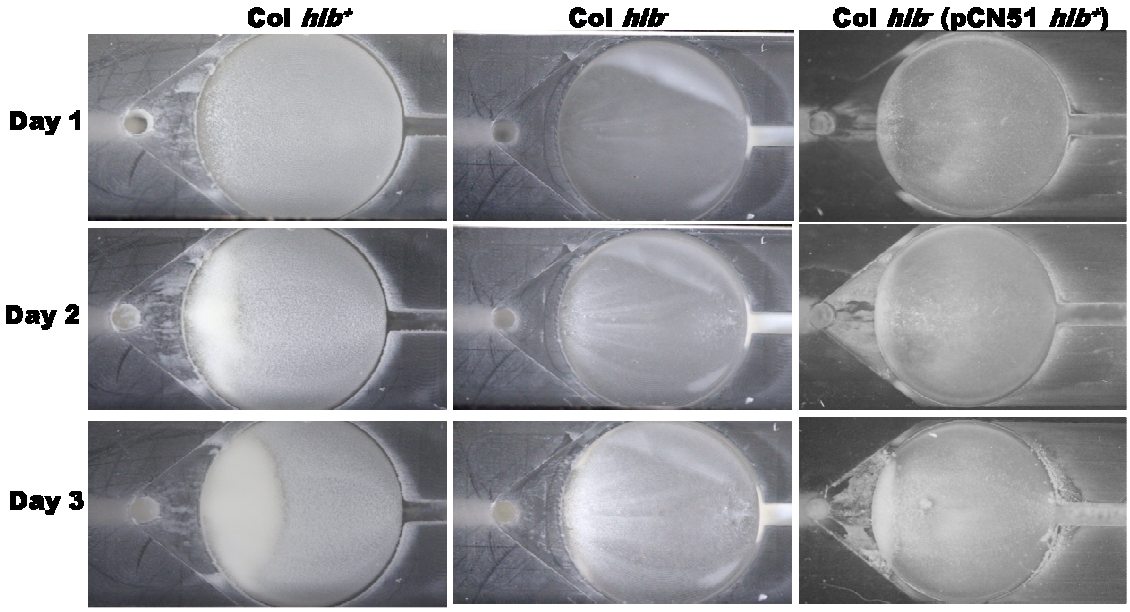

Figure 5.12 Beta toxin is an important biofilm factor. Pictures were taken over the course of three days of biofilm development. COL *hlb*$^{+}$ is on the left column, COL *hlb*$^{-}$ is in the middle, and COL *hlb*$^{-}$ pCN51 *hlb*$^{+}$ is on the right. Biofilm is the white fuzzy growth on the left of the circular cassette. COL *hlb*$^{-}$ pCN51 *hlb*$^{+}$ shows a partial rescue of the COL *hlb*$^{+}$ phenotype. Vector alone (COL *hlb*$^{-}$ pCN51) was similar to that of COL *hlb*$^{-}$ (not shown).

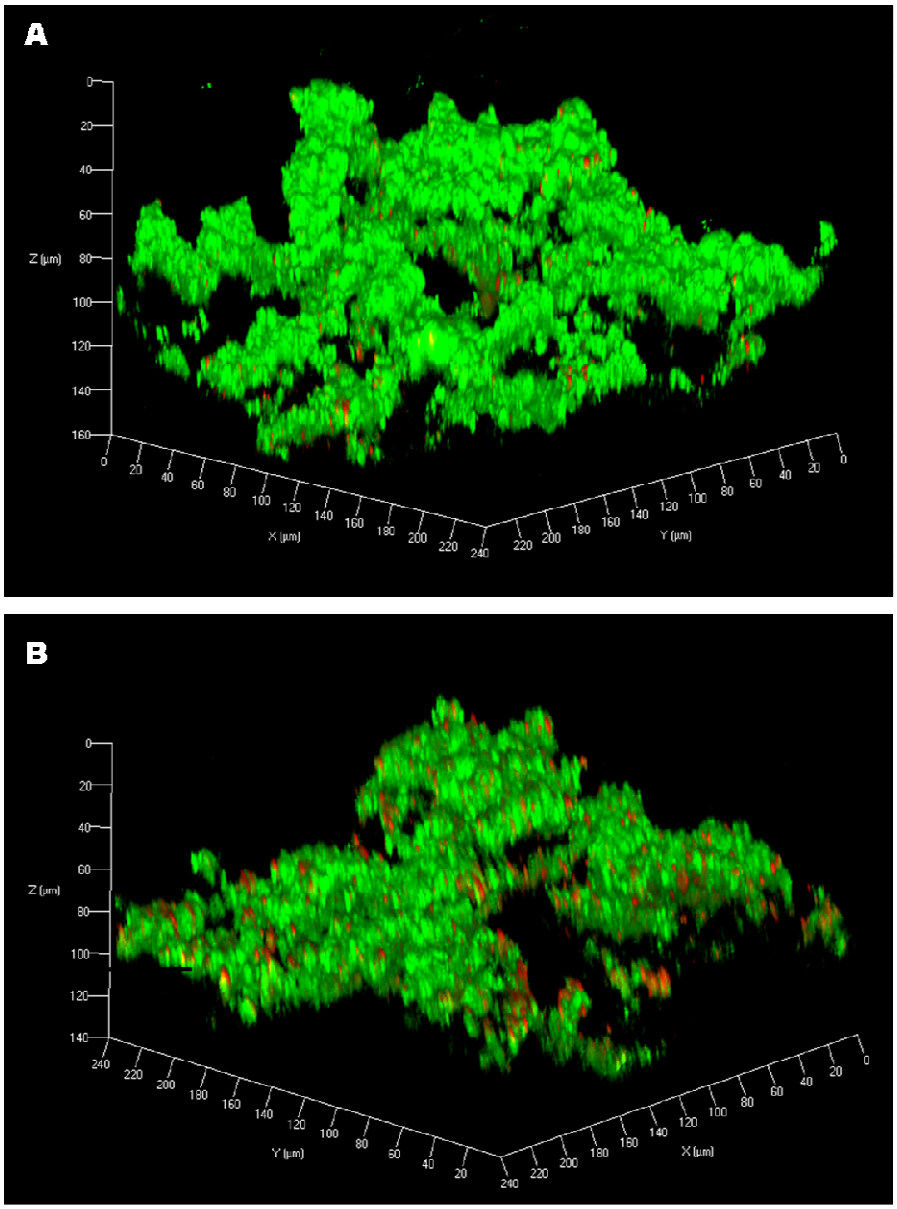

Figure 5.13 COL *hlb*$^{+}$ produces a thicker biofilm. Confocal microscopy images of COL *hlb*$^{+}$ and COL *hlb*$^{-}$. (A) Representative sample from the COL *hlb*$^{+}$ biofilm growth from figure 5.12 stained with syto-9 (green) and todo-3 (red). The average thickness is approximately 160 nm. (B) Representative sample from COL *hlb*$^{-}$ biofilm growth from figure 5.12. Stained identical to that of Figure 5.13A. The average thickness is approximately 100 nm.

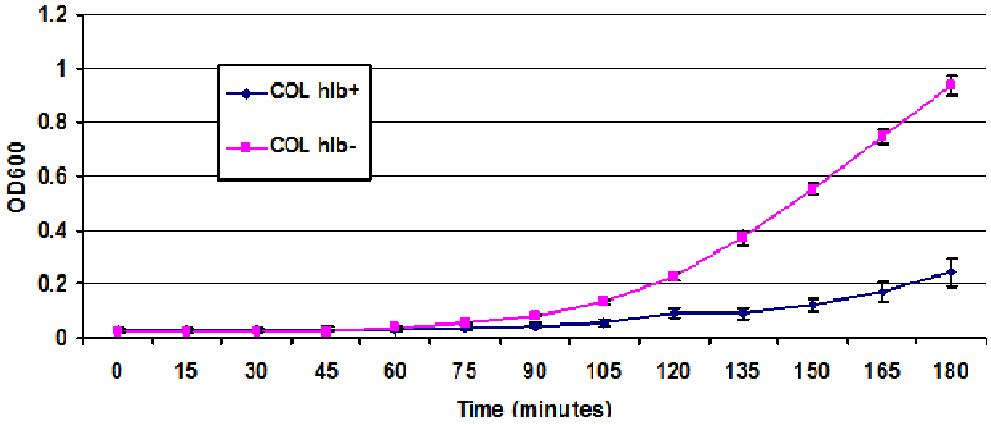

Figure 5.14 Growth curve analysis of COL *hlb*$^{+}$ and COL *hlb*$^{-}$. COL *hlb*$^{-}$ enters log phase after 120 min of growth. COL *hlb*$^{+}$ does not begin to enter log phase until 165 min of growth. Both strains were grown in triplicate and the experiment repeated twice. Error bars represent the standard deviation.

The *hlb* gene has been shown to be present in MRSA urinary tract infections, particularly those involving biofilm formation on catheters, as detected by PCR (5). This study is the first to show a direct role for the *hlb* gene product in biofilm formation. Some of the proteinacious components of *S. aureus* biofilms are known, such as Bap (biofilm association protein) (25), SasG (surface associated *Staphylococcus* Protein G) (22), and Protein A (57). However, this is the first evidence for the *hlb* gene product, beta toxin, having a direct role on biofilm formation.

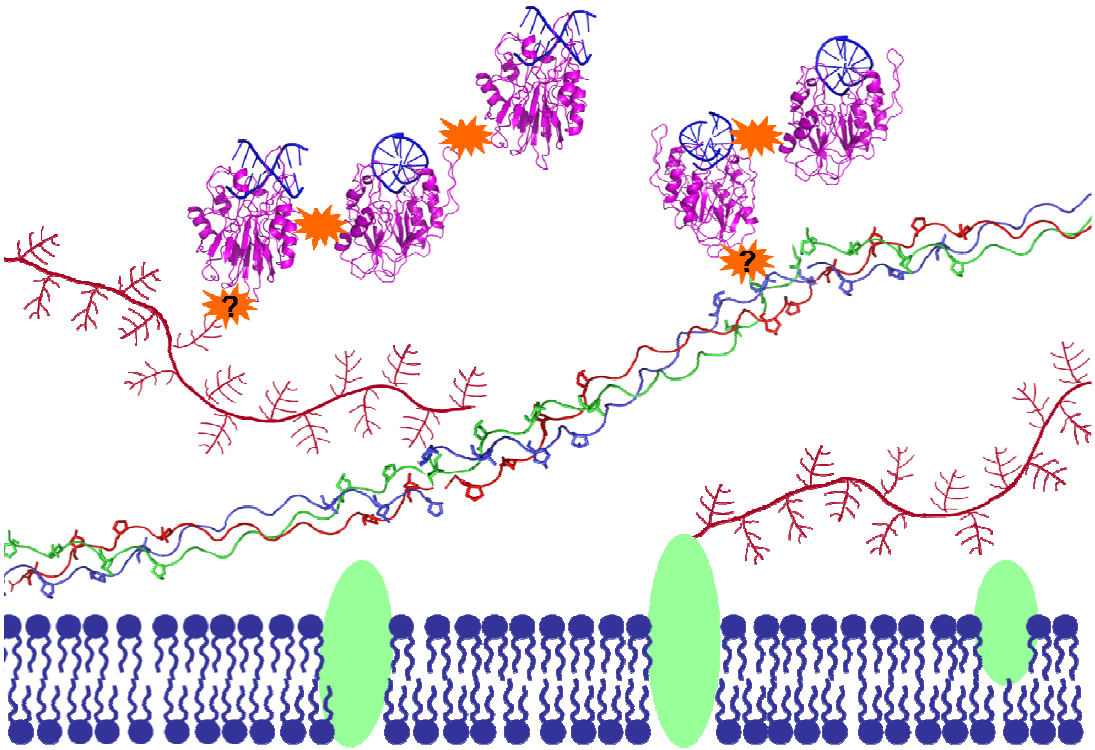

Figure 5.15 Model of beta toxin forming a nucleoprotein network in the extracellular matrix. Beta toxin (magenta cartoon) binds eDNA (blue helix) and cross-links non-specifically (orange star burst, question marks represent potential cross-links) to itself and other proteins. Other molecules that beta toxin may crosslink to are hyaluronic acid (red strands with branches) and collagen (PDB entry 1CDG, red, green, and blue fibrils). The plasma membrane (blue lipids) is punctuated with integral membrane proteins (light green ovals).

Conclusion

These experiments show that beta toxin in the presence of DNA is able to cross-link with itself or other proteins. The nature of the cross-link needs to be considered. It is possible that binding DNA triggers a conformational change that allows refolding of beta toxin into a molecule that forms an SDS and 8 M urea resistant interaction. The interaction has to be one-sided as adding a soluble quenching protein that does not

interact with DNA can accept these resistant interactions. While this is possible, a more likely explanation is the formation of a covalent bond.

Our initial hypothesis is that the cross-link is an isopeptide bond. Spontaneous isopeptide bond formation in gram positive bacterial pili has been documented (46). Assuming that the target of the beta toxin cross-link is something as simple as an amino or carboxyl group, it can form cross-links with nearly any protein. If the target protein is bound to eDNA or extracellular polysaccharides then a matrix is formed that can give stability to a biofilm. Moreover, with such a simple target, beta toxin could cross-link directly to carbohydrate in cell walls or in the extracellular matrix (Figure 5.15). Such direct interaction would be more efficient since cross-link formation would be first order (encountering target on an extracellular polymer) rather than second order (encountering target on protein bound to an extracellular polymer). This could explain the very strong stimulatory effect of beta toxin upon biofilm formation *in vivo*.

The connection between environmental signals and regulation of specific stages of biofilm formation is under investigation. Beta toxin is regulated post-exponentially by *agr* locus (61). This is consistent with studies reporting a role of *agr* in biofilm formation (48), (85). As no simple genetic switch has been identified to cause planktonic bacteria to switch to biofilm formation (58), it is not surprising that beta toxin can fill multiple virulence roles, i.e., lysis of cells and formation of a biofilm matrix.

The structural family of DNase I homologs is very large. The discovery of this activity in beta toxin suggests that similar activities might be present in molecules with the same fold and these molecules could also contribute to the formation of biofilms. Furthermore, viral eDNA has been found in amyloid plaques associated with Alzheimer's disease (97). It is possible that the nucleic acid induced non-specific cross linking mechanism is involved in this process, as well. It will be crucial to identify and characterize the chemistry of the crosslink to further understand this mechanism.

The importance of biofilms in pathogenic bacteria is well known. These studies point, for the first time, to a molecular mechanism for forming the structural framework of staphylococcal biofilms. This revelation opens the door to new avenues of treatment

as increased antibiotic resistance becomes more prevalent and as the critical role of biofilms in bacterial virulence becomes increasingly apparent.

REFERENCES

1. 2006. Introduction to Basic Crystallography. International Tables for Crystallography **F:**61-62.
2. **Aarestrup, F. M., H. D. Larsen, N. H. Eriksen, C. S. Elsberg, and N. E. Jensen.** 1999. Frequency of α- and β-haemolysin in Staphylococcus aureus of bovine and human origin. A comparison between pheno- and genotype and variation in phenotypic expression. APMIS **107:**425–430.
3. **Ago, H., M. Oda, M. Takahashi, H. Tsuge, S. Ochi, N. Katunuma, M. Miyano, and J. Sakurai.** 2006. Structural basis of the sphingomyelin phosphodiesterase activity in neutral sphingomyelinase from Bacillus cereus. J. Biol. Chem **281:**16157–16167.
4. **Alexander, G. A.** 1981. Improved lyophilization procedure for storage of reference cultures and clinical isolates. J Clin Microbiol **13:**805-6.
5. **Ando, E., K. Monden, R. Mitsuhata, R. Kariyama, and H. Kumon.** 2004. Biofilm formation among methicillin-resistant Staphylococcus aureus isolates from patients with urinary tract infection. Acta Med Okayama **58:**207-14.
6. **Archer, G. L.** 1998. Staphylococcus aureus: A well-armed pathogen. Clinical Infectious Diseases **26:**1179-81.
7. **Barsumian, E. L., P. M. Schlievert, and D. W. Watson.** 1978. Nonspecific and specific immunological mitogenicity by group A streptococcal pyrogenic exotoxins. Infect. Immun **22:**681–688.
8. **Beenken, K. E., J. S. Blevins, and M. S. Smeltzer.** 2003. Mutation of sarA in Staphylococcus aureus limits biofilm formation. Infect Immun **71:**4206-11.
9. **Beenken, K. E., P. M. Dunman, F. McAleese, D. Macapagal, E. Murphy, S. J. Projan, J. S. Blevins, and M. S. Smeltzer.** 2004. Global gene expression in Staphylococcus aureus biofilms. J Bacteriol **186:**4665-84.
10. **Berman, H. M., J. Westbrook, Z. Feng, G. Gilliland, T. N. Bhat, H. Weissig, I. N. Shindyalov, and P. E. Bourne.** 2000. The Protein Data Bank. Nucleic Acids Res **28:**235-42.
11. **Bigger, J., C. Borland, and R. O'Meara.** 1927. A new method of preparing staphylococcal haemolysin. J Pathol. Bacteriol. **30:**271-277.
12. **Bladon, C. M., P. Bladon, and J. A. Parkinson.** 1992. Delta-toxin and analogues as peptide models for protein ion channels. Biochem Soc Trans **20:**862-4.
13. **Blevins, J. S., K. E. Beenken, M. O. Elasri, B. K. Hurlburt, and M. S. Smeltzer.** 2002. Strain-dependent differences in the regulatory roles of sarA and agr in Staphylococcus aureus. Infect Immun **70:**470-80.

14. **Blomster-Hautamaa, D. A., and P. M. Schlievert.** 1988. Preparation of toxic shock syndrome toxin-1. Methods Enzymol **165**.
15. **Bramley, A. J., A. H. Patel, M. O'Reilly, R. Foster, and T. J. Foster.** 1989. Roles of alpha-toxin and beta-toxin in virulence of Staphylococcus aureus for the mouse mammary gland. Infect Immun **57:**2489-94.
16. **Briggs, P.** 2005. Notes on Twinning and CCP4 http://www.ccp4.ac.uk/peter/documents/twinning/twinning.html.
17. **Clarke, C. J., C. F. Snook, M. Tani, N. Matmati, N. Marchesini, and Y. A. Hannun.** 2006. The extended family of neutral sphingomyelinases. Biochemistry **45:**11247-56.
18. **Coleman, D., J. Knights, R. Russell, D. Shanley, T. H. Birkbeck, G. Dougan,, and a. I. Charles.** 1991. Insertional inactivation of the Staphylococcus aureus β-toxin by bacteriophage Φ13 occurs by site- and orientation-specific integration of the Φ13 genome. . Mol. Microbiol **5:**933–939.
19. **Coleman, D. C., D. J. Sullivan, R. J. Russell, J. P. Arbuthnott, B. F. Carey, and H. M. Pomeroy.** 1989. Staphylococcus aureus bacteriophages mediating the simultaneous lysogenic conversion of β-lysin, staphylokinase and enterotoxin A: molecular mechanism of triple conversion. J. Gen. Microbiol **135:**1679–1697.
20. **Coleman, D. C., J. P. Arbuthnott, H. M. Pomeroy, and T. H. Birkbeck.** 1986. Cloning and expression in Escherichia coli and Staphylococcus aureus of the β-lysin determinant from Staphylococcus aureus: evidence that bacteriophage conversion of β-lysin activity is caused by insertional inactivation of the β-lysin determinant. Microb. Pathog **1:**549–564.
21. **Collins, J., A. Buckling, and R. C. Massey.** 2008. Identification of factors contributing to T-cell toxicity of Staphylococcus aureus clinical isolates. J Clin Microbiol **46:**2112-4.
22. **Corrigan, R. M., D. Rigby, P. Handley, and T. J. Foster.** 2007. The role of Staphylococcus aureus surface protein SasG in adherence and biofilm formation. Microbiology **153:**2435-46.
23. **Costerton, J. W., K. J. Cheng, G. G. Geesey, T. I. Ladd, J. C. Nickel, M. Dasgupta, and T. J. Marrie.** 1987. Bacterial biofilms in nature and disease. Annu Rev Microbiol **41:**435-64.
24. **Costerton, J. W., Z. Lewandowski, D. E. Caldwell, D. R. Korber, and H. M. Lappin-Scott.** 1995. Microbial biofilms. Annu Rev Microbiol **49:**711-45.
25. **Cucarella, C., C. Solano, J. Valle, B. Amorena, I. Lasa, and J. R. Penades.** 2001. Bap, a Staphylococcus aureus surface protein involved in biofilm formation. J Bacteriol **183:**2888-96.
26. **Dao-pin, S., D. E. Anderson, W. A. Baase, F. W. Dahlquist, and B. W. Matthews.** 1991. Structural and thermodynamic consequences of burying a charged residue within the hydrophobic core of T4 lysozyme. Biochemistry **30:**11521–11529.
27. **De la Mora Rey, T.** 2008. Crystallographic and Biochemical Studies of Methylamine Dehydrogenase from *Paracoccus denitificans*: a Tryptophan

Tryptophylquinone Containing Enzyme. PhD Thesis. University of Minnesota, Minneapolis.

28. **Dinges, M. M., P. M. Orwin, and P. M. Schlievert.** 2000. Exotoxins of Staphylococcus aureus. Clin. Microbiol. Rev **13:**16–34.
29. **Dobrowsky, R. T., and Y. A. Hannun.** 1992. Ceramide stimulates a cytosolic protein phosphatase. J Biol Chem **267:**5048-51.
30. **Dunman, P. M., E. Murphy, S. Haney, D. Palacios, G. Tucker-Kellogg, S. Wu, E. L. Brown, R. J. Zagursky, D. Shlaes, and S. J. Projan.** 2001. Transcription profiling-based identification of Staphylococcus aureus genes regulated by the agr and/or sarA loci. J Bacteriol **183:**7341-53.
31. **Dziewanowska, K., V. M. Edwards, J. R. Deringer, G. A. Bohach, and D. J. Guerra.** 1996. Comparison of the β-toxins from Staphylococcus aureus and Staphylococcus intermedius. Arch. Biochem. Biophys **335:**102–108.
32. **Folk, J. E., and J. S. Finlayson.** 1977. The epsilon-(gamma-glutamyl)lysine crosslink and the catalytic role of transglutaminases. Adv Protein Chem **31:**1-133.
33. **Giacovazzo, C.** 1992. Fundamentals of Crystallography. Oxford Univ Press New York.
34. **Giantonio, B. J., R. K. Alpaugh, J. Schultz, C. McAleer, D. W. Newton, B. Shannon, Y. Guedez, M. Kotb, L. Vitek, R. Persson, P. O. Gunnarsson, T. Kalland, M. Dohlsten, B. Persson, and L. M. Weiner.** 1997. Superantigen-based immunotherapy: a phase I trial of PNU-214565, a monoclonal antibody-staphylococcal enterotoxin A recombinant fusion protein, in advanced pancreatic and colorectal cancer. J Clin Oncol **15:**1994-2007.
35. **Gonzalez-Zorn, B., G. Dominguez-Bernal, M. Suarez, M. T. Ripio, Y. Vega, S. Novella, and J. A. Vazquez-Boland.** 1999. The smcL gene of Listeria ivanovii encodes a sphingomyelinase C that mediates bacterial escape from the phagocytic vacuole. Mol Microbiol **33:**510-23.
36. **Gotz, F.** 2002. Staphylococcus and biofilms. Mol Microbiol **43:**1367-78.
37. **Gouaux, J. E., O. Braha, M. R. Hobaugh, L. Song, S. Cheley, C. Shustak, and H. Bayley.** 1994. Subunit stoichiometry of staphylococcal α-hemolysin in crystals and on membranes: a heptameric transmembrane pore. Proc. Natl. Acad. Sci. USA **91:**12828–12831.
38. **Hendrickson, W. A., J.R. Horton, and D.M. LeMaster.** 1990. Selenomethionyl proteins produced for analysis by multiwavelength anomalous diffraction (MAD): a vehicle for direct determination of three-dimensional structure. Embo J **9:**1665-72.
39. **Herbst-Irmer, R., and G. M. Sheldrick.** 2002. Refinement of obverse/reverse twins. Acta Crystallogr B **58:**477-81.
40. **Hershko, A., and A. Ciechanover.** 1992. The ubiquitin system for protein degradation. Annu Rev Biochem **61:**761-807.
41. **Hiramatsu, K., H. Hanaki, T. Ino, K. Yabuta, T. Oguri, and F. C. Tenover.** 1997. Methicillin-resistant Staphylococcus aureus clinical strain with reduced vancomycin susceptibility. Journal of Antimicrobial Chemotherapy **40:**135-6.

42. **Holm, L., and C. Sander.** 1997. DALI/FSSP classification of three-dimensional protein folds. Nucleic Acids Res. **25:**231–234.
43. **Holm, L., and C. Sander.** 1993. Protein structure comparison by alignment of distance matrices. J. Mol. Biol **233:**123–138.
44. **Huseby, M., K. Shi, C. K. Brown, J. Digre, F. Mengistu, K. S. Seo, G. A. Bohach, P. M. Schlievert, D. H. Ohlendorf, and C. A. Earhart.** 2007. Structure and biological activities of beta toxin from Staphylococcus aureus. J Bacteriol **189:**8719-26.
45. **Johnson, S. M., and R. Robinson.** 1979. The composition and fluidity of normal and leukaemic or lymphomatous lymphocyte plasma membranes in mouse and man. Biochim Biophys Acta **558:**282-95.
46. **Kang, H. J., F. Coulibaly, F. Clow, T. Proft, and E. N. Baker.** 2007. Stabilizing isopeptide bonds revealed in gram-positive bacterial pilus structure. Science **318:**1625-8.
47. **Krissinel, E., and K. Henrick.** 2004. Secondary-structure matching (SSM), a new tool for fast protein structure alignment in three dimensions. Acta Crystallogr. Sect. D **60:**2256–2268.
48. **Lauderdale, K. J., B. R. Boles, A. L. Cheung, and A. R. Horswill.** 2009. Interconnections between Sigma B, agr, and proteolytic activity in Staphylococcus aureus biofilm maturation. Infect Immun **77:**1623-35.
49. **Lowy, F. D.** 1998. Staphylococcus aureus infections. N. Engl. J. Med **339:**520–532.
50. **Mack, D., W. Fischer, A. Krokotsch, K. Leopold, R. Hartmann, H. Egge, and R. Laufs.** 1996. The intercellular adhesin involved in biofilm accumulation of Staphylococcus epidermidis is a linear beta-1,6-linked glucosaminoglycan: purification and structural analysis. J Bacteriol **178:**175-83.
51. **Maranan, M. C., B. Moreira, S. Boyle-Vavra, and R. S. Daum.** 1997. Antimicrobial resistance in staphylococci. Epidemiology, molecular mechanisms, and clinical relevance. Infectious Disease Clinics of North America **11:**813-49.
52. **Marrack, P., and J. Kappler.** 1990. The staphylococcal enterotoxins and their relatives. Science **248:**705–711.
53. **Marshall, M. J., G. A. Bohach, and D. F. Boehm.** 2000. Characterization of Staphylococcus aureus beta-toxin induced leukotoxicity. J Nat Toxins **9:**125-38.
54. **Marshall, M. J., G. A. Bohach, and D. F. Boehm.** 2000. Characterization of Staphylococcus aureus beta-toxin induced leukotoxicity. J. Nat. Toxins **9:**125–138.
55. **Matsuo, Y., A. Yamada, K. Tsukamoto, H. Tamura, H. Ikezawa, H. Nakamura, and K. Nishikawa.** 1996. A distant evolutionary relationship between bacterial sphingomyelinase and mammalian DNase I. Protein Sci **5:**2459–2467.
56. **McCormick, J. K., J. M. Yarwood, and P. M. Schlievert.** 2001. Toxic shock syndrome and bacterial superantigens: an update. Annu. Rev. Microbiol. **55:**77–104.

57. **Merino, N., A. Toledo-Arana, M. Vergara-Irigaray, J. Valle, C. Solano, E. Calvo, J. A. Lopez, T. J. Foster, J. R. Penades, and I. Lasa.** 2009. Protein A-mediated multicellular behavior in Staphylococcus aureus. J Bacteriol **191:**832-43.
58. **Monds, R. D., and G. A. O'Toole.** 2009. The developmental model of microbial biofilms: ten years of a paradigm up for review. Trends Microbiol **17:**73-87.
59. **Munch-Petersen, E., and C. Boundy.** 1962. Yearly incidence of penicillin-resistant staphylococci in man since 1942. Bulletin of the World Health Organization **26:**241-52.
60. **Murshudov, G. N., A. A. Vagin, and E. J. Dodson.** 1997. Refinement of macromolecular structures by the maximum-likelihood method. Acta Crystallogr. Sect. D **53:**240–255.
61. **Novick, R. P.** 2003. Autoinduction and signal transduction in the regulation of staphylococcal virulence. Mol Microbiol **48:**1429-49.
62. **Novick, R. P., and E. Geisinger.** 2008. Quorum sensing in staphylococci. Annu Rev Genet **42:**541-64.
63. **Obama, T., Y. Kan, H. Ikezawa, M. Imagawa, and K. Tsukamoto.** 2003. Glu-53 of Bacillus cereus sphingomyelinase acts as an indispensable ligand of Mg2+ essential for catalytic activity. J. Biochem. (Tokyo) **133:**279–286.
64. **Obeid, L. M., C. M. Linardic, L. A. Karolak, and Y. A. Hannun.** 1993. Programmed cell death induced by ceramide. Science **259:**1769-71.
65. **Olczak, A., M. Cianci, Q. Hao, P. J. Rizkallah, J. Raftery, and J. R. Helliwell.** 2003. S-SWAT (softer single-wavelength anomalous technique): potential in high-throughput protein crystallography. Acta Crystallogr A **59:**327-34.
66. **Openshaw, A. E., P. R. Race, H. J. Monzo, J. A. Vazquez-Boland, and M. J. Banfield.** 2005. Crystal structure of SmcL, a bacterial neutral sphingomyelinase C from Listeria. J. Biol. Chem **280:**35011–35017.
67. **Padilla, J. E., and T. O. Yeates.** 2003. A statistic for local intensity differences: robustness to anisotropy and pseudo-centering and utility for detecting twinning. Acta Crystallogr D Biol Crystallogr **59:**1124-30.
68. **Pearl, F. M., C. F. Bennett, J. E. Bray, A. P. Harrison, N. Martin, A. Shepherd, I. Sillitoe, J. Thornton, and C. A. Orengo.** 2003. The CATH database: an extended protein family resource for structural and functional genomics. Nucleic Acids Res.**:**452–455.
69. **Ren, S. X., G. Fu, X. G. Jiang, R. Zeng, Y. G. Miao, H. Xu, Y. X. Zhang, H. Xiong, G. Lu, L. F. Lu, H. Q. Jiang, J. Jia, Y. F. Tu, J. X. Jiang, W. Y. Gu, Y. Q. Zhang, Z. Cai, H. H. Sheng, H. F. Yin, Y. Zhang, G. F. Zhu, M. Wan, H. L. Huang, Z. Qian, S. Y. Wang, W. Ma, Z. J. Yao, Y. Shen, B. Q. Qiang, Q. C. Xia, X. K. Guo, A. Danchin, I. Saint Girons, R. L. Somerville, Y. M. Wen, M. H. Shi, Z. Chen, J. G. Xu, and G. P. Zhao.** 2003. Unique physiological and pathogenic features of Leptospira interrogans revealed by whole genome sequencing. Nature **422:**888–893.

70. **Rhodes, G.** 2000. Crystallography Made Crystal Clear: A Guide for Users of Macromolecular Models, Second ed. Academic Press, San Diego, CA.
71. **Rice, K. C., E. E. Mann, J. L. Endres, E. C. Weiss, J. E. Cassat, M. S. Smeltzer, and K. W. Bayles.** 2007. The cidA murein hydrolase regulator contributes to DNA release and biofilm development in Staphylococcus aureus. Proc Natl Acad Sci U S A **104:**8113-8.
72. **Roblin, P., V. Guillet, O. Joubert, D. Keller, M. Erard, L. Maveyraud, G. Prevost, and L. Mourey.** 2008. A covalent S-F heterodimer of leucotoxin reveals molecular plasticity of beta-barrel pore-forming toxins. Proteins **71:**485-96.
73. **Rose, J., C. Wu, Z. Liu, G. Newton, and B. Wang.** 2001. Using single wavelength anomalous scattering data from in-house protein structrue determination. Rigaku Journal **18:**4-12.
74. **Sawai, H., and Y. A. Hannun.** 1999. Ceramide and sphingomyelinases in the regulation of stress responses. Chem Phys Lipids **102:**141-7.
75. **Sawai, H., T. Okazaki, H. Yamamoto, H. Okano, Y. Takeda, M. Tashima, H. Sawada, M. Okuma, H. Ishikura, H. Umehara, and et al.** 1995. Requirement of AP-1 for ceramide-induced apoptosis in human leukemia HL-60 cells. J Biol Chem **270:**27326-31.
76. **Schlievert, P. M., and L. C. Case.** 2007. Molecular analysis of staphylococcal superantigens. Methods Mol Biol **391:**113-26.
77. **Schneider, T., and G. Sheldrick.** 2002. Substructure solution with SHELXD. Acta Crystallogr. Sect. D **58:**1772–1779.
78. **Segers, R. P., A. van der Drift, A. de Nijs, P. Corcione, B. A. van der Zeijst, and W. Gaastra.** 1990. Molecular analysis of a sphingomyelinase C gene from Leptospira interrogans serovar hardjo. Infect Immun **58:**2177-85.
79. **Seto, M., M. Whitlow, M. A. McCarrick, S. Srinivasan, Y. Zhu, R. Pagila, R. Mintzer, D. Light, A. Johns, and J. A. Meurer-Ogden.** 2004. A model of the acid sphingomyelinase phosphoesterase domain based on its remote structural homolog purple acid phosphatase. Protein Sci. **13:**3172–3186.
80. **Sheldrick, G. M.** 1997. SHELXTL Reference Manual. Bruker-AXS, Inc., Madison, WI
81. **Song, L., M. R. Hobaugh, C. Shustak, S. Cheley, H. Bayley, and J. E. Gouaux.** 1996. Structure of staphylococcal alpha-hemolysin, a heptameric transmembrane pore. Science **274:**1859-66.
82. **Speziale, P., L. Visai, S. Rindi, G. Pietrocola, G. Provenza, and M. Provenzano.** 2008. Prevention and treatment of Staphylococcus biofilms. Curr Med Chem **15:**3185-95.
83. **Staudt, C., H. Horn, D. C. Hempel, and T. R. Neu.** 2004. Volumetric measurements of bacterial cells and extracellular polymeric substance glycoconjugates in biofilms. Biotechnol Bioeng **88:**585-92.
84. **Sueyoshi, N., K. Kita, N. Okino, K. Sakaguchi, T. Nakamura, and M. Ito.** 2002. Molecular cloning and expression of Mn(2+)-dependent sphingomyelinase/hemolysin of an aquatic bacterium, Pseudomonas sp. strain TK4. J Bacteriol **184:**540-6.

85. **Tamber, S., and A. L. Cheung.** 2009. SarZ promotes the expression of virulence factors and represses biofilm formation by modulating SarA and agr in Staphylococcus aureus. Infect Immun **77:**419-28.
86. **Terwilliger, T. C.** 1997. Multiwavelength anomalous diffraction phasing of macromolecular structures: analysis of MAD data as single isomorphous replacement with anomalous scattering data using the MADMRG Program. Methods Enzymol **276:**530-7.
87. **Todar, K.** 2009. Todar's Online Textbook of Bacteriology http://www.textbookofbacteriology.net/.
88. **Torres, V., G. Pishchany, M. Humayuu, O. Schneewind, and E. Skaar. .** 2006. Staphylococcus aureus IsdB is a hemoglobin receptor required for heme iron utilization. J. Bacteriol **188:**8421–8429.
89. **van Belkum, A.** 2006. Staphylococcal colonization and infection: homeostasis versus disbalance of human (innate) immunity and bacterial virulence. Curr Opin Infect Dis **19:**339-44.
90. **Verdon, J., N. Girardin, C. Lacombe, J. M. Berjeaud, and Y. Hechard.** 2009. delta-hemolysin, an update on a membrane-interacting peptide. Peptides **30:**817-23.
91. **Voet, D. V., Judith G. .** 2004. Biochemistry, 3rd ed. Wiley and Co.
92. **Walev, I., U. Weller, S. Strauch, T. Foster, and S. Bhakdi.** 1996. Selective killing of human monocytes and cytokine release provoked by sphingomyelinase (β-toxin) of Staphylococcus aureus. Infect. Immun **64:**2974–2979.
93. **Walev, I., U. Weller, S. Strauch, T. Foster, and S. Bhakdi.** 1996. Selective killing of human monocytes and cytokine release provoked by sphingomyelinase (beta-toxin) of Staphylococcus aureus. Infect Immun **64:**2974-9.
94. **Wallace, A. C., R. A. Laskowski, and J. M. Thornton.** 1995. LIGPLOT a program to generate schematic diagrams of protein ligand interactions. Protein Eng **8:**127–134.
95. **Westerlund, B., and J. P. Slotte.** 2009. How the molecular features of glycosphingolipids affect domain formation in fluid membranes. Biochim Biophys Acta **1788:**194-201.
96. **Whitchurch, C. B., T. Tolker-Nielsen, P. C. Ragas, and J. S. Mattick.** 2002. Extracellular DNA required for bacterial biofilm formation. Science **295:**1487.
97. **Wozniak, M. A., A. P. Mee, and R. F. Itzhaki.** 2009. Herpes simplex virus type 1 DNA is located within Alzheimer's disease amyloid plaques. J Pathol **217:**131-8.
98. **Xu, H., C. Yang, L. Chen, I. A. Kataeva, W. Tempel, D. Lee, J. E. Habel, D. Nguyen, J. W. Pflugrath, J. D. Ferrara, W. B. Arendall, 3rd, J. S. Richardson, D. C. Richardson, Z. J. Liu, M. G. Newton, J. P. Rose, and B. C. Wang.** 2005. Away from the edge II: in-house Se-SAS phasing with chromium radiation. Acta Crystallogr D Biol Crystallogr **61:**960-6.
99. **Yeates, T. O.** 1997. Detecting and overcoming crystal twinning. Methods Enzymol **276:**344-58.

100. **Zhang, P., B. Liu, G. M. Jenkins, Y. A. Hannun, and L. M. Obeid.** 1997. Expression of neutral sphingomyelinase identifies a distinct pool of sphingomyelin involved in apoptosis. J Biol Chem **272:**9609-12.
101. **Zhang, Y. X., Y. Geng, B. Bi, J. Y. He, C. F. Wu, X. K. Guo, and G. P. Zhao.** 2005. Identification and classification of all potential hemolysin encoding genes and their products from Leptospira interrogans serogroup Icterohaemorrhagiae serovar Lai. Acta Pharmacol. Sin **26:**453–461.